

Coverage Performance Analysis of Reconfigurable Intelligent Surface-aided Millimeter Wave Network with Blockage Effect



Zeyang Li

Department of Electronic and Electrical Engineering
University of Sheffield

Supervisors: Prof. Jie Zhang, Dr. Wei Liu

This thesis is submitted for the approval of the
Doctor of Philosophy

January 2023

This thesis is dedicated to my beloved family. Without their unconditional love, encouragement and support, I would not be the person I am today.

Acknowledgements

First and foremost, I would like to thank my supervisor Professor Jie Zhang for his consistent guidance during my Ph.D. study. His insightful ideas and valuable suggestions have been a great help for my research. His enthusiasm and rigorous attitude towards academic research have encouraged and inspired me all the time. I am also very grateful to my second supervisor Dr. Wei Liu for providing guidance for my academic training. It is such a pleasure to have the opportunity to work with them.

I would like to express my gratitude to Dr. Jiliang Zhang and Dr. Haonan Hu for their valuable guidance. Their insightful suggestions and comments during our weekly discussion have been a great support for my academic research. They inspired me to be an independent researcher. I would also like to extend my gratitude to all the colleagues in the Communication Group at the University of Sheffield for their assistance in many aspects of my PhD life.

Above all, I would like to express my gratitude to my family and friends for their love and support. I would not be who I am today without them.

Abstract

In order to solve spectrum resource shortage and satisfy immense wireless data traffic demands, millimeter wave (mmWave) frequency with large available bandwidth has been proposed for wireless communication in 5G and beyond 5G. However, mmWave communications are susceptible to blockages. This characteristic limits the network performance. Meanwhile, reconfigurable intelligent surface (RIS) has been proposed to improve the propagation environment and extend the network coverage. Unlike traditional wireless technologies that improve transmission quality from transceivers, RISs enhance network performance by adjusting the propagation environment. One of the promising applications of RISs is to provide indirect line-of-sight (LoS) paths when the direct LoS path between transceivers does not exist. This application makes RIS particularly useful in mmWave communications. With effective RIS deployment, the mmWave RIS-aided network performance can be enhanced significantly. However, most existing works have analyzed RIS-aided network performance without exploiting the flexibility of RIS deployment and/or considering blockage effect, which leaves huge research gaps in RIS-aided networks. To fill the gaps, this thesis develops RIS-aided mmWave network models considering blockage effect under the stochastic geometry framework. Three scenarios, i.e., indoor, outdoor and outdoor-to-indoor (O2I) RIS-aided networks, are investigated.

Firstly, LoS propagation is hard to be guaranteed in indoor environments since blockages are densely distributed. Deploying RISs to assist mmWave transmission is a promising way to overcome this challenge. In the first paper, we propose an indoor mmWave RIS-aided network model capturing the characteristics of indoor environments. With a given base station (BS) density, whether deploying RISs or increasing BS density to further enhance the

network coverage is more cost-effective is investigated. We present a coverage calculation algorithm which can be adapted for different indoor layouts. Then, we jointly analyze the network cost and coverage probability. Our results indicate that deploying RISs with an appropriate number of BSs is more cost-effective for achieving an adequate coverage probability than increasing BSs only.

Secondly, for a given total number of passive elements, whether fewer large-scale RISs or more small-scale RISs should be deployed has yet to be investigated in the presence of the blockage effect. In the second paper, we model and analyze a 3D outdoor mmWave RIS-aided network considering both building blockages and human-body blockages. Based on the proposed model, the analytical upper and lower bounds of the coverage probability are derived. Meanwhile, the closed-form coverage probability when RISs are much closer to the UE than the BS is derived. In terms of coverage enhancement, we reveal that sparsely deployed large-scale RISs outperform densely deployed small-scale RISs in scenarios of sparse blockages and/or long transmission distances, while densely deployed small-scale RISs win in scenarios of dense blockages and/or short transmission distances.

Finally, building envelope (the exterior wall of a building) makes outdoor mmWave BS difficult to communicate with indoor UE. Transmissive RISs with passive elements have been proposed to refract the signal when the transmitter and receiver are on the different side of the RIS. Similar to reflective RISs, the passive elements of a transmissive RIS can implement phase shifts and adjust the amplitude of the incident signals. By deploying transmissive RISs on the building envelope, it is feasible to implement RIS-aided O2I mmWave networks. In the third paper, we develop a 3D RIS-aided O2I mmWave network model with random indoor blockages. Based on the model, a closed-form coverage probability approximation considering blockage spatial correlation is derived, and multiple-RIS deployment strategies are discussed. For a given total number of RIS passive elements, the impact of blockage density, the number and locations of RISs on the coverage probability is analyzed.

All the analytical results have been validated by Monte Carlo simulation. The observations from the result analysis provide guidelines for the future deployment of RIS-aided mmWave networks.

Table of contents

Acknowledgements	v
Abstract	vii
List of Figures	xii
List of Tables	xiii
List of Abbreviations	xv
I Introduction and Overview	1
1 Introduction	3
1.1 Background	3
1.1.1 Millimeter Wave Networks	3
1.1.2 Reconfigurable Intelligent Surface	4
1.1.3 RIS-aided mmWave Networks	4
1.2 Motivation and Objectives	5
1.3 Contributions	8
1.3.1 Papers Included in the Thesis	8
1.3.2 Papers not Included in the Thesis	8
1.3.3 Contributions of the Thesis	9
1.4 Structure of the Thesis	11

2	Literature Review	13
2.1	Modelling of Blockages in Network Performance Evaluation	13
2.2	Modelling of Millimeter-wave Networks	17
2.3	Performance Analysis of RIS-aided Networks	18
2.3.1	Single-input Single-output RIS-aided Networks	18
2.3.2	Comparison between RIS and Relay	18
2.3.3	Imperfect Phase Shifts of RIS	19
2.3.4	Spatially Correlated Channels	20
2.3.5	Multiple RIS-aided Networks	20
2.4	Modelling of RIS-aided Networks Using Stochastic Geometry	21
2.4.1	RIS-aided Networks without Blockage	22
2.4.2	RIS-aided Networks with Blockage Model	24
3	Conclusion and Future Work	27
3.1	Conclusion	27
3.2	Future Work	29
II	Published Papers	43
4	Paper I - Enhancing Indoor mmWave Wireless Coverage: Small-Cell Densification or Reconfigurable Intelligent Surfaces Deployment?	45
5	Paper II - RIS-assisted mmWave Networks with Random Blockages: Fewer Large RISs or More Small RISs?	63
6	Paper III - Coverage Analysis of Multiple Transmissive RIS-aided Outdoor-to-Indoor mmWave Networks	104

List of figures

1.1	Illustration of RIS-aided mmWave network.	5
2.1	The 2D LoS ball model.	14
2.2	A top view to show the blockage correlation between two links.	15
2.3	Illustration of a 2D self-body blockage model.	16
4.1	The LoS area and RIS-extended area of a randomly located UE in the indoor environment. Note that the LoS area and RIS-extended area can be applied to both uplink and downlink networks. If any BSs locate in the LoS area or RIS-extended area, the UE is in coverage.	50
4.2	The considered indoor layouts.	55
4.3	The network coverage probability with different BS density and RIS density.	56
4.4	The cost comparison between RIS deployment and small-cell BS densification to achieve same coverage probability in indoor layout 1.	57
4.5	The cost comparison between RIS deployment and small-cell BS densification to achieve same coverage probability in indoor layout 2.	58
5.1	Top view of the BS, UE, RIS and buildings.	71
5.2	Human-body blockages.	71
5.3	Nearby-user blockage model.	72
5.4	Self-body blockage model.	72
5.5	The SNR of the received signal when the RIS is located at (x,y) . The locations of the UE and the BS are $(0,0)$ and $(150,0)$, respectively.	76

5.6	The RIS area when the SNR threshold $T = 7\text{dB}$	77
5.7	The RIS area when the SNR threshold $T = 18\text{dB}$	77
5.8	The RIS area when the SNR threshold $T = 23\text{dB}$	78
5.9	The RIS area when the SNR threshold $T = 36\text{dB}$	78
5.10	The coverage probability versus the density of building blockages for different distance between the BS and the UE.	88
5.11	The coverage probability versus the density of nearby-user blockages for different distance between the BS and the UE.	88
5.12	The coverage probability versus the SNR threshold and n	90
5.13	The coverage probability when RISs are much closer to the UE than the BS.	91
5.14	Cost effectiveness: the function of coverage probability to cost for different cost exponent ζ . $R_b = 50$ m.	92
6.1	Network model.	109
6.2	Top views to show blockage region/regions.	113
6.3	The overlapped blockage region (red) of two RISs.	114
6.4	Multi-RIS deployment strategy.	121
6.5	The effect of W_{r2} and x_d on the average coverage probability when 4 RISs are deployed.	122
6.6	With different number of RISs, the coverage probability when the UE is 10 m away from the building envelope. In case 1, the RIS providing the highest average received power is selected to transmit the signal; in case 2, all the RISs that are not blocked are selected to transmit the signal.	123
6.7	Considering the blockages with different size, the coverage probability when the UE is 10 m away from the building envelope.	124
6.8	The network coverage in the room with different number of RISs deployed in the building envelope.	125
6.9	The coverage probability considering / without considering blockage spatial correlation.	132

List of tables

4.1	Simulation Parameters	55
5.1	$\rho_u, \rho_b, \tau_b, \tau_u$ when $\Delta = 0, AB > 0$ and $C \neq 0$	80
5.2	$\rho_u, \rho_b, \tau_b, \tau_u$ when $\Delta > 0, x_1 < 0$ and $x_2 > R_b$	80
5.3	$\rho_u, \rho_b, \tau_b, \tau_u$ when $\Delta > 0$ (except the case that $x_1 < 0$ and $x_2 > R_b$)	81
5.4	Simulation Parameters	89
6.1	Main Notations	110
6.2	$\Phi_{1,2}$ for event $E_{1,2}$	118
6.3	Simulation Parameters	122
6.4	With different room size $W_r \times L_r$ and different number of RISs, the optimized length W_{r2} and the optimized location x_d of the RIS-deployment wall, and the optimal average coverage probability A_h of the room.	126
6.5	With different blockage density λ_b and different number of RISs, the optimized length W_{r2} and the optimized location x_d of the RIS-deployment wall, and the optimal average coverage probability A_h of the room with size 30 m \times 30 m.	126

List of Abbreviations

2D two-dimensional

3D three-dimensional

AF amplify-and-forward

AoA angle of arrival

ASE area spectral efficiency

BER bit error rate

BPP binomial point process

BS base station

CLT central limit theorem

CSI channel state information

DF decode-and-forward

LoS line-of-sight

MIMO multiple input multiple output

mmWave millimeter wave

NLoS none-line-of-sight

NOMA	non-orthogonal multiple access
O2I	outdoor-to-indoor
PDF	probability density function
PLE	path loss exponent
PPP	Poisson point process
RHH	Remote Radio Heads
RIS	reconfigurable intelligent surface
SCN	small-cell network
SER	symbol error rate
SIR	signal-to-interference ratio
SISO	single-input single-output
SNR	signal-to-noise ratio
STAR	simultaneously transmitting and reflecting
UDN	ultra-dense network
UDSC	ultra-dense small cell
UE	user equipment

Part I

Introduction and Overview

Chapter 1

Introduction

1.1 Background

1.1.1 Millimeter Wave Networks

Due to the large available bandwidth ranging from 30 GHz to 300 GHz, millimeter wave (mmWave) frequencies have been regarded as one of the promising technologies to provide multi-giga-bits-per-second data rates [1]. MmWave band has already been considered in many wireless systems, e.g., personal area networking in IEEE 802.15.3c [2], fixed point access links in IEEE 802.16.1 [3], and local area networking in IEEE 802.11ad [4]. However, mmWave frequencies suffer from high penetration loss when the waves pass through common blockages, e.g., walls, trees and human bodies, because of the shorter wavelength [5]. Therefore, line-of-sight (LoS) transmission needs to be guaranteed in mmWave networks. One of the feasible solutions to guarantee LoS transmission is ultra-dense small cell (UDSC) networks [6], in which small cell base stations (BSs) are densely deployed to increase LoS probability. Nevertheless, small cell density cannot increase boundlessly. Research has shown that further increasing small cell density after reaching a certain threshold leads to a decrease of network coverage [7], [8]. Accordingly, a new technology needs to be adopted for mmWave wireless coverage enhancement.

1.1.2 Reconfigurable Intelligent Surface

Reconfigurable intelligent surface (RIS) has been proposed to intelligently reconfigure wireless propagation environment [9]. Specifically, a RIS is a two-dimensional (2D) surface composed of a large number of passive elements (also known as unit cells). Each passive element is software-controlled to modify the phase and amplitude of the incident signal, so that the RIS can form passive analog beamforming in the direction of the receiver [10]. The function of passive elements can be implemented by adopting different technologies, e.g., using small-scale discrete antenna elements [11] or metallic/dielectric patches [12] as passive elements. In the literature, sometimes other terms such as intelligent reflecting surfaces, software controllable surfaces, large intelligent surfaces and digitally controllable scatters are used to refer to RISs. RISs can provide several promising applications in wireless communication, e.g., generating indirect LoS link between transceivers, suppressing inter-cell interference and improving physical layer security [13]. In addition, RISs are more energy efficient than conventional communication technologies, e.g., amplify-and-forward relaying [14], since RISs do not require any power amplifiers. RISs can be categorised into three types [15]: (i) reflective RISs, which fully reflect the incident signal; (ii) transmissive RISs, which fully refract the incident signal; and (iii) simultaneously transmitting and reflecting (STAR) RISs, which partially reflect and partially refract the incident signal. From the perspective of practicability, two prototypes of the RIS have been designed by two different research groups, i.e., the Massachusetts Institute of Technology (MIT) [11], USA, and NTT DOCOMO [12], Japan.

1.1.3 RIS-aided mmWave Networks

Adopting RISs to reflect or refract signals can create extra transmission paths between a serving BS and a UE, as shown in Fig. 1.1, so that LoS probability, which is crucial in mmWave communication [16], can be improved, and thereby, the coverage probability can be improved. Meanwhile, the size and inter-element distance of the passive elements on RIS are sub-wavelength, this characteristic allows the size of RIS to be smaller, and thereby a large

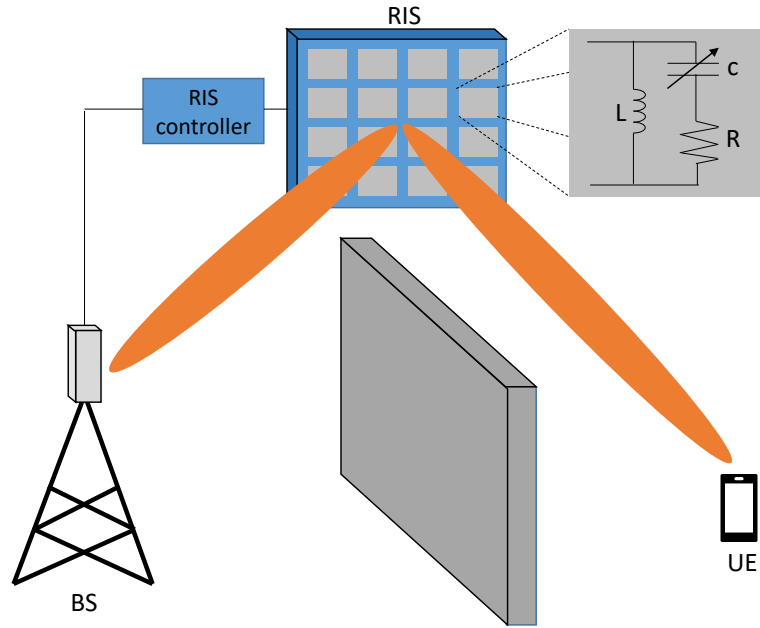


Fig. 1.1 Illustration of RIS-aided mmWave network.

number of passive elements can be deployed on a RIS with acceptable size to provide a high array gain [17]. With an effective RIS deployment strategy, the performance of RIS-aided mmWave networks can be enhanced significantly. Research has shown that the RIS-aided transmission has the highest received power if the RIS is near either the transmitter or receiver [3]. In multi-RIS-aided mmWave networks, RIS deployment strategies need to be further studied to improve LoS probability and provide enough path gain.

1.2 Motivation and Objectives

As mentioned in Section 1.1, RISs can create an indirect LoS link when the direct link between the BS and UE is blocked, thereby enhancing the coverage probability. However, the coverage enhancement of RIS-aided networks considering blockage effect still requires further investigation. In this thesis, we aim to investigate the RIS-aided network coverage under blockage effect and to provide critical and valuable insights for practical RIS deployment. Specifically, several research gaps remain to be filled:

Gap 1: RISs are passive devices, and thereby cost less energy than the alternative technologies requiring active devices [14, 18], e.g., UDSC, massive multiple input multiple output (MIMO) and relay. However, RIS-aided transmission suffers high attenuation because of the double path loss and absence of signal amplifier [19–21]. To compensate for the high attenuation, the size and the number of RISs need to be sufficiently large so that enough passive elements in the suitable positions can reflect signals effectively [10, 22]. In other words, large-scale RISs need to be massively deployed in wireless networks. As a result, the number of RISs required in RIS-aided networks might be much higher than the number of active devices required in other technologies [20]. Previous work [23] defined the network cost as the quantity of the network equipment multiples with the unit cost. For example, the network cost of UDSC networks is the quantity of small-cell BSs multiple with the unit cost of small-cell BSs. In addition, the network cost of RIS is that the quantity of RISs multiples with the unit cost of RISs. Given a fixed network cost, it remains unknown whether RISs are more cost-effective to enhance network performance compared with alternative technologies. Meanwhile, existing works mainly focus on the modelling of either small-cell networks (SCN) [8, 24–26] or RIS-aided networks [27–30], where the results are not applicable for comparison because of different system models. To have a fair comparison between RIS deployment and small-cell densification, a system model that applies to both RIS-aided networks and UDSC networks needs to be built.

Based on Gap 1, the following question is investigated:

Question 1: Which technology can achieve higher indoor mmWave network coverage with lower network cost: small-cell densification or RIS deployment?

Gap 2: Large-scale RISs need to be massively deployed in RIS-aided networks to compensate for the high attenuation and generate indirect LoS paths [10, 22]. Meanwhile, RIS-aided transmission has the highest received power when the RIS is near either the transmitter or receiver [9]. Accordingly, effective RIS deployment strategies are essential for wireless coverage enhancement. The technical challenge of stochastic geometry-based RIS-aided network modelling is: different from traditional transmission where only the distance between BS and

UE needs to be considered, three geometrical factors need to be considered for RIS-aided transmission, i.e., the distance between BS and UE, the distance between BS and RIS, and distance between RIS and UE. Considering random locations of RIS, high complexity is introduced into the model. Previous stochastic geometry-based works [28, 29, 31, 32] have analyzed RIS-aided network coverage based on numerical integrals. The results showed that the optimal RIS deployment depends on various factors, e.g., blockage density, RIS density, user demand and transmission distance. However, demonstrating the interplay/tradeoff among these factors requires some closed-form expressions, which have not been presented in existing works. Meanwhile, for a given total number of passive elements, whether fewer large-scale RISs or more small-scale RISs should be deployed for higher network coverage needs to be investigated.

Based on Gap 2, the following questions are investigated:

Question 2: What are the critical network parameters that need to be considered in the RIS deployment, and how do they affect the RIS-aided network coverage?

Question 3: For a fixed total number of passive elements, should fewer large-scale RISs or more small-scale RISs be deployed to maximize the coverage probability?

Gap 3: In mmWave communications, signals suffer from high penetration losses when passing through obstacles. Hence, it is challenging to adopt mmWave transmission in outdoor-to-indoor (O2I) networks because of the building envelope (the exterior wall of a building). The work in [33] investigated transmissive RIS-aided O2I mmWave networks and showed that the network coverage can be enhanced significantly by deploying transmissive RISs on the building envelope. Nevertheless, the work might have overestimated the coverage probability by ignoring blockage spatial correlation. In an indoor environment where the space is limited, RISs which are close to each other might be blocked by the same blockage. Therefore, the spatial correlation of blockages needs to be investigated. In addition, it is not cost-effective to deploy transmissive RISs on the whole building envelope. Accordingly, the RIS deployment strategies (the positions of RISs on the building envelope) need to be studied for effective RIS deployment.

Based on Gap 3, the following question is investigated:

Question 4: Considering blockage spatial correlation, how to deploy transmissive RISs on the building envelope to enhance O2I network coverage?

1.3 Contributions

1.3.1 Papers Included in the Thesis

- **Paper I: Enhancing Indoor mmWave Wireless Coverage: Small-cell Densification or Reconfigurable Intelligent Surfaces Deployment?**, Zeyang Li, Haonan Hu, Jiliang Zhang and Jie Zhang. This paper has been published in IEEE Wireless Communications Letters, Volume: 10, Number: 11, Pages: 2547-2551, Nov. 2021.
- **Paper II: RIS-assisted mmWave Networks with Random Blockages: Fewer Large RISs or More Small RISs?**, Zeyang Li, Haonan Hu, Jiliang Zhang and Jie Zhang. This paper has been accepted to publish in IEEE Transactions on Wireless Communications.
- **Paper III: Coverage Analysis of Multiple Transmissive RIS-aided Outdoor-to-Indoor mmWave Networks**, Zeyang Li, Haonan Hu, Jiliang Zhang and Jie Zhang. This paper has been published in IEEE Transactions on Broadcasting, Early Access, Aug. 2022.

1.3.2 Papers not Included in the Thesis

- **Impact of Wall Penetration Loss on Indoor Wireless Networks**, Zeyang Li, Haonan Hu, Jiliang Zhang and Jie Zhang. This paper has been published in IEEE Antennas Wireless Propagation Letter, Volume: 20, Number: 10, Pages: 1888-1892, Oct. 2021.
- **Computation Offloading Analysis in Clustered Fog Radio Access Networks with Repulsion**, Haonan Hu, Jiliang Zhang, Yan Jiang, Zeyang Li, Qianbin Chen and Jie Zhang. This paper has been published in IEEE Transactions on Vehicular Technology, Volume: 70, Number: 10, Pages: 10804-10819, Oct. 2021.

1.3.3 Contributions of the Thesis

This thesis investigates the RIS-aided mmWave networks under blockage effect based on stochastic geometry. Question 1 is addressed in Paper I, Question 2 and Question 3 are addressed in Paper II, Question 3 and Question 4 are addressed in Paper III. The main contributions of this thesis are summarized as follows:

- In Paper I, we are the first to compare RIS deployment with small-cell densification regarding coverage enhancement. We consider a general scenario that the BS distribution follows Poisson point process (PPP), and the UE is randomly distributed within the indoor layout. Firstly, we calculate the indoor coverage probability based on a Monte Carlo-based algorithm that computes the channel quality of each BS to the UE. This algorithm needs to be re-run for different BS densities. Then, we define the coverage area as the area of the LoS region and RIS-extended LoS region of a UE in the indoor environment. Next, we propose a coverage area calculation algorithm. Because the coverage area is independent of BS density, the algorithm does not need to be re-run for different BS densities. After calculating the coverage area, the coverage probability can be obtained based on equations from stochastic geometry theory. The proposed algorithm can be applied to different indoor layouts. Meanwhile, it can be applied to both UDSC networks and RIS-aided networks. Moreover, the coverage probability obtained from the coverage area calculation algorithm matches well with that obtained from Monte Carlo-based algorithm. Furthermore, we define the cost of deploying small-cell BSs and RISs as functions of the quantity of BSs and RISs. Finally, we jointly analyze the coverage probability and network cost to compare the cost effectiveness of UDSC networks and RIS-aided networks. More specifically, we compare the network cost of UDSC networks and RIS-aided networks when both networks achieve the same coverage probability.
- In Paper II, we investigate the coverage probability of a downlink RIS-aided mmWave networks. By considering the height of BS, UE and random blockages, we present a three-dimensional (3D) RIS-aided mmWave network model. We assume that the

centers of RISs, building blockages and human-body blockages are distributed following two-dimensional (2D) independent PPPs with fixed heights. Different from previous stochastic geometry-based works which have analyzed RIS-aided network coverage based on numerical integrals [28, 29, 31, 32], we derive the tractable analytical coverage probability upper and lower bounds of the RIS-aid mmWave networks based on a novel two-step approach. Specifically, in the first step, we analyse the received signal-to-noise ratio (SNR) without considering blockage. We first define the RIS-acceptable region. The SNR threshold of the UE is satisfied if a RIS located in the RIS-acceptable region. Then, we adopt circles which cover or be contained by the RIS acceptable region as the upper and lower bounds of the RIS acceptable region. Based on the region's upper and lower bounds, we derive the probability that the received SNR is higher than the SNR threshold. In the second step, we analyse the LoS probability, i.e., the probability that either the direct or RIS-aided transmission is unblocked. We derive the probability that an indirect LoS transmission exists within a given circle centered on the BS or the UE. Finally, by combining the results from the two steps, we derive and validate the analytical upper and lower bounds of the coverage probability as the functions of network parameters and blockage densities. We also derive and validate the closed-form coverage probability when RISs are much closer to UE than BS. Finally, we propose a general network cost model for RIS-assisted networks. For a given number of passive elements, we analyse the impact of building density, nearby-user density, SNR threshold, the RIS size and RIS density on the coverage probability, respectively.

- In Paper III, we investigate the coverage probability of a multiple transmissive RIS-aided O2I mmWave network. By considering the heights of the BS, transmissive RISs and UE, we propose a 3D multiple transmissive RIS-aided O2I mmWave network model with random indoor blockages. The scenario in which different transmission paths are blocked by the same blockage, which has a high probability to happen in indoor environment with limited space, has not been considered in previous work about transmissive RIS-aided O2I networks [33]. Therefore, we first consider the

same-size blockages, incorporate the blockage spatial correlation into our system model and derive the blockage probability, i.e., the probability that all the transmission paths between the BS and UE are blocked. Next, we consider that the sizes of blockages follow a probability density function, and extend the blockage probability to different-size blockages. Moreover, we derive and verify a closed-form approximation of the coverage probability. Finally, our results show that the coverage probability without considering blockage spatial correlation leads to an overestimation of the actual network coverage. In addition, we evaluate multi-RIS deployment strategies for a given total number of passive elements, and analyse the impact of blockage density, room size, the number and locations of RISs on the coverage probability.

The author of this thesis plays a key role as the first author of Paper I-III, including presenting original ideas, problem formulation, mathematical modelling and analysis, verifying analytical derivations by simulations, designing algorithm, and writing papers. Dr. Haonan Hu and Dr. Jiliang Zhang provide guidance in the analytical derivations and result analysis. Prof. Jie Zhang supervises the contents and significance of these research. All authors contribute to the main idea formulation and manuscript polishing.

1.4 Structure of the Thesis

The thesis is composed of two parts. For Part I, we provide a general introduction and overview, including three chapters. For Part II, we present three journal papers as main technical contributions of this thesis.

In Chapter 1, we introduce the background, motivations, objectives, and contributions of the research on the coverage performance of RIS-aided mmWave network with blockage effect. In addition, the outline of this thesis is provided.

In Chapter 2, Section 2.1 introduces blockage modelling in existing research about network performance evaluation. Section 2.2 introduces the major characteristics of mmWave frequency in network modelling. Section 2.3 reviews performance analysis of RIS-aided

networks in various scenarios. Section 2.4 reviews RIS-aided network modelling based on stochastic geometry.

In Chapter 3, we present the contributions of the three journal papers, including the main insights discovered from the result analysis. In addition, we discuss the extensive research for future works.

Chapter 2

Literature Review

This chapter first introduces the modelling of blockages in network performance evaluation. Then, it introduces the major characteristics of mmWave frequency in network modelling. Moreover, it reviews RIS-aided network performance analysis in different scenarios. Finally, it introduces RIS-aided network modelling based on stochastic geometry in previous works.

2.1 Modelling of Blockages in Network Performance Evaluation

The blockage effect has a significant impact on network performance. Previous works have shown that the network performance evaluation with/without considering the blockage effect can lead to quite different results. For instance, in [34], the blockage effect was not considered, and the results revealed that the area spectral efficiency (ASE) monotonically increases as the BS density rises. However, in [8], different path loss exponents (PLEs) were considered for LoS links and none-line-of-sight (NLoS) links. Moreover, the results showed that the ASE may decrease as the BS density exceeds a certain threshold. The reason is that more interference signals with LoS links are created as the BS density rises. Accordingly, an accurate blockage model is crucial for network performance evaluation.

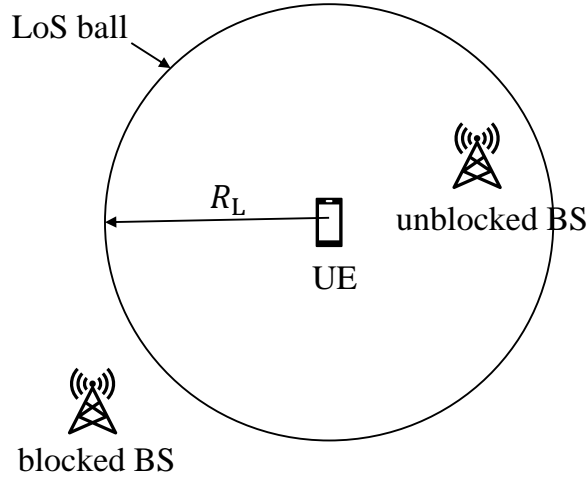


Fig. 2.1 The 2D LoS ball model.

A 2D LoS ball model was proposed to incorporate the blockage effect into the network model in [35]. As shown in Fig. 2.1, the LoS ball model is a circle centered at the UE and with radius R_L . The transmission is LoS if the transmitter is located within the circle and is none-line-of-sight (NLoS) otherwise. The Blockage effect was expressed by distinguishing LoS and NLoS links with different PLEs.

A mathematical framework for random building blockage modelling based on Boolean scheme was presented in [36]. The building blockages were modelled as rectangles and the centers of blockages formed a PPP with density λ . In addition, the width W , length L and orientation θ of each blockage were independently and randomly decided. The work proved that the number of blockages K on a transmission link with distance R follows Poisson distribution with mean value $\beta R + p$, where $\beta = 2\lambda(\mathbb{E}[W] + \mathbb{E}[L])/\pi$ and $p = \lambda\mathbb{E}[W]\mathbb{E}[L]$. And the LoS probability of the transmission with distance R is:

$$\mathbb{P}(K = 0) = e^{-(\beta R + p)}. \quad (2.1)$$

The network performance analysis with a random building blockage model was compared with the actual building layout. The results showed that the proposed blockage model fits the actual scenarios well. Based on the blockage model in [36], different types of blockages were modelled as line segments and circles in many later works. For example, in [37], macro-

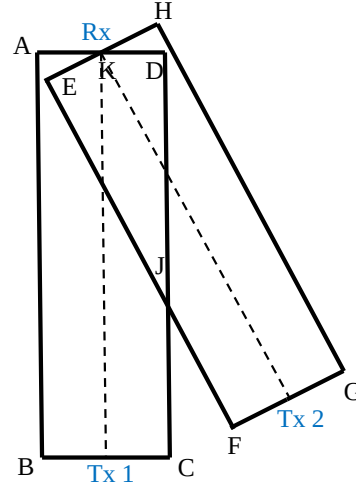


Fig. 2.2 A top view to show the blockage correlation between two links.

diversity, i.e., multiple BSs serve one UE simultaneously, was investigated considering blockages of line segments. In addition, the blockage correlation among different links was studied.

A human body blockage model was proposed in [38]. The human body blockages were modelled as cylinders with the constant diameter d and random height H . The centers of the blockages follow a PPP with the density λ_h . Moreover, in [39], spatial correlation, which has been regarded as one of the significant factors in mmWave channel modelling, was analyzed by considering the blockage correlation between different transmission links. For example, in Fig. 2.2, region ABCD and region EFGH are the blockage region for TX1-RX and TX2-RX links, respectively. The link is blocked if any centers of blockages are located in its blockage region. Blockage correlation needs to be considered when the overlapped blockage region of the two links, i.e., Region DKEJ, exists. The probability that the two links are blocked by the same blockages can be calculated by $P_{bc} = 1 - e^{-S\lambda_h}$, where S is the area of region DKEJ.

To better characterize the indoor environment for network performance evaluation, indoor blockage models have been studied by many works. In [40] and [41], based on Boolean scheme, binary-oriented line segments were used to model the indoor walls. In [42], Poisson grid model was proposed for modelling indoor walls and floors in a multi-storey building. In [43], multi-storey small-cell networks were investigated, and the joint analysis of BS density and storey height was presented.

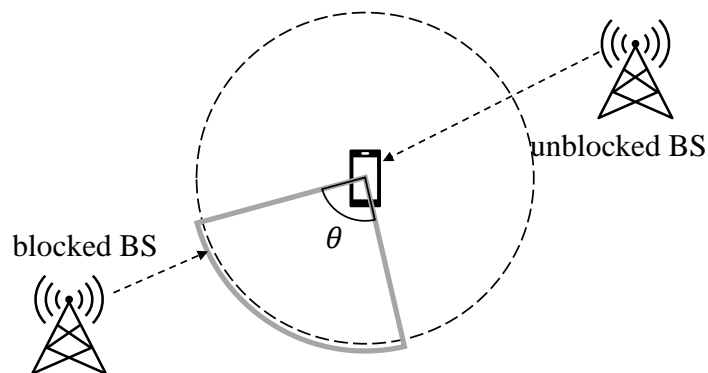


Fig. 2.3 Illustration of a 2D self-body blockage model.

A 2D self-body blockage model was proposed in [44] to incorporate the self-body blockage effect into the mmWave network modelling. As shown in Fig. 2.3, a blocking angle θ was adopted to represent a certain angle of the user's body to the UE. The value of θ is decided by the width of the user's body and the position of the user. Constant penetration loss is assumed when the signal's angle of arrival (AoA) falls in the blocking angle. BSs are assumed to follow a PPP, and thereby the probability that a BS is blocked by the body of the user is $P_{bs} = \frac{\theta}{2\pi}$.

Summary

In this section, the blockage models in network performance evaluation proposed in literature have been reviewed. Random-located blockages are an acceptable assumption for the tractable network performance in general scenarios, while only providing limited accuracy for a specific propagation environment. On the other hand, deterministic blockage models deliver more insights but are more time-consuming and only apply to limited scenarios. An adequate blockage model should facilitate a tractable network performance analysis while reflecting the practical blockage environment. The LoS ball model in Fig. 2.1 [35] enables the tractability of performance analysis but only reflects the practical blockage environment to a certain degree. Therefore, to keep tractability and accuracy, the building blockage modelling based on Boolean scheme [36], which has been proved to fit well with the actual scenarios, is adopted in this thesis [36] for modelling buildings. The blockage model in [39] has incorporated blockage spatial correlation. However, a tractable approach to describing the blockage probability considering multiple transmission paths has yet to be developed.

The self-body blockage model in Fig. 2.3 [44] can only adopt to 2D scenarios where the heights of BSs and self-body blockage are ignored, while the 3D self-body blockage model requires further investigation.

2.2 Modelling of Millimeter-wave Networks

Compared with traditional communication, MmWave communication has different characteristics for antenna radiation and channel propagation, which need to be modelled in a tractable and accurate way for network performance analysis:

(1) Transceivers in mmWave systems are equipped with massive antennas to enhance the transmission in the target direction and suppress the transmissions in other directions, i.e., analog beamforming. To approximately characterize analog beamforming, a simplified beamforming antenna model considering a main-lobe gain, side-lobe gain and main-lobe width was adopted, i.e., flat-top antenna model [35, 26, 45–48]. Particularly, in [45], the impact of imperfect beam alignment on ergodic rate and coverage probability was investigated. Moreover, different from the flat-top antenna model, a sinc and cosine antenna model was used to incorporate antenna size into network performance analysis at the cost of analytical tractability [25, 49].

(2) MmWave frequency has sparse scattering characteristics. Hence, Rayleigh fading channels, commonly assumed in traditional channel models, are not suitable for mmWave transmission [50]. Instead, Nakagami- m channels are assumed for mmWave transmissions [35, 26, 51].

(3) A large number of antenna elements are implemented in mmWave systems, e.g., massive MIMO mmWave systems/RIS-aided mmWave systems. As a result, channel responses are smoothed by the extremely large spatial diversity as a result of the favourable action of the law of large numbers [52, 53]. These smooth channel responses are called channel hardening, which means that fading channels behave as if they were non-fading channels.

(4) MmWave frequency has high penetration loss through blockages. Hence, the impact of blockages needs to be investigated. In [35, 26, 25], an LoS ball model was adopted.

Moreover, in [47, 48, 54], a random blockage model based on random shape theory was applied. Numerical results indicated that blockage density has a significant impact on the network throughput [48, 54].

2.3 Performance Analysis of RIS-aided Networks

The performance analysis of RIS-aided networks has been investigated under various scenarios and assumptions, i.e., single-RIS network, multi-RIS network, imperfect phase shifts, and spatially correlated channels. In this section, the works on RIS-aided networks with different emphases are introduced.

2.3.1 Single-input Single-output RIS-aided Networks

The coverage/outage probability of a single-input single-output (SISO) RIS-aided system has been widely analyzed. Specifically, Rayleigh fading channels [18, 55] and Rician fading channels [56] were assumed for the channels between the BS/UE and each passive element of the RIS. Then, the channel distribution of the RIS-aided transmission was approximated based on central limit theorem (CLT). This approximation is accurate when the number of passive elements $N \gg 1$. Then, the channel distribution of the RIS-aided transmission with an arbitrary number of passive elements N was approximated assuming Rayleigh fading channels in [57, 58] and Rician fading channels in [59] and Nakagami- m fading channels in [60].

2.3.2 Comparison between RIS and Relay

The comparison between RIS and relay has been discussed by many works since RIS and relay offer similar functions with different mechanisms. In [14, 16, 61], the comparison between a RIS and an amplify-and-forward (AF) relay has been presented. In [14], the energy efficiency maximization problem was formulated. The transmit power allocation and RIS phase shifts were optimized. The results showed that the RIS-aided networks can

achieve higher energy efficiency compared with the AF relay. In [61], assuming Rayleigh fading channels, the outage probability and ergodic capacity of both the RIS-aided system and AF-relaying system were studied. The results indicated that the RIS-aided system outperforms the AF-relaying system. In [16], fluctuating two-ray distribution was adopted to model small-scale fading in mmWave communication. The outage probability and bit error rate (BER) of both systems were analyzed, and results showed that the RIS-aided system with a small number of passive elements can achieve the same performance as the AF-relaying system. In [20], the RIS-aided system was compared with decode-and-forward (DF)-relaying in terms of transmit power and energy efficiency for achieving the same data rate. The results revealed that a RIS requires hundreds of passive elements to be competitive with the DF relay.

2.3.3 Imperfect Phase Shifts of RIS

Perfect phase shifts on the RIS/RISs have been assumed in the above works. However, imperfect phase shifts are more practical because 1) discrete phase shifts are implemented instead of continuous phase shifts; 2) perfect channel state information (CSI) is unavailable. Therefore, the impact of discrete phase shifts and phase error on the network performance has been studied. In [62], the data rate of an uplink RIS-aided network was evaluated. The required number of phase shifts was derived with a given data rate threshold. In [63], the number of discrete phase shifts for achieving full diversity order was investigated. In [64], the interplay between the amplitude and phase of each passive element on the RIS was considered. The closed-form outage probability of the RIS-aided network was derived. In [65], the distribution of the signal-to-noise ratio (SNR) and the diversity order of the error probability were evaluated assuming that phase error follows a generic distribution. In [66], the impact of phase error on the ergodic capacity was investigated. In [67] and [68], Von Mises distribution was adopted to model phase error. Specifically, in [67], the BER of the RIS-aided network assuming Nakagami- m fading was derived. In [68], the outage probability approximation of the RIS-aided network was derived. In [69], the average data rate and error probability of the RIS-aided network were derived assuming the phase error follows a

uniform distribution. In [70], the impact of discrete phase shifts on the outage probability assuming Rician fading channels was analyzed.

2.3.4 Spatially Correlated Channels

The passive elements of the RIS are separated by no more than half of the wavelength, which leads to spatially correlated channels for RIS-aided communication. Accordingly, performance analysis of RIS-aided networks considering spatially correlated channels has been studied. In [53], a spatially correlated Rayleigh fading channel model for RIS-aided communication was proposed. Moreover, in [71] and [72], the outage/coverage probability of the RIS-aided network assuming spatially correlated Rayleigh fading channels was evaluated. Furthermore, in [73], the symbol error rate (SER) and channel capacity of the RIS-aided network with spatially correlated channels were analyzed.

2.3.5 Multiple RIS-aided Networks

The works introduced above have presented performance analysis of RIS-aided networks in the presence of a single RIS. The performance of multiple RIS-aided networks has also been evaluated. Specifically, in [74], the outage probability and average sum rate were analyzed assuming that the RIS providing the highest instantaneous SNR is chosen to assist the transmission. In [75], the BER, SER and achievable rate of the multiple RIS-aided networks in indoor and outdoor scenarios were investigated. In indoor scenarios, the RIS providing the highest SNR is chosen to assist the transmission. In outdoor scenarios, 2-hop RIS-aided transmission is adopted. The 2-RIS path which provides the highest SNR is selected to assist the transmission. In [76], multiple RISs with different sizes were adopted, and the channels of different RISs were assumed to be independent but nonidentical. Two RIS-selected schemes were considered, i.e., 1) all the RISs serve the UE; 2) a scheduled RIS serve the UE. The outage probability and ergodic capacity of the network were evaluated. In [77], the co-channel interference was considered in the multiple RIS-aided networks. The outage probability and BER were analyzed. In the above works, the impact of the RIS

deployment strategy on the network performance was not discussed. Accordingly, in [78] and [79], whether centralized RIS deployment or distributed RIS deployment should be adopted has been discussed. Specifically, in [78], a single-antenna BS serves 2 single-antenna UEs by adopting either a centralized RIS which closes to the BS or 2 distributed RISs which close to the UEs. The achievable data rate of the uplink RIS-aided network was analyzed. In [79], a single-antenna BS serves a single-antenna UE with either a centralized RIS or multiple distributed RISs. Outdated CSI was considered and the ergodic capacity was evaluated. The work in [80] considered simultaneous transmission by multiple RISs with indoor blockages. The BER and achievable data rate were analyzed.

Summary

In this section, the RIS-aided network performance evaluation under different scenarios has been reviewed. The above works assumed fixed locations of RISs without exploiting the impact of the spatial locations. Considering the flexibility of RIS locations, the network performance and deployment analysis of RIS-aided networks need to be analyzed. Meanwhile, research has shown that both the number of RISs and the number of passive elements per RIS have a significant impact on network performance. Therefore, a further question is: for large-scale RIS-aided networks, whether fewer large RISs or more small RISs should be deployed for higher network coverage.

2.4 Modelling of RIS-aided Networks Using Stochastic Geometry

Different from traditional BS-UE transmission where only the distance between BS and UE needs to be considered, three factors need to be considered for RIS-aided transmission, i.e., the distance between BS and UE, the distance between RIS and UE, and the distance between BS and RIS. Considering random locations of RISs, high complexity is introduced into the model. Meanwhile, the spatial locations of RISs significantly influence the network performance. Previous works have shown that the received signal power is the highest when

a RIS is close to either the transmitter or receiver [3]. To further investigate the impact of random spatial locations of multiple RISs on network performance, network modelling based on stochastic geometry needs to be studied. In this section, the network models of existing works using stochastic geometry are reviewed.

2.4.1 RIS-aided Networks without Blockage

The single-cell multi-RIS system has been investigated in [27] and [28]. In [27], the locations of RISs follow a PPP within a circle centered at the UE, and the distance between the BS and UE is fixed. Specifically, the work studied the scenario that the distance between the BS and UE is much longer than the distance between the UE and RISs, so that it assumed that the distances from the BS to the UE and to the RISs are approximately the same. In addition, the direct transmission between the BS and UE is assumed to be blocked. Outage probability and energy efficiency were derived and evaluated. In [28], a given number of UEs are randomly distributed in a circle with radius R_c and centered at the BS, and a given number of RISs are randomly deployed in a circular ring with inner radius R_{in} , outer radius R_{out} and centered at the BS, where $R_{in} < R_{out} < R_c$. Each UE is served by its closest RIS if the distance between the UE and the RIS is shorter than D , where D is the RIS coverage range within which the ratio of the average channel power gain of RIS transmission and that of direct transmission is higher than a threshold. If UEs are located outside the coverage range of any RIS, then they are served by the BS only. The spatial throughput of the RIS-aided network was calculated based on numerical integrals.

Except for the works about single-cell RIS-aided systems, the work in [29] studied the multi-cell RIS-aided system where BSs and RISs are distributed based on two independent PPPs. The work assumed that RIS-aided transmission happens when the distance r_2 between the UE and the RIS is shorter than the distance r_0 between the UE and the BS. Meanwhile, the UE can choose either the direct transmission from the BS or the RIS-aided transmission. Interference from BSs was considered while reflected interference from RISs was ignored. The signal-to-interference ratio (SIR) coverage probability of the RIS-aided transmission

was approximated by assuming $r_2 = \rho r_0$, where ρ is a proportion decided by the density of BSs and RISs, and the approximation was calculated based on numerical integral.

Different from the above works, interference induced by reflecting the signals from interference BSs has been studied in [81]. The work evaluated the coverage probability of the RIS-aided two-UE non-orthogonal multiple access (NOMA) system where one UE is served by both direct transmission and RIS-aided transmission and the other UE is served by the BS only. BSs and UEs were distributed according to two independent PPPs. UEs are associated with the BS which is closest to the RIS for the highest average received signal power. The distance between the UE and the RIS is fixed and is assumed to be much shorter than the distance between any BSs and the UE, thereby, the distances from any BSs to the UE and to the RIS are regarded as the same. Only the interference from a portion interference BSs can be reflected by the RIS because the RIS only reflects the signals when the UE and the BSs are on the same side of the surface. The portion of interference BSs is decided by a fixed coefficient ρ_1 . The Laplace transform of interference was derived, moreover, the coverage probability was derived and evaluated.

Different from the work in [81] which considered the reflected signal and interference from the associated RIS only, the work in [82] considered the reflected signal and interference from all the RISs within a certain range D_2 of the UE. The locations of RISs follow a PPP. In addition, the same definition of RIS coverage range in [28] was also adopted. With given locations of the serving BS and RIS, the distributions of signal and interference power were approximated by assuming the distances from a BS to a RIS and to the UE are equal and adopting the Gamma distribution. Moreover, the coverage probability and spatial throughput of the multi-cell RIS-aided networks were presented and evaluated. However, the work did not consider one of the most promising scenarios for RIS application, i.e., the direct transmission from the serving BS is blocked. Therefore, in [83], UEs were divided into two groups, i.e., direct UEs and RIS-aided UEs, based on a given proportion. For the RIS-aided transmission, the UE associates with the closest RIS and the associated RIS associates with the closest BS. The received signal power of the RIS-aided UE was approximated as a summation of scaled generalized gamma random variables. Meanwhile, the upper

bound of the aggregate interference from RISs was considered by assuming that the reflected interference from each passive element of RISs is aligned in phase at the receiver, and was approximated as the summation of normal random variables. Furthermore, the overall coverage probability and ergodic capacity were derived.

2.4.2 RIS-aided Networks with Blockage Model

It is important to study the blockage effect on the performance of the RIS-aided networks since one of the most promising applications for RIS is to provide indirect LoS transmission when the direct transmission from the BS is blocked. Accordingly, the same research group in [81] further studied the RIS-aided two-UE NOMA system by inducing the LoS ball model in [84] and [85]. The RIS was assumed to be randomly distributed within the LoS ball and all the BSs were distributed outside the LoS ball. Meanwhile, the transmissions between the RIS and BSs were assumed to be LoS. Therefore, any direct transmission from BSs to the UE is always blocked and thereby ignored in this work, and the RIS-aided transmissions are always LoS. Another major difference from the previous work [81] is that the effect of the incident angle and reflected angle of the signal at the RIS is considered into the path loss model. The coverage probability was evaluated in [84] and the ergodic rate was evaluated in [85].

A random blockage model has been adopted in the performance analysis of RIS-aided networks. In the following works, blockages were modelled as 2D lines with random orientations and fixed/random lengths. The centers of the blockages were distributed as a PPP. In [86], with a given pair of BS and UE, the probability that the location and orientation of a RIS allow the RIS to reflect the desired signal was derived. Furthermore, in [30], [87] and [88], a portion $\kappa \in [0, 1]$ of the blockages were deployed with a RIS on one of the sides. The LoS probabilities of both the direct transmission and the RIS-aided transmission were considered by adopting equation (2.1). A single-cell RIS-aided system was studied in [30]. With a given distance between the BS and the UE, the outage probabilities of the RIS-aided networks under three different RIS association strategies, i.e., a random RIS, the closest RIS, and K random RISs, were provided based on numerical integrals. A multi-cell RIS-aided

system was investigated in [87] and [88]. In [87], the locations of BSs follow a PPP and each BS has an associated UE which locates at a distance R . The SIR coverage probability considering the interference from both direct transmission and reflective transmission was calculated based on numerical integrals. In [88], the locations of BSs and UEs follow two independent PPPs. UEs associate with the BS which provides the highest average received signal power through either the direct or RIS-aided transmission. Meanwhile, RIS-aided transmission was only adopted when the direct transmission is blocked. The probability that a UE associates with a BS through RIS-aided transmission was derived. Moreover, the probability distribution of the path loss from the serving BS to the UE was derived. Finally, the coverage probability, defined as the probability that the path loss from the serving BS is below a threshold, was derived. However, the probability distribution of the path loss only applies to the near-field path loss model of RIS-aided transmission while the far-field path loss model was not studied in this work. In [31] and [32], BSs and UEs were distributed according to two independent PPPs. The location and orientation of buildings were randomly distributed. In addition, a subset of blockages were equipped with RISs. In [31], direct interferences from BSs were considered, and in [32], both direct interferences from BSs and reflected interferences from RISs were considered. Both works derived coverage probability based on numerical integrals.

Since the publication of our works in Paper I, several more studies have investigated indoor RIS-aided networks. The work in [89] analyzed indoor mmWave coverage enhancement of a RIS deployment strategy considering the mobility of human blockages. An outage probability minimization algorithm was proposed. In [90], the locations and orientations of RISs were optimized to maximize the coverage of indoor mmWave RIS-aided networks. Obstacles in indoor scenarios were considered. A coverage probability optimization algorithm based on gradient descent was proposed.

An O2I single-cell RIS-aided system was investigated in [33]. A RIS was assumed to be deployed in the building envelope to guide the signal from the outdoor BS to the indoor UE. Both static blockages and dynamic blockages were considered. Static blockages were modelled based on the work in [36], which have random length, width and orientation, and

the locations of the static blockages follow a PPP. Static blockages were assumed to locate in both indoor and outdoor environments. In addition, dynamic blockages were modelled based on queueing theory and assumed to be located in an indoor environment only. Finally, the SNR coverage probability was derived and evaluated. However, the spatial correlation of blockages was not considered in the work. Therefore, the coverage probability might be overestimated.

Summary

In this section, the RIS-aided network modelling based on stochastic geometry has been reviewed. Because of the random distances between RISs and BSs/UEs, high complexity is introduced into the network model. Some research works simplified the model by only considering specific scenarios, e.g., the scenario in which the RISs are much closer to the UE than the BS, and thereby assuming that the distances from the BS to the UE and to the RIS are the same. Therefore, the randomness in transmission distances is reduced. Other research works derived the performance matrices, e.g., coverage probability, using multiple numerical integrals, which only provided limited insights into the interplay among network parameters. To demonstrate the tradeoff/interplay among different network parameters, tractable analytical (closed-form) approaches for RIS-aided network coverage based on novel methods need to be proposed.

Chapter 3

Conclusion and Future Work

3.1 Conclusion

In this thesis, the coverage performance of RIS-aided networks in indoor, outdoor and O2I scenarios under blockage effect have been investigated to provide guidelines for the network deployment in reality.

In indoor RIS-aided networks, the coverage performance has been compared with UDSC networks. A coverage area calculation algorithm has been proposed and verified by Monte Carlo simulations. The results showed that different network deployment strategies, i.e., UDSC networks, RIS-aided networks with fewer BSs and more RISs or with more BSs and fewer RISs, can achieve the same coverage probability, and RIS-aided networks with an appropriate number of BSs are more cost-effective to achieve an adequate coverage probability than UDSC networks. On the other hand, since RIS is only a passive array, a minimal number of BSs are essential to achieve a high coverage probability, e.g., above 80%, for a RIS-aided network.

In outdoor RIS-aided networks, the RIS deployment strategy for a given total number of passive elements has been investigated. The analytical upper and lower bounds of coverage probability have been derived and matched with the trend of simulation results closely. Meanwhile, the coverage probability when RISs are much closer to UE than BS has been derived in closed form and verified. The analytical results showed the interplay/tradeoff

amongst the factors such as RIS density, blockage density, SNR threshold and other network parameters. In terms of coverage enhancement, sparsely deployed large-scale RISs lead to a higher coverage probability than densely deployed small-scale RISs for low blockage density and/or long transmission distance, e.g., rural area, while densely deployed small-scale RISs are a better choice for a high blockage density and/or short transmission distance, e.g., urban area. The reason is that sparsely deployed large-scale RISs provide higher compensation for path loss while densely deployed small-scale RISs increase LoS probability. Accordingly, densely deployed small-scale RISs are more suitable for the networks with low SNR threshold and higher blockage density. Meanwhile, in the same cell of a BS, small-scale RISs are preferable to be deployed around the cell center to decrease blockage probability, while large-scale RISs are preferable to be deployed in the cell edge to decrease blockage probability and compensate for path loss.

In O2I RIS-aided networks, the network coverage considering the spatial correlation of blockages has been evaluated. Given the location of the UE, the closed-form approximation of the coverage probability has been derived and verified. Furthermore, the average coverage probability is that the average value of the coverage probabilities in all the considered locations (the whole room in this case). Moreover, the impact of blockage density, room size, the number and locations of RISs on the average coverage probability has been analyzed. Numerical results considered the scenarios in which 1) the distance between any two adjacent RISs is the same; 2) all the RISs are located in a line on the RIS-deployment building envelope (exterior building wall where transmissive RISs are deployed). The results have revealed that the highest coverage enhancement caused by four small-scale RISs with appropriate locations reaches 69.5% higher compared with a large-scale RIS located at the center of the building envelope. Meanwhile, for the same room area, the room with a longer building envelope has a higher average RIS coverage probability. In addition, the optimal distance between any two adjacent RISs decreases as the blockage density rises when the number of RISs is relatively low, e.g., 2 deployed RISs, while the optimal distance between any two adjacent RISs increases as the blockage density rises when the number of RISs is relatively high, e.g., 3 or 4 deployed RISs.

3.2 Future Work

Future research directions are summarized as follows:

- Recent research [91], [92] and [93] have shown that building structures have a huge impact on wireless network performance and should be considered in the design stage. In Paper I, the results showed that indoor layouts have a significant influence on the cost effectiveness of RIS-aided networks, for example, compared with rooms separated from other rooms by walls, rooms connected with other rooms through entrances are better for RISs to reflect the signals from one room to the other. Hence, in terms of coverage enhancement, wireless performance evaluation of buildings equipped with RIS-aided networks is worth investigating in future work.
- In RIS-aided networks, besides signals from the serving BS, inter-user interference and inter-cell interference can also be reflected to the UE. However, the modelling of reflected interference has been either ignored or over-simplified in existing works. To evaluate the impact of reflected interference on network performance, large-scale RIS-aided networks considering both direct interferences from BSs and reflected interference from RISs need to be investigated. In addition, the interference-suppressing application of RISs can be analyzed in future work.
- In reality, BS locations, RIS locations and blockage locations are correlated. To our best knowledge, this correlation has never been considered in existing works. Additional design guidelines for RIS-aided network deployment might be obtained by incorporating this correlation into RIS-aided network performance analysis.
- Paper II and Paper III have indicated that RIS deployment strategy has a significant impact on network performance. However, RIS deployment optimization is very complicated and needs to consider a large number of factors, e.g., RIS locations, RIS sizes and RIS density. Meanwhile, the application of machine learning on complex wireless network optimization problems has drawn increasing attention. Therefore, RIS deployment optimization based on machine learning is a promising research direction.

References

- [1] S. A. Busari, S. Mumtaz, S. Al-Rubaye, and J. Rodriguez, “5G millimeter-wave mobile broadband: Performance and challenges,” *IEEE Commun. Mag.*, vol. 56, no. 6, pp. 137–143, Jun. 2018.
- [2] T. Baykas, C.-S. Sum, Z. Lan, J. Wang, M. A. Rahman, H. Harada, and S. Kato, “IEEE 802.15.3c: the first IEEE wireless standard for data rates over 1 gb/s,” *IEEE Commun. Mag.*, vol. 49, no. 7, pp. 114–121, Jul. 2011.
- [3] “IEEE standard for wireless MAN-advanced air interface for broadband wireless access systems,” 2012.
- [4] “IEEE standard—part 11: Wireless LAN MAC and PHY specifications amendment 3: Enhancements for very high throughput in the 60 ghz band,” 2012.
- [5] T. S. Rappaport, S. Sun, R. Mayzus, H. Zhao, Y. Azar, K. Wang, G. N. Wong, J. K. Schulz, M. Samimi, and F. Gutierrez, “Millimeter wave mobile communications for 5G cellular: It will work!” *IEEE Access*, vol. 1, pp. 335–349, May 2013.
- [6] I. Hwang, B. Song, and S. S. Soliman, “A holistic view on hyper-dense heterogeneous and small cell networks,” *IEEE Commun. Mag.*, vol. 51, no. 6, pp. 20–27, Jun. 2013.
- [7] D. López-Pérez, M. Ding, H. Claussen, and A. H. Jafari, “Towards 1 gbps/ue in cellular systems: Understanding ultra-dense small cell deployments,” *IEEE Commun. Surv. Tutor.*, vol. 17, no. 4, pp. 2078–2101, Jun. 2015.

- [8] M. Ding, P. Wang, D. López-Pérez, G. Mao, and Z. Lin, “Performance impact of LoS and NLoS transmissions in dense cellular networks,” *IEEE Trans. Wirel. Commun.*, vol. 15, no. 3, pp. 2365–2380, Mar. 2016.
- [9] Q. Wu and R. Zhang, “Towards smart and reconfigurable environment: Intelligent reflecting surface aided wireless network,” *IEEE Commun. Mag.*, vol. 58, no. 1, pp. 106–112, Jan. 2020.
- [10] M. Di Renzo, A. Zappone, M. Debbah, M.-S. Alouini, C. Yuen, J. de Rosny, and S. Tretyakov, “Smart radio environments empowered by reconfigurable intelligent surfaces: How it works, state of research, and the road ahead,” *IEEE J. Sel. Areas Commun.*, vol. 38, no. 11, pp. 2450–2525, Nov. 2020.
- [11] V. Arun and H. Balakrishnan, “RFocus: Beamforming using thousands of passive antennas,” in *17th USENIX Symposium on Networked Systems Design and Implementation (NSDI 20)*. Santa Clara, CA: USENIX Association, Feb. 2020, pp. 1047–1061.
- [12] N. DOCOMO, “Press releases: Docomo conducts world’s first successful trial of transparent dynamic metasurface.” [Online]. Available: https://www.docomo.ne.jp/english/info/media_center/pr/2020/0117_00.html
- [13] Q. Wu, S. Zhang, B. Zheng, C. You, and R. Zhang, “Intelligent reflecting surface-aided wireless communications: A tutorial,” *IEEE Trans. Commun.*, vol. 69, no. 5, pp. 3313–3351, May 2021.
- [14] C. Huang, A. Zappone, G. C. Alexandropoulos, M. Debbah, and C. Yuen, “Reconfigurable intelligent surfaces for energy efficiency in wireless communication,” *IEEE Trans. Wirel. Commun.*, vol. 18, no. 8, pp. 4157–4170, Aug. 2019.
- [15] S. Zeng, H. Zhang, B. Di, Y. Tan, Z. Han, H. V. Poor, and L. Song, “Reconfigurable intelligent surfaces in 6G: Reflective, transmissive, or both?” *IEEE Commun. Lett.*, vol. 25, no. 6, pp. 2063–2067, Jun. 2021.

-
- [16] H. Du, J. Zhang, J. Cheng, and B. Ai, "Millimeter wave communications with reconfigurable intelligent surfaces: Performance analysis and optimization," *IEEE Trans. Commun.*, vol. 69, no. 4, pp. 2752–2768, Apr. 2021.
- [17] C. Pradhan, A. Li, L. Song, B. Vucetic, and Y. Li, "Hybrid precoding design for reconfigurable intelligent surface aided mmwave communication systems," *IEEE Wireless Commun. Lett.*, vol. 9, no. 7, pp. 1041–1045, Jul. 2020.
- [18] E. Basar, M. Di Renzo, J. De Rosny, M. Debbah, M.-S. Alouini, and R. Zhang, "Wireless communications through reconfigurable intelligent surfaces," *IEEE Access*, vol. 7, pp. 116 753–116 773, Aug. 2019.
- [19] Özdogan, E. Björnson, and E. G. Larsson, "Intelligent reflecting surfaces: Physics, propagation, and pathloss modeling," *IEEE Wireless Commun. Lett.*, vol. 9, no. 5, pp. 581–585, May 2020.
- [20] E. Björnson, Özdogan, and E. G. Larsson, "Intelligent reflecting surface versus decode-and-forward: How large surfaces are needed to beat relaying?" *IEEE Wireless Commun. Lett.*, vol. 9, no. 2, pp. 244–248, Feb. 2020.
- [21] W. Tang, M. Z. Chen, X. Chen, J. Y. Dai, Y. Han, M. Di Renzo, Y. Zeng, S. Jin, Q. Cheng, and T. J. Cui, "Wireless communications with reconfigurable intelligent surface: Path loss modeling and experimental measurement," *IEEE Trans. Wirel. Commun.*, vol. 20, no. 1, pp. 421–439, Sep. 2021.
- [22] E. Björnson, Özdogan, and E. G. Larsson, "Reconfigurable intelligent surfaces: Three myths and two critical questions," *IEEE Commun. Mag.*, vol. 58, no. 12, pp. 90–96, Dec. 2020.
- [23] C. Bouras, V. Kokkinos, and A. Papazois, "Financing and pricing small cells in next-generation mobile networks," *Wired/Wireless Internet Communications*, pp. 41–54, 2014.

- [24] J. Liu, M. Sheng, L. Liu, and J. Li, "Effect of densification on cellular network performance with bounded pathloss model," *IEEE Commun. Lett.*, vol. 21, no. 2, pp. 346–349, Feb. 2017.
- [25] X. Yu, J. Zhang, M. Haenggi, and K. B. Letaief, "Coverage analysis for millimeter wave networks: The impact of directional antenna arrays," *IEEE J. Sel. Areas Commun.*, vol. 35, no. 7, pp. 1498–1512, Jul. 2017.
- [26] J. G. Andrews, T. Bai, M. N. Kulkarni, A. Alkhateeb, A. K. Gupta, and R. W. Heath, "Modeling and analyzing millimeter wave cellular systems," *IEEE Trans. Commun.*, vol. 65, no. 1, pp. 403–430, Jan. 2017.
- [27] J. Ye, A. Kammoun, and M.-S. Alouini, "Spatially-distributed RISs vs relay-assisted systems: A fair comparison," *IEEE open j. Commun. Soc.*, vol. 2, pp. 799–817, Feb. 2021.
- [28] J. Lyu and R. Zhang, "Spatial throughput characterization for intelligent reflecting surface aided multiuser system," *IEEE Wireless Commun. Lett.*, vol. 9, no. 6, pp. 834–838, Feb. 2020.
- [29] M. Nemati, J. Park, and J. Choi, "RIS-assisted coverage enhancement in millimeter-wave cellular networks," *IEEE Access*, vol. 8, pp. 188 171–188 185, Oct. 2020.
- [30] C. Psomas, H. A. Suraweera, and I. Krikidis, "On the association with intelligent reflecting surfaces in spatially random networks," in *Proc. IEEE Int. Conf. Commun. (ICC)*, Montreal, QC, Canada, 2021, pp. 1–6.
- [31] S. Bagherinejad, M. Bayanifar, M. Sattari Maleki, and B. Maham, "Coverage probability of RIS-assisted mmwave cellular networks under blockages: A stochastic geometric approach," *Physical Communication*, vol. 53, p. 101740, 2022.
- [32] L. Yang, X. Li, S. Jin, M. Matthaiou, and F.-C. Zheng, "Fine-grained analysis of reconfigurable intelligent surface-assisted mmwave networks," *IEEE Trans. Commun.*, vol. 70, no. 9, pp. 6277–6294, Sep. 2022.

- [33] M. Nemati, B. Maham, S. R. Pokhrel, and J. Choi, "Modeling RIS empowered outdoor-to-indoor communication in mmwave cellular networks," *IEEE Trans. Commun.*, vol. 69, no. 11, pp. 7837–7850, Aug. 2021.
- [34] J. G. Andrews, F. Baccelli, and R. K. Ganti, "A tractable approach to coverage and rate in cellular networks," *IEEE Trans. Commun.*, vol. 59, no. 11, pp. 3122–3134, Nov. 2011.
- [35] T. Bai and R. W. Heath, "Coverage and rate analysis for millimeter-wave cellular networks," *IEEE Trans. Wirel. Commun.*, vol. 14, no. 2, pp. 1100–1114, Feb. 2015.
- [36] T. Bai, R. Vaze, and R. W. Heath, "Analysis of blockage effects on urban cellular networks," *IEEE Trans. Wirel. Commun.*, vol. 13, no. 9, pp. 5070–5083, Jun. 2014.
- [37] A. K. Gupta, J. G. Andrews, and R. W. Heath, "Macrodiversity in cellular networks with random blockages," *IEEE Trans. Wirel. Commun.*, vol. 17, no. 2, pp. 996–1010, Feb. 2018.
- [38] M. Gapeyenko, A. Samuylov, M. Gerasimenko, D. Moltchanov, S. Singh, E. Aryafar, S.-p. Yeh, N. Himayat, S. Andreev, and Y. Koucheryavy, "Analysis of human-body blockage in urban millimeter-wave cellular communications," in *2016 IEEE Int. Conf. Commun. (ICC)*, Kuala Lumpur, Malaysia, 2016, pp. 1–7.
- [39] M. Gapeyenko, A. Samuylov, M. Gerasimenko, D. Moltchanov, S. Singh, M. R. Akdeniz, E. Aryafar, S. Andreev, N. Himayat, and Y. Koucheryavy, "Spatially-consistent human body blockage modeling: A state generation procedure," *IEEE Trans. Mob. Comput.*, vol. 19, no. 9, pp. 2221–2233, Sep. 2020.
- [40] M. K. Müller, M. Taranetz, and M. Rupp, "Analyzing wireless indoor communications by blockage models," *IEEE Access*, vol. 5, pp. 2172–2186, Dec. 2017.
- [41] W. Yang, J. Zhang, and J. Zhang, "On evaluation of indoor to outdoor communications using neighbourhood small cells," *IEEE Trans. Veh. Technol.*, vol. 69, no. 7, pp. 8045–8050, Jul. 2020.

- [42] J. Lee, X. Zhang, and F. Baccelli, “A 3-D spatial model for in-building wireless networks with correlated shadowing,” *IEEE Trans. Wirel. Commun.*, vol. 15, no. 11, pp. 7778–7793, Nov. 2016.
- [43] C. Chen, Y. Zhang, J. Zhang, X. Chu, and J. Zhang, “On the performance of indoor multi-story small-cell networks,” *IEEE Trans. Wirel. Commun.*, vol. 20, no. 2, pp. 1336–1348, Feb. 2021.
- [44] T. Bai and R. W. Heath, “Analysis of self-body blocking effects in millimeter wave cellular networks,” in *Proc. 48th Asilomar Conf. Signals Syst. Comput.*, Pacific Grove, CA, USA, 2014, pp. 1921–1925.
- [45] M. Di Renzo, “Stochastic geometry modeling and analysis of multi-tier millimeter wave cellular networks,” *IEEE Trans. Wirel. Commun.*, vol. 14, no. 9, pp. 5038–5057, Sep. 2015.
- [46] Y. Li, J. G. Andrews, F. Baccelli, T. D. Novlan, and C. J. Zhang, “Design and analysis of initial access in millimeter wave cellular networks,” *IEEE Trans. Wirel. Commun.*, vol. 16, no. 10, pp. 6409–6425, Oct. 2017.
- [47] A. K. Gupta, J. G. Andrews, and R. W. Heath, “On the feasibility of sharing spectrum licenses in mmwave cellular systems,” *IEEE Trans. Commun.*, vol. 64, no. 9, pp. 3981–3995, Sep. 2016.
- [48] J. Kim, J. Park, S. Kim, S.-L. Kim, K. W. Sung, and K. S. Kim, “Millimeter-wave interference avoidance via building-aware associations,” *IEEE Access*, vol. 6, pp. 10 618–10 634, Feb. 2018.
- [49] D. Maamari, N. Devroye, and D. Tuninetti, “Coverage in mmwave cellular networks with base station co-operation,” *IEEE Trans. Wirel. Commun.*, vol. 15, no. 4, pp. 2981–2994, Apr. 2016.

-
- [50] J. Park, S.-L. Kim, and J. Zander, "Tractable resource management with uplink decoupled millimeter-wave overlay in ultra-dense cellular networks," *IEEE Trans. Wirel. Commun.*, vol. 15, no. 6, pp. 4362–4379, Jun. 2016.
- [51] H.-M. Wang, K.-W. Huang, and T. A. Tsiftsis, "Base station cooperation in millimeter wave cellular networks: Performance enhancement of cell-edge users," *IEEE Trans. Commun.*, vol. 66, no. 11, pp. 5124–5139, Nov. 2018.
- [52] E. Björnson, J. Hoydis, and L. Sanguinetti, "Massive mimo networks: Spectral, energy, and hardware efficiency," *Found. Trends Signal Process.*, 2017.
- [53] E. Björnson and L. Sanguinetti, "Rayleigh fading modeling and channel hardening for reconfigurable intelligent surfaces," *IEEE Wireless Commun. Lett.*, vol. 10, no. 4, pp. 830–834, Apr. 2021.
- [54] H. Shokri-Ghadikolaei and C. Fischione, "The transitional behavior of interference in millimeter wave networks and its impact on medium access control," *IEEE Trans. Commun.*, vol. 64, no. 2, pp. 723–740, Feb. 2016.
- [55] L. Yang, Y. Yang, M. O. Hasna, and M.-S. Alouini, "Coverage, probability of SNR gain, and DOR analysis of RIS-aided communication systems," *IEEE Wireless Commun. Lett.*, vol. 9, no. 8, pp. 1268–1272, Aug. 2020.
- [56] Q. Tao, J. Wang, and C. Zhong, "Performance analysis of intelligent reflecting surface aided communication systems," *IEEE Commun. Lett.*, vol. 24, no. 11, pp. 2464–2468, Nov. 2020.
- [57] L. Yang, F. Meng, Q. Wu, D. B. da Costa, and M.-S. Alouini, "Accurate closed-form approximations to channel distributions of RIS-aided wireless systems," *IEEE Wireless Commun. Lett.*, vol. 9, no. 11, pp. 1985–1989, Nov. 2020.
- [58] Z. Cui, K. Guan, J. Zhang, and Z. Zhong, "SNR coverage probability analysis of RIS-aided communication systems," *IEEE Trans. Veh. Technol.*, vol. 70, no. 4, pp. 3914–3919, Apr. 2021.

- [59] A. M. Salhab and M. H. Samuh, “Accurate performance analysis of reconfigurable intelligent surfaces over rician fading channels,” *IEEE Wireless Commun. Lett.*, vol. 10, no. 5, pp. 1051–1055, May 2021.
- [60] A. Bhowal and S. Aissa, “RIS-aided communications in indoor and outdoor environments: Performance analysis with a realistic channel model,” *IEEE Trans. Veh. Technol.*, vol. early access, pp. 1–1, Jan. 2022.
- [61] A.-A. A. Boulogeorgos and A. Alexiou, “Performance analysis of reconfigurable intelligent surface-assisted wireless systems and comparison with relaying,” *IEEE Access*, vol. 8, pp. 94 463–94 483, Jun. 2020.
- [62] H. Zhang, B. Di, L. Song, and Z. Han, “Reconfigurable intelligent surfaces assisted communications with limited phase shifts: How many phase shifts are enough?” *IEEE Trans. Veh. Technol.*, vol. 69, no. 4, pp. 4498–4502, Apr. 2020.
- [63] P. Xu, G. Chen, Z. Yang, and M. D. Renzo, “Reconfigurable intelligent surfaces-assisted communications with discrete phase shifts: How many quantization levels are required to achieve full diversity?” *IEEE Wireless Commun. Lett.*, vol. 10, no. 2, pp. 358–362, Feb. 2021.
- [64] Y. Zhang, J. Zhang, M. D. Renzo, H. Xiao, and B. Ai, “Performance analysis of RIS-aided systems with practical phase shift and amplitude response,” *IEEE Trans. Veh. Technol.*, vol. 70, no. 5, pp. 4501–4511, May 2021.
- [65] M.-A. Badiu and J. P. Coon, “Communication through a large reflecting surface with phase errors,” *IEEE Wireless Commun. Lett.*, vol. 9, no. 2, pp. 184–188, Feb. 2020.
- [66] D. Li, “Ergodic capacity of intelligent reflecting surface-assisted communication systems with phase errors,” *IEEE Commun. Lett.*, vol. 24, no. 8, pp. 1646–1650, Aug. 2020.

- [67] R. C. Ferreira, M. S. P. Facina, F. A. P. De Figueiredo, G. Fraidenraich, and E. R. De Lima, "Bit error probability for large intelligent surfaces under double-nakagami fading channels," *IEEE Open J. Commun. Soc.*, vol. 1, pp. 750–759, Jun. 2020.
- [68] T. Wang, M.-A. Badiu, G. Chen, and J. P. Coon, "Outage probability analysis of RIS-assisted wireless networks with von mises phase errors," *IEEE Wireless Commun. Lett.*, vol. 10, no. 12, pp. 2737–2741, Dec. 2021.
- [69] R. Hashemi, S. Ali, N. H. Mahmood, and M. Latva-aho, "Average rate and error probability analysis in short packet communications over RIS-aided URLLC systems," *IEEE Trans. Veh. Technol.*, vol. 70, no. 10, pp. 10 320–10 334, Oct. 2021.
- [70] P. Xu, W. Niu, G. Chen, Y. Li, and Y. Li, "Performance analysis of RIS-assisted systems with statistical channel state information," *IEEE Trans. Veh. Technol.*, vol. 71, no. 1, pp. 1089–1094, Jan. 2022.
- [71] T. Van Chien, A. Papazafeiropoulos, L. T. Tu, R. Chopra, S. Chatzinotas, and B. Ottersten, "Outage probability analysis of IRS-assisted systems under spatially correlated channels," *IEEE Wireless Commun. Lett.*, vol. 10, no. 8, pp. 1815–1819, Aug. 2021.
- [72] A. Papazafeiropoulos, C. Pan, A. Elbir, P. Kourtessis, S. Chatzinotas, and J. M. Senior, "Coverage probability of distributed irts systems under spatially correlated channels," *IEEE Wireless Commun. Lett.*, vol. 10, no. 8, pp. 1722–1726, Aug. 2021.
- [73] A. P. Ajayan, S. P. Dash, and B. Ramkumar, "Performance analysis of an IRS-aided wireless communication system with spatially correlated channels," *IEEE Wireless Commun. Lett.*, vol. 11, no. 3, pp. 563–567, Mar. 2022.
- [74] L. Yang, Y. Yang, D. B. d. Costa, and I. Trigui, "Outage probability and capacity scaling law of multiple RIS-aided networks," *IEEE Wireless Commun. Lett.*, vol. 10, no. 2, pp. 256–260, Feb. 2021.

- [75] I. Yildirim, A. Uyrus, and E. Basar, "Modeling and analysis of reconfigurable intelligent surfaces for indoor and outdoor applications in future wireless networks," *IEEE Trans. Commun.*, vol. 69, no. 2, pp. 1290–1301, Feb. 2021.
- [76] T. N. Do, G. Kaddoum, T. L. Nguyen, D. B. da Costa, and Z. J. Haas, "Multi-RIS-aided wireless systems: Statistical characterization and performance analysis," *IEEE Trans. Commun.*, vol. 69, no. 12, pp. 8641–8658, Dec. 2021.
- [77] L. Yang, P. Li, Y. Yang, S. Li, I. Trigui, and R. Ma, "Performance analysis of RIS-aided networks with co-channel interference," *IEEE Commun. Lett.*, vol. 26, no. 1, pp. 49–53, Jan. 2022.
- [78] S. Zhang and R. Zhang, "Intelligent reflecting surface aided multi-user communication: Capacity region and deployment strategy," *IEEE Trans. Commun.*, vol. 69, no. 9, pp. 5790–5806, Sep. 2021.
- [79] Y. Zhang, J. Zhang, M. Di Renzo, H. Xiao, and B. Ai, "Reconfigurable intelligent surfaces with outdated channel state information: Centralized vs. distributed deployments," *IEEE Trans. Commun.*, vol. 70, no. 4, pp. 2742–2756, Apr. 2022.
- [80] I. Yildirim, A. Uyrus, and E. Basar, "Modeling and analysis of reconfigurable intelligent surfaces for indoor and outdoor applications in future wireless networks," *IEEE Trans. Commun.*, vol. 69, no. 2, pp. 1290–1301, Feb. 2021.
- [81] C. Zhang, W. Yi, Y. Liu, and Q. Wang, "Multi-cell NOMA: Coherent reconfigurable intelligent surfaces model with stochastic geometry," in *Proc. IEEE Int. Conf. Commun. (ICC)*, Montreal, QC, Canada, 2021, pp. 1–6.
- [82] J. Lyu and R. Zhang, "Hybrid active/passive wireless network aided by intelligent reflecting surface: System modeling and performance analysis," *IEEE Trans. Wirel. Commun.*, vol. 20, no. 11, pp. 7196–7212, May 2021.

- [83] T. Shafique, H. Tabassum, and E. Hossain, “Stochastic geometry analysis of IRS-assisted downlink cellular networks,” *IEEE Trans. Commun.*, vol. 70, no. 2, pp. 1442–1456, Jan. 2022.
- [84] C. Zhang, W. Yi, Y. Liu, Z. Qin, and K. K. Chai, “Downlink analysis for reconfigurable intelligent surfaces aided NOMA networks,” in *Proc. IEEE Glob. Commun. Conf. (GLOBECOM)*, Taipei, Taiwan, 2020, pp. 1–6.
- [85] C. Zhang, W. Yi, Y. Liu, K. Yang, and Z. Ding, “Reconfigurable intelligent surfaces aided multi-cell NOMA networks: A stochastic geometry model,” *IEEE Trans. Commun.*, vol. 70, no. 2, pp. 951–966, Feb. 2022.
- [86] M. D. Renzo and J. Song, “Reflection probability in wireless networks with metasurface-coated environmental objects: An approach based on random spatial processes,” *EURASIP J. Wireless Commun. Netw.*, vol. 2019, no. 1, p. 99, Dec. 2019.
- [87] Y. Chen, B. Zhang, M. Ding, D. López-Pérez, and H. Zheng, “Performance analysis of wireless networks with intelligent reflecting surfaces,” in *IEEE Wirel. Commun. Netw. Conf. (WCNC)*, Nanjing, China, 2021, pp. 1–6.
- [88] M. A. Kishk and M.-S. Alouini, “Exploiting randomly located blockages for large-scale deployment of intelligent surfaces,” *IEEE J. Sel. Areas Commun.*, vol. 39, no. 4, pp. 1043–1056, Apr. 2021.
- [89] H. Qin, Z. Liu, and C. Yang, “Indoor mm-wave coverage enhancement: Reconfigurable intelligent surface deployment strategy based on human mobility model,” *IEEE Commun. Lett.*, vol. Early Access, Jul. 2022.
- [90] J. Zhang and D. M. Blough, “Optimizing coverage with intelligent surfaces for indoor mmwave networks,” in *IEEE INFOCOM 2022 - IEEE Conference on Computer Communications*, 2022, pp. 830–839.

- [91] J. Zhang, A. A. Glazunov, and J. Zhang, “Wireless energy efficiency evaluation for buildings under design based on analysis of interference gain,” *IEEE Trans. Veh. Technol.*, vol. 69, no. 6, pp. 6310–6324, Jun. 2020.
- [92] W. Yang, J. Zhang, H. Song, and J. Zhang, “Partition-based analytic evaluation of building wireless performance,” *IEEE Trans. Veh. Technol.*, vol. 70, no. 9, pp. 9036–9049, Sep. 2021.
- [93] J. Zhang, A. A. Glazunov, and J. Zhang, “Wireless performance evaluation of building layouts: Closed-form computation of figures of merit,” *IEEE Trans. Commun.*, vol. 69, no. 7, pp. 4890–4906, Jul. 2021.

Part II

Published Papers

Chapter 4

Paper I - Enhancing Indoor mmWave Wireless Coverage: Small-Cell Densification or Reconfigurable Intelligent Surfaces Deployment?

Zeyang Li, Haonan Hu, Jiliang Zhang and Jie Zhang.

This paper has been published in IEEE Wireless Communications Letters, Volume: 10, Number: 11, Pages: 2547-2551, Nov. 2021.

Enhancing Indoor mmWave Wireless Coverage: Small-Cell Densification or Reconfigurable Intelligent Surfaces Deployment?

Zeyang Li¹, Haonan Hu^{1,2}, Jiliang Zhang^{1,3}, Jie Zhang^{1,3}

¹ Department of Electronic and Electrical Engineering, the University of Sheffield, Sheffield, S10 2TN, UK

² Chongqing Key Laboratory of Mobile Communications Technology Engineering Research Center of Mobile Communications, the School of Communication and Information Engineering, Chongqing University of Posts and Telecommunications, Chongqing 400065

³ Ranplan Wireless Network Design Ltd., Cambridge, CB23 3UY, UK

Abstract

Both reconfigurable intelligent surfaces (RISs) and ultra-dense (UD) small-cell (SC) base stations (BSs) are investigated for indoor mmWave wireless coverage enhancement. To explore which deployment strategy is more cost-effective, the costs of deploying both RISs and UD SCs are defined and calculated. Through jointly analyzing coverage probability and network cost in typical indoor environments, we conclude that the same network coverage can be achieved by multiple deployment strategies. To achieve certain level of coverage probability with the lowest network cost, a proper number of BSs are crucial for RIS-assisted networks.

1 Introduction

It is predicted that wireless data traffic will rise by up to 1000 times in the next decade, with nearly 80% of data traffic consumed indoors [1, 2]. Meanwhile, due to the spectral resource shortage in microwave frequencies, millimeter-wave (mmWave) frequencies have been employed on wireless communication, which suffer severe wall penetration loss in indoor

environments [19, 4]. Both the rapidly growing data traffic demand and high wall penetration loss of mmWave bring great challenges to indoor mmWave network deployment. Fortunately, two promising technologies can address the problem: Ultra-dense (UD) small-cell (SC) and reconfigurable intelligent surfaces (RISs).

The basic idea of UD SC is to densely deploy small cells, i.e., fully-functioning base stations (BSs) (femtocells and picocells) and radio access points (Remote Radio Heads (RRHs)), to satisfy the immense traffic demand [5]. However, the small-cell density cannot grow infinitely due to fundamental limits of network densification [6]. The wireless coverage can be maximized by reaching certain cell density, and decrease with further increase of cell density [7, 8]. In [9], the indoor network coverage is analyzed based on Poisson grid blockage model. The indoor multi-story small-cell networks are investigated in [10]. The results in [9, 10] show that wall penetration loss has a great impact on indoor network coverage.

On the other hand, RIS is an alternative technology for indoor coverage enhancement. A RIS is a meta-surface with unit cells (integrated electronic circuits), each unit cell can implement phase shift and modify amplitude on the incident signal independently. RISs can provide additional transmission paths by altering reflected signal propagation [11]. The RIS deployment is particularly useful when the line-of-sight (LoS) transmission is blocked or not strong enough [12, 13]. This makes RIS an alternative technology for coverage enhancement. The work in [14] shows that the coverage probability of RIS-assisted wireless networks is higher compared with the networks without RISs. A closed-form expression of the outage probability for RIS-assisted networks with spatially correlated channels is derived in [15], the results show that the outage probability decreases significantly after considering the spatial correlation. In addition, achievable data rate and error performance of indoor and outdoor RIS-assisted wireless networks are investigated in [16] and shown great improvement.

Even though previous research has shown that both UD SC and RIS can enhance the network coverage, it remains unknown which technology is more efficient in terms of coverage enhancement. Moreover, whether combining both technologies will result in better coverage performance than only employing anyone of them has never been investigated.

This letter is the first to compare the performance of UD SC and RIS and to make the best use of both for cost-effective indoor coverage. We first define the cost of deploying UD SC BSs and RISs. Then, we present a joint analysis of coverage probability and network cost. Our main observations are that: 1) the same coverage probability can be achieved by different network deployment strategies, i.e., fewer BSs and more RISs, more BSs and fewer RISs, and only BSs; 2) to achieve certain level of coverage probability with the lowest network cost, a proper number of BSs are crucial; and 3) even with the assistance of RISs, a minimal number of BSs are required for high network coverage.

2 System Model

The system model of the wireless networks in the indoor environment is presented in this section. In this work, downlink network is considered while the system model also applies to the uplink network with few changes. To investigate general scenarios, both Poisson point process (PPP) [17] and Binomial point process (BPP) [18] are employed for BS distribution. The BS density is denoted by ψ_b . PPP is adopted for more general scenarios where a various number of BSs are deployed, and BPP is employed for the scenarios where a fixed number of BSs are deployed. The assumption that BS distribution follows PPP is also used in the existing works regarding indoor networks [10, 9]. The typical user equipment (UE) is randomly distributed in the indoor environment. The locations of RISs are assumed to follow one-dimensional PPP on the RIS-deployed walls, as shown in Fig. 4.1. The RIS density is ψ_r . The length of all the RIS-deployed walls in the considered indoor layout is expressed by ξ . On the other hand, no RIS is deployed on the non-RIS-deployed walls, since no coverage gain can be obtained by deploying RISs on these walls.

Two types of transmission, i.e., the direct transmission from the BS to the UE and the RIS-assisted transmission, are considered in this letter. In addition, Rician fading channel and Rayleigh fading channel are adopted for LoS transmission and NLoS transmission, respectively. The wavelength of the signal is denoted by λ and the path loss exponent is α . Let P_t and d denote the transmit power and the transmission distance, respectively.

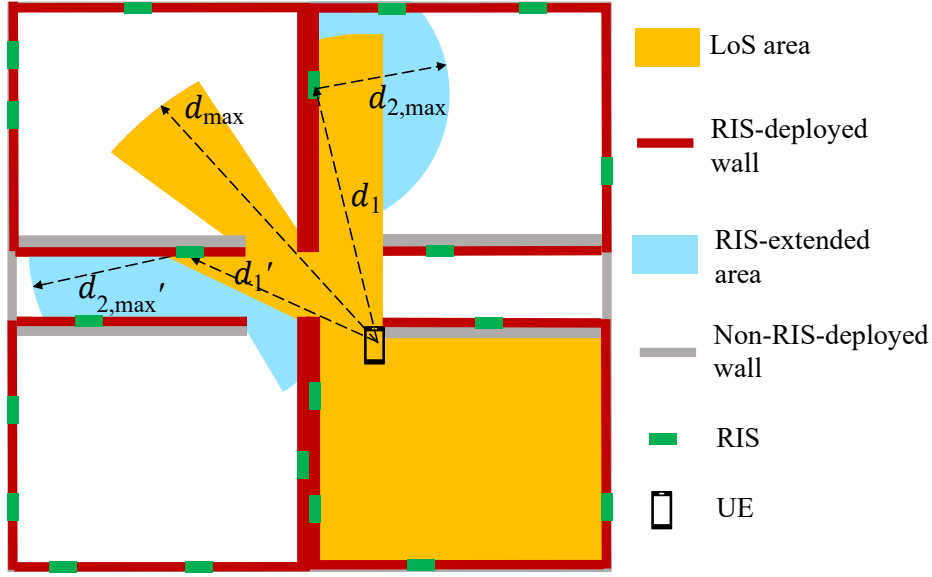


Fig. 4.1 The LoS area and RIS-extended area of a randomly located UE in the indoor environment. Note that the LoS area and RIS-extended area can be applied to both uplink and downlink networks. If any BSs locate in the LoS area or RIS-extended area, the UE is in coverage.

Furthermore, the received signal power of the direct transmission from the BS to the UE is as follows:

$$P_r = \begin{cases} \frac{P_t |h|^2 \lambda^2}{16\pi^2 d^\alpha}, & n_w = 0, \\ \frac{P_t \omega^{n_w} |g|^2 \lambda^2}{16\pi^2 d^\alpha}, & \text{otherwise,} \end{cases} \quad (1)$$

where ω denotes the wall penetration loss and n_w represents the number of passed walls. h and g follow Rician distribution and Rayleigh distribution, respectively.

The RIS-assisted transmission is adopted when the following two conditions are met: 1) the direct transmission from the BS to the UE suffers from severe wall penetration loss; 2) the transmission from the BS to the RIS and from the RIS to the UE is LoS transmission. To analyze the RIS-assisted transmission, the physical properties of the RIS must be considered. Each RIS is made of $M \times N$ unit cells, hence, the total number of unit cells per RIS is $\kappa = MN$. The size of each unit cell is $d_u \times d_u$. We assume that the power radiation pattern of RIS is independent of the incident/reflected angle of the signal and consider peak radiation in all the directions. All the unit cells have the same amplitude value A of the reflection coefficient but different phase shift [21]. By aligning in phase of the reflected signals from

the unit cells, the received signal power can be enhanced. In this letter, we investigate an upper bound of the RIS-assisted network coverage by assuming perfect phase shift control. Hardware imperfections [19, 20], e.g., discrete phase shifts and phase-dependent reflection coefficient amplitude, will be analyzed in the future works. Moreover, the received signal power of the RIS-assisted transmission is formulated as [16, 21]:

$$P_r = \frac{P_t G \left(\sum_{i=1}^K \phi_i \varphi_i \right)^2 d_u^2 \lambda^2 A^2}{64\pi^3 d_1^2 d_2^2}, \quad (2)$$

where G is the gain of the unit cell, ϕ_i and φ_i , which follow Rician distribution, represent the channel fading coefficient of the BS to the i th unit cell link and of the i th unit cell to the UE link, d_1 and d_2 denote the distance between the UE and the RIS, the distance between the BS and the RIS. We assume that walls cannot reflect signals unless RISs are deployed and signals can only be reflected one time.

3 Coverage Probability and Cost Analysis

To enhance the wireless coverage of the indoor mmWave networks, the two options are RIS deployment and SC densification. To investigate which option is more cost-effective, we define coverage probability and network cost for the RIS-assisted networks and UD SC networks.

3.1 Coverage Probability

The coverage probability is defined as the probability that the received signal power from at least one BS is higher than the power threshold T . T can be understood as the minimum received signal power that a receiver can detect. In other words, outage happens only when the signals from all the BSs are undetectable by the UE. Then, the coverage probability can be expressed as follows:

$$C = \Pr\{P_r \geq T\}. \quad (3)$$

Algorithm 1 The Coverage Probability Calculation Algorithm

```

1: Generate walls according to the considered indoor layout;
2: for Different BS density  $\psi_b$  do
3:   for Different RIS density  $\psi_r$  do
4:     Let  $\chi = 0$ ;
5:     for  $i = 1 : \eta$  do
6:       Generate a randomly distributed UE in the considered indoor layout;
7:       Generate randomly distributed BSs with BS density  $\psi_b$  in the considered indoor layout;
8:       Generate randomly distributed RISs with RIS density  $\psi_r$  on the RIS-deployed walls;
9:       Calculate the received signal power from each BS using equation (1) or (2);
10:      if the received signal power from at least one BS satisfy  $P_r \geq T$  then
11:         $\chi = \chi + 1$ ;
12:      end if
13:    end for
14:    The coverage probability  $C(\psi_b, \psi_r) = \chi/\eta$ .
15:  end for
16: end for

```

C can be calculated by Monte-Carlo simulations with η simulation times.

Algorithm 1 shows Monte-Carlo simulations for the coverage probability considering fading channels and wall penetration loss. For each different BS density, η times of simulations need to be run. In addition, the time of each simulation rises as the BS density increases. Accordingly, Algorithm 1 is very time-consuming and inconvenient for network coverage analysis. Therefore, we propose Algorithm 2 whose simulation time is not affected by the increase of BS density. In addition, the simulation results can be applied for different BS density. The principle of Algorithm 2 is presented in the following paragraphs.

According to the properties of mmWave frequency, two assumptions are made for the transmission model in Algorithm 2: 1) due to the high wall penetration loss of mmWave [19], we assume that signals cannot penetrate walls; 2) since small-scale fading is not significant in the LoS mmWave transmission [21, 30], a deterministic channel model is employed. Furthermore, given the power threshold T , the maximum LoS transmission distance is computed by:

$$d_{\max} = \frac{\lambda^{\frac{2}{\alpha}}}{(4\pi)^{\frac{2}{\alpha}} T^{\frac{1}{\alpha}}} P_t^{\frac{1}{\alpha}}. \quad (4)$$

For RIS-assisted transmission, given the distance d_1 between the UE and the RIS, the maximum distance $d_{2,\max}$ between the BS and the RIS is represented as:

$$d_{2,\max} = \sqrt{\frac{GM^2 N^2 d_u^2 \lambda^2 A^2}{64\pi^3 d_1^2 T}} P_t. \quad (5)$$

Note that $d_{2,\max} \leq d_{\max}$.

Based on the assumptions and equation (4) and (5), the LoS area and RIS-extended area of a randomly located UE in the indoor environment are shown in Fig. 4.1. The boundary of the LoS area is determined by either the maximum LoS transmission distance (equation (4)) or the wall which blocks the UE. In Fig. 4.1, 6 RISs are located in the LoS area of the UE, but only 2 of them have the RIS-extended area which is not overlapped with the LoS area. The boundary of the RIS-extended area is decided by either the maximum reflected transmission distance (equation (5)) or the wall which blocks the RIS. Moreover, the two scenarios that a UE is in network coverage are: 1) a BS is located in the LoS area; 2) a BS is located in the RIS-extended area. We denote the size of the LoS area and the RIS-extended area by S_L and $S_\Delta(\psi_r)$, respectively. Note that $S_\Delta(\psi_r)$ is a function of RIS density ψ_r . In addition, the average number of BSs in PPP scenario and the number of BSs in BPP scenario are expressed by $n_{BS} = \psi_b WL$. The average number of RISs is denoted by $n_{RIS} = \psi_r \xi$.

For the scenario that the locations of BSs follow PPP, the probability that no BS is located in the LoS area and the RIS-extended area is $P_{\text{out}} = \exp\left(-\psi_b(S_L + S_\Delta(\psi_r))\right)$ [17]. Accordingly, the network coverage probability can be expressed by:

$$C_{\text{PPP}} = 1 - \exp\left(-\psi_b(S_L + S_\Delta(\psi_r))\right). \quad (6)$$

For the scenario that the locations of BSs follow BPP, the probability that no BS is located in the LoS area and the RIS-extended area is $P_{\text{out}} = \left(1 - \frac{S_L + S_\Delta(\psi_r)}{WL}\right)^{n_{BS}}$. Therefore, the network coverage probability can be expressed by:

$$C_{\text{BPP}} = 1 - \left(1 - \frac{S_L + S_\Delta(\psi_r)}{WL}\right)^{n_{BS}}. \quad (7)$$

Algorithm 2 The Coverage Area Calculation Algorithm

- 1: Generate walls according to the considered indoor layout;
 - 2: Divide the whole indoor area into $k \times k$ unit square with size S_{unit} ;
 - 3: **for** Different RIS density ψ_r **do**
 - 4: **for** $i = 1 : \tau$ **do**
 - 5: Generate a randomly distributed UE in the considered indoor layout;
 - 6: Generate randomly distributed RISs with RIS density ψ_r on the RIS-deployed walls;
 - 7: Find all the RISs located in the LoS area of the UE;
 - 8: Let $S_L = 0$ and $S_\Delta = 0$;
 - 9: **for** $j = 1 : k^2$ **do**
 - 10: **if** {the distance between the UE and the center of the j th unit square does not exceed d_{max} } && {no wall blocks the UE from the center of the j th unit square} **then**
 - 11: $S_L = S_L + S_{\text{unit}}$;
 - 12: **else if** {no wall blocks the center of the j th unit square from the RIS which locates in the LoS area} && {the distance between the RIS and the center of the j th unit square does not exceed $d_{2,\text{max}}$ } **then**
 - 13: $S_\Delta = S_\Delta + S_{\text{unit}}$;
 - 14: **end if**
 - 15: **end for**
 - 16: For different BS density ψ_b , calculate the coverage probability using the equation (6) and (7);
 - 17: **end for**
 - 18: Calculate the average coverage probability $C(\psi_b, \psi_r)$.
 - 19: **end for**
-

S_L and S_Δ are obtained by Monte-Carlo simulations. Let τ be the Monte-Carlo simulation times. The procedures of the simulation are shown in Algorithm 2.

3.2 Cost Analysis

The network cost includes deployment cost and operational cost. For deployment cost, some facilities are the prerequisites for both the UD SC networks and RIS-assisted networks, e.g., both require an indoor broadband connection for providing connectivity to the BSs as backhaul. The common facilities for both networks are not considered into the cost since our aim is to compare the difference. The work in [24] defines the unit cost which is determined by the cost per equipment, the time length of the installment and the interest rate. Moreover, the total network cost is that the quantity of the network equipments multiples with the

Table 4.1 Simulation Parameters

parameter	value	parameter	value
λ	0.01 m	ω	-20 dB
L_r	10 m	T/P_t	-90 dB
W_c	5 m	d_u	0.005 m
W_d	2 m	A	0.9
α	2	G	8

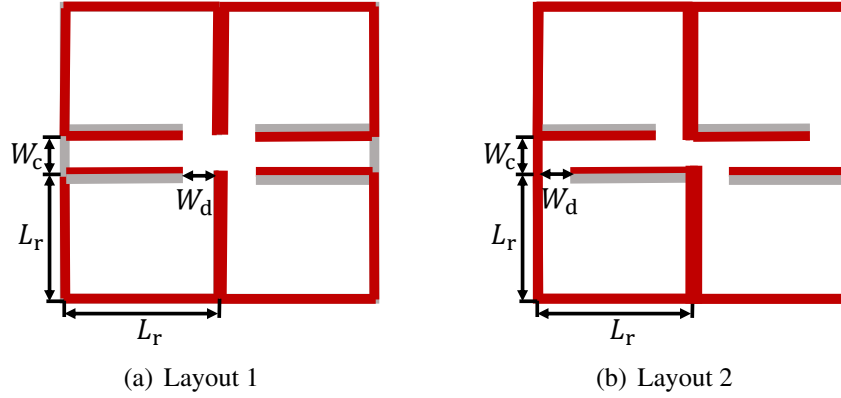


Fig. 4.2 The considered indoor layouts.

unit cost. Hence, we denote the unit cost of BSs and RISs by a_{BS} and a_{RIS} , respectively. Furthermore, the costs of BSs are that the average number of BSs multiples with the BS unit cost, i.e., $\eta_{BS} = n_{BS}a_{BS}$. And the costs of RISs are that the average number of RISs multiples with the RIS unit cost, i.e., $\eta_{RIS} = n_{RIS}a_{RIS}$. Hence, the expression of the total network cost is provided as follows:

$$\eta = \eta_{BS} + \eta_{RIS} = a_{BS}\psi_bWL + a_{RIS}\psi_r\xi. \quad (8)$$

The coverage probability and the network cost are correlated, since both are the functions of the BS density and the RIS density, i.e., $C(\psi_b, \psi_r)$ and $\eta(\psi_b, \psi_r)$. Hence, the function of the coverage probability to the network cost, i.e., $\eta(C)$, can be built. Moreover, we can find out the more cost-effective network by comparing $\eta(C)$ of the UD SC networks and that of the RIS-assisted networks. Specifically, when the UD SC networks and the RIS-assisted networks have the same coverage probability, i.e., $C(\psi_{b1}, 0) = C(\psi_{b2}, \psi_r)$, the network with lower network cost is more cost-effective than the network with higher network cost.

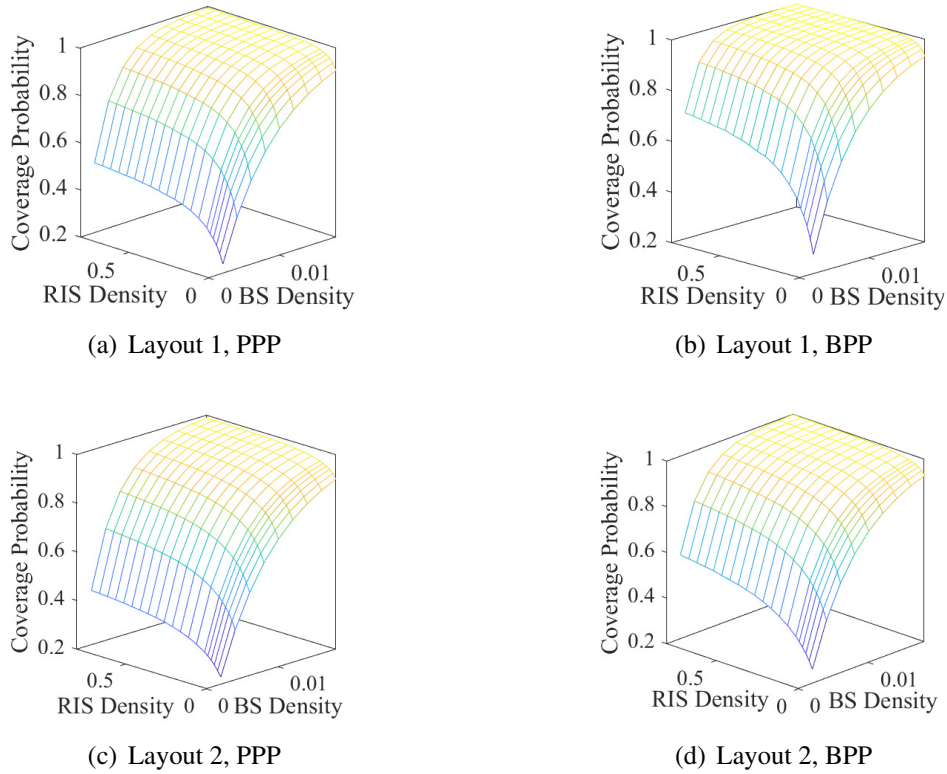


Fig. 4.3 The network coverage probability with different BS density and RIS density.

4 Simulation Results

In this section, the coverage probabilities of RIS-assisted networks and UD SC networks are evaluated, respectively. Moreover, the cost effectiveness of RIS deployment and that of UD SC deployment are compared. The considered indoor layouts are shown in Fig. 4.2. The size of each room is $L_r \times L_r$. The size of the door in each room is denoted by W_d . In addition, the width of the corridor is W_c . The simulation parameters are provided in Table 4.1. The Rician fading parameter $K = 10\text{dB}$ and the Rayleigh fading coefficient $g \sim CN(0, 1)$.

Based on Algorithm 1, the network coverage probability with different BS density and RIS density is shown in Fig. 4.3. The RIS with 50×50 unit cells is employed. Note that when RIS density is 0, only UD SC networks are employed. Fig. 4.3 indicates that: the coverage probability rises significantly as RIS density increases from 0 to 0.2. Further increase of RIS density can only lead to slight growth of the coverage probability. More importantly, the same coverage probability can be achieved by multiple deployment strategies, i.e., fewer BSs

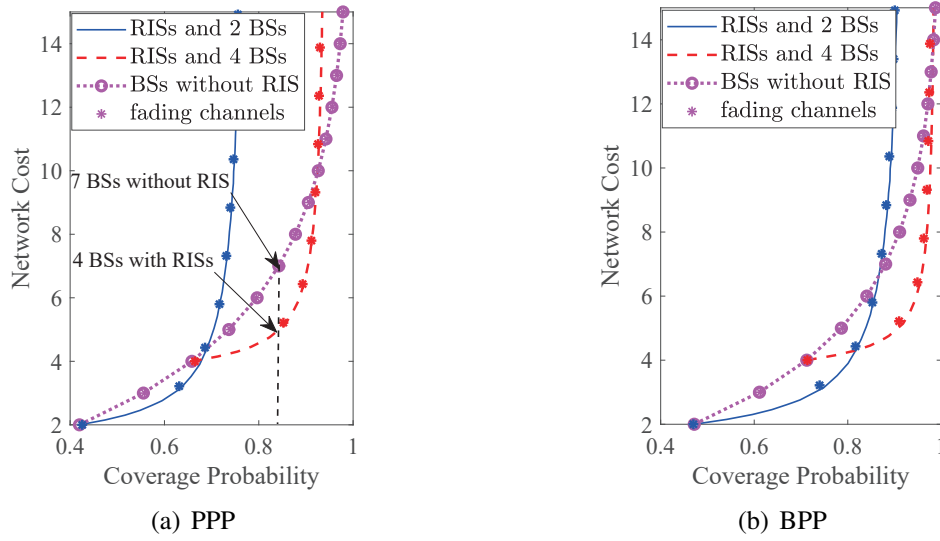


Fig. 4.4 The cost comparison between RIS deployment and small-cell BS densification to achieve same coverage probability in indoor layout 1.

and more RISs, more BSs and fewer RISs, and only BSs. To find out which strategy is the most cost-effective, we need to jointly analyze the coverage probability and network cost.

In each subfigure of Fig. 4.4 and Fig. 4.5, the coverage probabilities obtained from both Algorithm 1 and Algorithm 2 are shown, and the comparison of the network cost between RIS-assisted networks and UD SC networks is presented. Without loss of generality, we normalise the unit cost of UD SC BSs as 1. And the unit cost of RISs is assumed to be 20 times lower than the unit cost of UD SC BSs. Fig. 4.4 and Fig. 4.5 can be understood as: with the same network cost, different deployment strategies can be adopted, i.e., fewer BSs and more RISs, more BSs and fewer RISs, and only BSs. Each deployment strategy leads to a different coverage probability. Note that the indoor coverage considering deterministic channels has the same trend as the indoor coverage considering fading channels and wall penetration loss, and the two indoor coverage probabilities are very close to each other. Therefore, Algorithm 2 can be adopted for performance analysis with little accuracy loss. To achieve certain level of coverage probability with the lowest network cost, a proper number of BSs are crucial, e.g., in Fig. 4.4 (a), RISs with 4 BSs have the lowest network cost to achieve 82% coverage, compared with 7 BSs without RIS and RISs with 2 BSs. In addition, to achieve high coverage probability, i.e., above 90%, a minimal number of BSs are required,

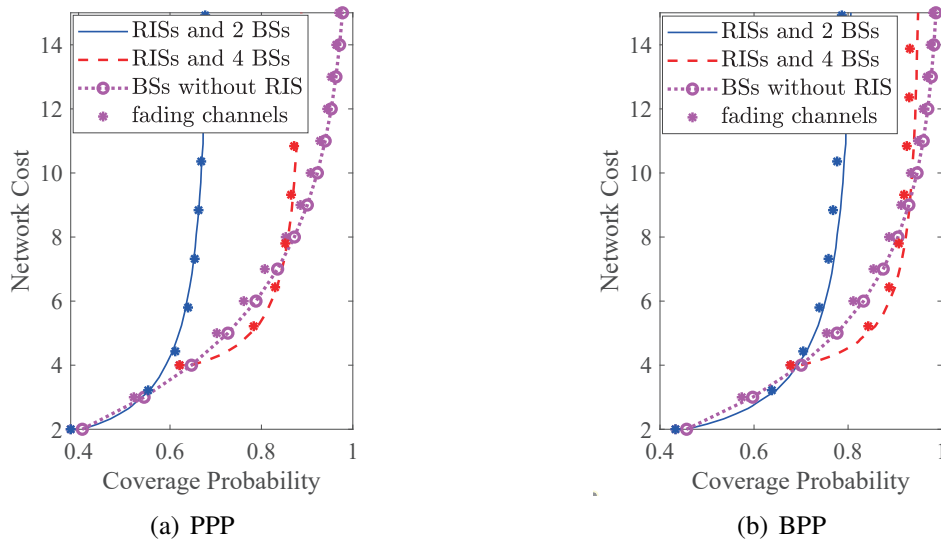


Fig. 4.5 The cost comparison between RIS deployment and small-cell BS densification to achieve same coverage probability in indoor layout 2.

even with the assistance of RISs, e.g., 2 BSs with RISs are not cost-effective to achieve high coverage. On the other hand, the indoor layouts have a great impact on the cost-effectiveness of the RIS-assisted networks, e.g., for the scenario that the BS distribution follows BPP, in layout 1, RISs with 2 BSs have lower cost to achieve 80% coverage than BSs without RIS, while it is the exact opposite in layout 2.

5 Conclusion

In this letter, we have compared RIS deployment with UD SC in terms of coverage enhancement. The main observations are: 1) the same coverage probability can be achieved by different network deployment strategies; 2) to achieve certain network coverage with a cost-effective deployment strategy, a proper number of BSs are necessary; and 3) since RIS is only a passive array, a minimal number of BSs are essential for high network coverage.

For future works, the comparison between UD SC networks and RIS-assisted networks in terms of the network capacity will be investigated. In addition, the network cost can be decreased significantly with the acceptable degradation of network performance by

employing low-cost devices, e.g., RIS with discrete phase shifts. The tradeoff between hardware imperfections and network cost will be analyzed in the future works.

References

- [1] Huawei, (Feb. 2016) *Five Trends to Small Cell 2020*. [online]. Available: <http://www-file.huawei.com/~media/CORPORATE/PDF/News/Five-Trends-To-Small-Cell-2020-en.pdf>.
- [2] V. Chandrasekhar, J. G. Andrews and A. Gatherer, "Femtocell networks: a survey," *IEEE Commun. Mag.*, vol. 46, no. 9, pp. 59-67, Sep. 2008.
- [3] T. S. Rappaport, S. Sun, R. Mayzus *et al.*, "Millimeter wave mobile communications for 5G cellular: It will work!," *IEEE Access*, vol. 1, pp. 335-349, May 2013.
- [4] F. Boccardi, R. W. Heath, A. Lozano *et al.*, "Five disruptive technology directions for 5G," *IEEE Commun. Mag.*, vol. 52, no. 2, pp. 74-80, Feb. 2014.
- [5] M. Kamel, W. Hamouda and A. Youssef, "Ultra-dense networks: A survey," *IEEE Commun. Surveys Tuts.*, vol. 18, no. 4, pp. 2522-2545, May 2016.
- [6] J. G. Andrews, X. Zhang, G. D. Durgin *et al.*, "Are we approaching the fundamental limits of wireless network densification?" *IEEE Commun. Mag.*, vol. 54, no. 10, pp. 184-190, Oct. 2016.
- [7] D. López-Pérez, M. Ding, H. Claussen *et al.*, "Towards 1 Gbps/UE in cellular systems: Understanding ultra-dense small cell deployments," *IEEE Commun. Surveys Tuts.*, vol. 17, no. 4, pp. 2078-2101, Jun. 2015.

- [8] M. Ding, P. Wang, D. López-Pérez *et al.*, “Performance impact of LoS and NLoS transmissions in dense cellular networks,” *IEEE Trans. Wireless Commun.*, vol. 15, no. 3, pp. 2365-2380, Mar. 2016.
- [9] J. Lee, X. Zhang and F. Baccelli, “A 3-D spatial model for in-building wireless networks with correlated shadowing,” *IEEE Trans. Wireless Commun.*, vol. 15, no. 11, pp. 7778-7793, Nov. 2016.
- [10] C. Chen, Y. Zhang, J. Zhang *et al.*, “On the performance of indoor multi-story small-cell networks,” *IEEE Trans. Wireless Commun.*, vol. 20, no. 2, pp. 1336-1348, Feb. 2021.
- [11] Q. Wu and R. Zhang, “Intelligent reflecting surface enhanced wireless network via joint active and passive beamforming,” *IEEE Trans. Wireless Commun.*, vol. 18, no. 11, pp. 5394-5409, Nov. 2019.
- [12] Q. Wu and R. Zhang, “Towards smart and reconfigurable environment: Intelligent reflecting surface aided wireless network,” *IEEE Commun. Mag.*, vol. 58, no. 1, pp. 106-112, Jan. 2020.
- [13] E. Basar, M. Di Renzo, J. De Rosny *et al.*, “Wireless communications through reconfigurable intelligent surfaces,” *IEEE Access*, vol. 7, pp. 116753-116773, 2019.
- [14] T. Van Chien, L. T. Tu, S. Chatzinotas *et al.*, “Coverage probability and ergodic capacity of intelligent reflecting surface-enhanced communication systems,” *IEEE Commun. Lett.*, vol. 25, no. 1, pp. 69-73, Jan. 2021.
- [15] T. Van Chien, A. K. Papazafeiropoulos, L. T. Tu *et al.*, “Outage probability analysis of IRS-assisted systems under spatially correlated channels,” *IEEE Wireless Commun. Lett.*, early access, May 2021.
- [16] I. Yildirim, A. Uyrus and E. Basar, “Modeling and analysis of reconfigurable intelligent surfaces for indoor and outdoor applications in future wireless networks,” *IEEE Trans. Commun.*, vol. 69, no. 2, pp. 1290-1301, Feb. 2021.

-
- [17] J. G. Andrews, F. Baccelli and R. K. Ganti, "A tractable approach to coverage and rate in cellular networks," *IEEE Trans. Commun.*, vol. 59, no. 11, pp. 3122-3134, Nov. 2011.
- [18] M. Afshang and H. S. Dhillon, "Fundamentals of modeling finite wireless networks using binomial point process," *IEEE Trans. Wireless Commun.*, vol. 16, no. 5, pp. 3355-3370, May 2017.
- [19] Q. Wu and R. Zhang, "Beamforming optimization for wireless network aided by intelligent reflecting surface with discrete phase shifts," *IEEE Trans. Commun.*, vol. 68, no. 3, pp. 1838-1851, Mar. 2020.
- [20] S. Abeywickrama, R. Zhang, Q. Wu *et al.*, "Intelligent reflecting surface: Practical phase shift model and beamforming optimization," *IEEE Trans. Commun.*, vol. 68, no. 9, pp. 5849-5863, Sep. 2020.
- [21] W. Tang, M. Chen, X. Chen *et al.*, "Wireless communications with reconfigurable intelligent surface: Path loss modeling and experimental measurement," *IEEE Trans. Wireless Commun.*, vol. 20, no. 1, pp. 421-439, Jan. 2021.
- [22] Y. Zhu, G. Zheng and K. -K. Wong, "Stochastic geometry analysis of large intelligent surface-assisted millimeter wave networks," *IEEE J. Sel. Areas Commun.*, vol. 38, no. 8, pp. 1749-1762, Aug. 2020.
- [23] Y. Zhu, L. Wang, K.-K. Wong, and R. W. Heath, Jr., "Secure communications in millimeter wave ad hoc networks," *IEEE Trans. Wireless Commun.*, vol. 16, no. 5, pp. 3205-3217, May 2017.
- [24] C. Bouras, V. Kokkinos, and A. Papazois, "Financing and pricing small cells in next-generation mobile networks," *Wired/Wireless Internet Communications*, Paris, France, May 2014, pp. 41-54.

Chapter 5

Paper II - RIS-assisted mmWave

Networks with Random Blockages: Fewer Large RISs or More Small RISs?

Zeyang Li, Haonan Hu, Jiliang Zhang and Jie Zhang.

This paper has been accepted to publish in IEEE Transactions on Wireless Communication.

RIS-assisted mmWave networks with Random Blockages: Fewer Large RISs or More Small RISs?

Zeyang Li¹, Haonan Hu^{1,2}, Jiliang Zhang^{1,3}, Jie Zhang^{1,3}

¹ Department of Electronic and Electrical Engineering, the University of Sheffield, Sheffield, S10 2TN, UK

² Chongqing Key Laboratory of Mobile Communications Technology Engineering Research Center of Mobile Communications, the School of Communication and Information Engineering, Chongqing University of Posts and Telecommunications, Chongqing 400065

³ Ranplan Wireless Network Design Ltd., Cambridge, CB23 3UY, UK

Abstract

Reconfigurable intelligent surface (RIS), which provides indirect line-of-sight (LoS) transmission paths between the receiver and its blocked transmitter, has been proposed as one of the promising technologies for network performance enhancement. Recent works indicate that both the numbers of RISs and unit cells per RIS have a significant impact on network performance. However, with a given total number of unit cells, the joint analysis of these two factors considering blockage effect has not been investigated. In this paper, the coverage probability of a three-dimensional downlink millimeter wave RIS-assisted network is analyzed. We first derive the acceptable area where a LoS RIS is capable to satisfy the signal-to-noise ratio threshold at the receiver. Next, we model the centers of building blockages and human-body blockages as two independent Poisson point processes and derive the probability that indirect LoS transmissions exist. Then, we derive and validate the analytical upper and lower bounds of the coverage probability as the functions of network parameters and blockage densities. We also derive and validate the closed-form coverage probability when RISs are much closer to UE than BS. Finally, we propose a general network cost model for RIS-assisted network. Results show that in terms of coverage enhancement, densely deployed small-scale RISs outperform sparsely deployed large-scale RISs in scenarios with

dense blockages or short transmission distances, while sparsely deployed large-scale RISs are preferable in scenarios with sparse blockages or long transmission distances.

1 Introduction

Wireless data traffic will grow by up to 1000 times in the next decade [1]. To satisfy the immense data traffic demand, promising technologies, e.g., massive multiple-input multiple-output (MIMO) and ultra-dense network (UDN), have been proposed. By deploying more base stations (BSs) and more active antennas, the network capacity can be enhanced significantly. However, the hardware cost and energy consumption also increase dramatically. Therefore, reconfigurable intelligent surfaces (RISs), which have the advantage of less energy consumption and lower cost, have emerged to enhance the network performance. The work in [2] showed that the RIS-assisted networks with the proper number of BSs can achieve the highest cost effectiveness for coverage enhancement.

A RIS is a planar surface consisting of a large number of low-cost integrated electronic circuits (unit cells). Each integrated electronic circuit can be controlled to alter the phase and amplitude of the incident signal, so that the signal can be reconfigured to achieve different purpose, e.g., received power enhancement and signal/interference cancellation [3, 4]. An important application of RISs is to provide indirect line-of-sight (LoS) transmission paths when the direct transmission between the BS and user equipment (UE) is blocked. This is extremely useful in the millimeter wave (mmWave) networks [5, 6]. Besides, RISs are easy and flexible to be installed on the existing objects in both indoor and outdoor environments, which can significantly reduce the deployment cost. With all these advantages, RISs have drawn increasingly attention from various research, such as beamforming design based on deep reinforcement learning [7, 8], and channel estimation [9].

The performance of RIS-assisted networks under various scenarios has been widely studied recently. The coverage probability and ergodic capacity of the RIS-assisted single-input single-output (SISO) network have been derived [10–12]. The results in [11] indicated that both the number of RISs and the number of unit cells have a significant impact on the outage probability and average sum rate. The RIS-assisted networks under spatial correlated

Rayleigh fading channels have been investigated in [13, 14] and closed-form coverage probabilities have been derived. The results in [13] demonstrated that increasing the number of RISs is more beneficial than increasing unit cells. Different from above works which only considered Rayleigh fading channels, the RIS-assisted networks considering Rician fading channels have been investigated in [15] and [16]. The results in [15] showed that increasing the number of unit cells can significantly improve the network performance. For the above works, the spatial locations of RISs are not considered, or only one RIS/a given number of RISs at fixed locations are considered, and the impact of random spatial locations of RISs on the network performance were ignored.

Stochastic geometry has proved a tractable mathematical tool to model the spatial distribution of wireless nodes [17], and has been used to analyze the performance of RIS-assisted networks in only a few works. The works in [18] and [19] have studied RIS-assisted single-cell network with randomly distributed RISs and compared with decode-and-forward relays. The spatial throughput of the network by averaging the transmission distances was provided in [18] and the results indicated that given the total number of unit cells for RISs, the networks with fewer RISs but more unit cells per RIS have higher spatial throughput than the networks with more RISs but fewer unit cells per RIS. Nonetheless, the works in both [18] and [19] have only considered the scenario that the distance between the UE and RIS is much shorter than the distance between the UE and BS, so that the distances from the BS to RIS and to UE can be assumed to be approximately equal, which is less accurate. Multi-cell networks assisted by randomly distributed RISs have been investigated in [20–23]. The work in [20] provided the approximations for the coverage of the RIS-assisted mmWave networks. However, only the interference direct from BSs was considered. In [21] and [22], the interference reflected by RISs has been analyzed. The results in [21] showed that RIS-assisted networks can enhance network capacity and energy efficiency when the BSs are not densely deployed. Nevertheless, the interference reflected by the RISs will limit the network performance when the BS density is higher than the RIS density. The power distributions of the signal and interference reflected by RISs were derived in [22]. Moreover, with a given total deployment cost and individual costs, the results revealed the existence

of an optimal ratio between the density of RIS and BS for achieving the highest network throughput. The approximations of the coverage probability, ergodic capacity and energy efficiency of the RIS-assisted networks were derived in [23]. The LoS probability of direct transmission was considered in the work. For the above works, LoS transmission has been assumed between the BS/UE and RIS. However, there is no guarantee that RIS-assisted transmission will always be LoS in practice. Therefore, the probability that the RIS-assisted transmission is blocked needs to be investigated.

Blockage models based on Boolean line segments have been employed in the performance analysis of RIS-assisted networks. The work in [24] presented the probability that a randomly distributed RIS can be employed for RIS-assisted transmission. With RISs deployed on a subset of the blockages, the performance of RIS-assisted networks considering blockage effect was analyzed in [27, 25, 26]. In [25], with a given distance between the BS and the UE, the outage probabilities of the RIS-assisted networks under three different RIS association strategies, i.e., a random RIS, the closest RIS, and multiple random RISs, were provided based on numerical integrals. In [26], the work assumed that the locations of BSs follow a PPP and each BS has a associated UE which locates at a fixed distance. The SIR coverage probability considering the interference from both direct transmission and reflective transmission of other BSs was calculated based on numerical integrals. In [27], the probability distribution of the path loss between the UE and its serving BS was derived. However, the path loss model of the RIS-assisted transmission in [27] can only be applied when either the transmitter or the receiver or both of them is/are in the near field of RIS [20], which is very uncommon especially when the size of the RIS is not large enough as compared with the transmission distances.

Research has shown that both the number of RISs and the number of unit cells per RIS have a great impact on the network performance. However, the effect of blockages on the RIS-assisted transmission, which plays an important role in the performance of mmWave RIS-assisted networks [29, 30], has been ignored in most of the above works. Only the work in [27] considered the blockage probability of the RIS-assisted transmission, but the path loss model can only apply to limited scenario. With a given total number of unit cells,

the joint analysis of the RIS number and RIS size under various scenarios, e.g., different blockage density, transmission distance and received signal power requirement, has never been investigated so far. More specifically, whether fewer large RISs or more small RISs should be deployed for better network performance, and how to find the optimal number of unit cells per RIS still need to be studied with consideration of randomly distributed blockages.

Therefore, in this paper, we investigate the RIS-assisted mmWave networks considering random blockages. Our main contributions are summarized as follows.

- We propose the earliest joint analysis on the impact of the RIS number and RIS size on the coverage probability considering blockage models. We consider both building blockage model and human-body blockage model. Meanwhile, we adopt Poisson point process (PPP) for the RIS distribution and blockage models. We present the three-dimensional (3D) communication model by considering the height of the blockages and wireless devices. In addition, we introduce the RIS size and density factor to determine the number of RISs and the number of unit cells per RIS, so that different RIS deployment strategies can be evaluated and compared.
- We derive the analytical upper bound and lower bound of the coverage probability considering the network parameters and blockage densities, and derive the closed-form coverage probability when the connected RIS is much closer to the UE than the BS. Meanwhile, we provide the simulation results to validate our analytical results. In addition, we present a general cost model for RIS-assisted network.
- We analyze the effect of building density, nearby-user density, SNR threshold, the RIS size and RIS density on the coverage probability, respectively. We observe that more small RISs are a better option for a high building blockage density and/or short transmission distance, e.g., urban area, whereas fewer large RISs is more suitable for low building blockage density and/or long transmission distance, e.g., rural area. In addition, more small RISs is more applicable for small-cell networks and high human

density, e.g., malls and airports. On the other hand, fewer large RISs is a better choice for the networks with a high SNR requirement.

The paper is organized as follows. In the next section, we present the system model of the RIS-assisted network considering both building blockages and human-body blockages. In Section III, we derive the upper and lower bounds of the coverage probability. In Section IV, we verify the analytical results and analyze blockage effects, SNR threshold, the size and number of RISs on the network coverage. In Section V, we draw conclusions.

2 System Model

In this section, we present the system model of the RIS-assisted single-cell mmWave downlink networks. We first provide network model. Next, we describe blockage models, i.e., human-body blockage model and building blockage model. Finally, we describe the path loss model of both direct LoS transmission from the BS to the UE and indirect RIS-assisted transmission.

2.1 Network Model

The 3D RIS-assisted single-cell mmWave downlink networks are investigated in this paper. The BS has N_t antennas and the UE has a single antenna. RISs are assumed to be distributed according to a PPP with density λ_r , as shown in Fig. 5.1. The horizontal distance between the BS and the UE, the BS and the k th RIS, the UE and the k th RIS is R_b , l_k and r_k , respectively. In addition, the horizontal angle between the BS and the k th RIS at the UE is β_k . We assume that all the RISs have the same height h_r and the angles of all the RISs are suitable for transmission [21, 22, 19]. Meanwhile, the height of the BS and UE is h_b and h_u , as shown in Fig. 5.2.

Remark 1: To investigate that whether large RISs with low density or small RISs with high density have higher network performance, first, we assume that the largest permitted RIS is made of $N \times M$ regularly arranged unit cells, where N and M represent the number of rows and columns of the unit cells for each RIS. Hence, the total number of unit cells per largest permitted RIS is $m_c = NM$. And the width of each unit cell along both the x axis and

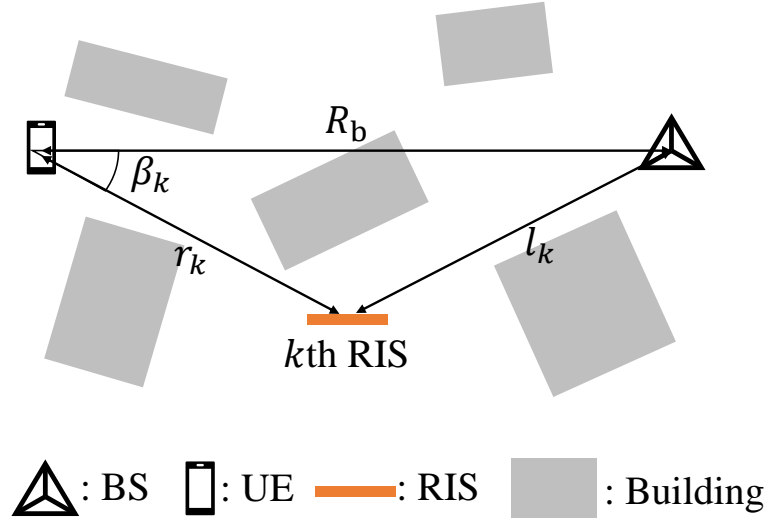


Fig. 5.1 Top view of the BS, UE, RIS and buildings.

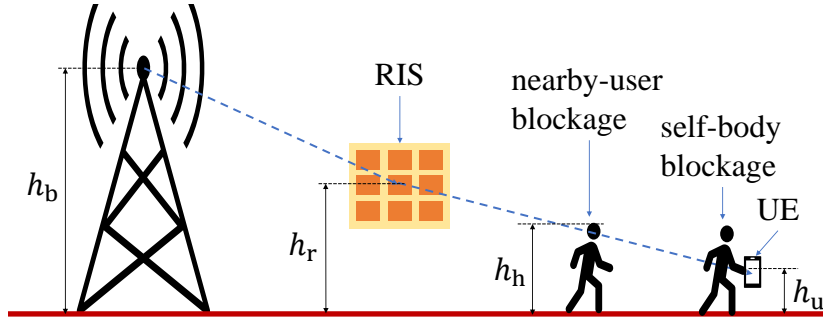


Fig. 5.2 Human-body blockages.

y axis is l_u . In addition, the density of the largest permitted RISs is denoted by λ_r' . Then, we define the RIS size and density factor n , so that the largest permitted RIS is divided into n small RISs. N_d and M_d denote the number of rows and columns of the unit cells per RIS. Moreover, the total number of unit cells per RIS is $m_d = N_d M_d = \lfloor m_c/n \rfloor$ and $N_d/M_d \approx N/M$. Meanwhile, the density of divided RISs is denoted by $\lambda_r = n\lambda_r'$. n determines both the size of each RIS and the RIS density, thus it is a significant parameter to evaluate the network performance of different RIS deployment strategies.

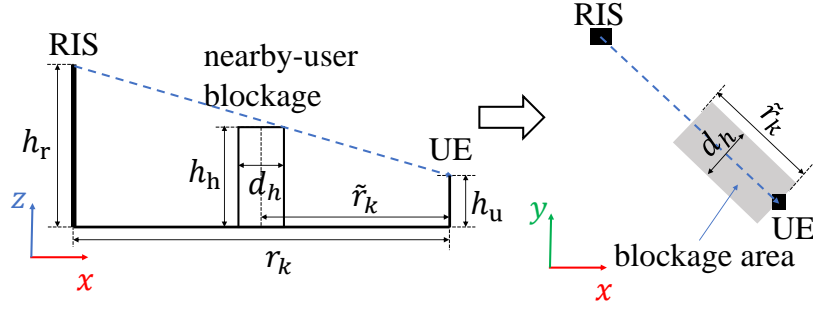


Fig. 5.3 Nearby-user blockage model.

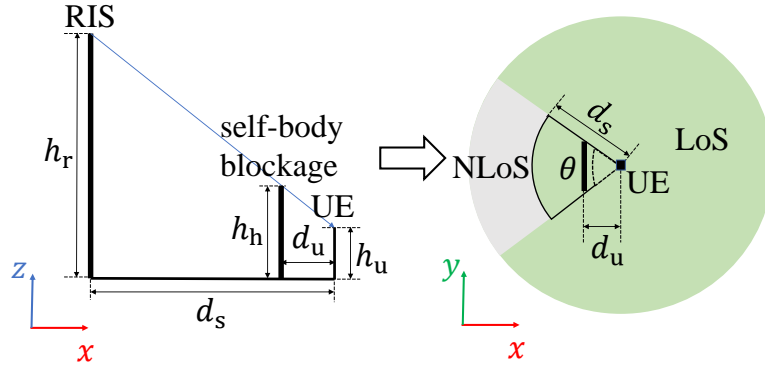


Fig. 5.4 Self-body blockage model.

2.2 Human-body Blockage Model

As shown in Fig. 5.2, two types of human-body blockages are investigated: nearby-user blockages and self-body blockage. The 3D nearby-user blockage model and 3D self-body blockage model are shown in Fig. 5.3 and Fig. 5.4, respectively.

For nearby-user blockage model, each blockage is modeled as a cylinder with diameter d_h and height h_h . The centers of the cylinders are distributed according to a 2D homogeneous PPP with intensity λ_h . Due to the limited height of the nearby-user blockages, given the horizontal distance r_k between the k th RIS and the UE, the horizontal distance of the transmission which can be blocked by nearby-user blockages is $\tilde{r}_k = \frac{h_h - h_u}{h_r - h_u} r_k$. Moreover, the transmission is blocked when the center of a blockage is located in the blockage area with size $d_h \times \tilde{r}_k$, as shown in Fig. 5.3. In PPP, the number of points in a certain area with size S follows Poisson distribution with mean value $\lambda_h S$. Therefore, the probability that the

transmission from the k th RIS to the UE is not blocked by nearby-user blockages is:

$$p_{\text{nu}}(r_k) = e^{-\lambda_{\text{h}} d_{\text{h}} \frac{h_{\text{r}} - h_{\text{u}}}{h_{\text{r}} - h_{\text{u}}} r_k}. \quad (1)$$

Besides, we assume that both the BS and RISs are higher than nearby-user blockages. Therefore, the transmission between the BS and the RIS cannot be blocked by nearby-user blockages.

For self-body blockage model, since the height h_{h} of the blockage is limited, the transmission cannot be blocked by self-body blockage if the horizontal distance between the RIS and the UE is less than $d_{\text{s}} = \frac{h_{\text{r}} - h_{\text{u}}}{h_{\text{h}} - h_{\text{u}}} d_{\text{u}}$, where d_{u} is the horizontal distance between the UE and the user, as shown in Fig. 5.4. On the other hand, when the horizontal distance between the UE and the RIS is larger than d_{s} , the angle of the self-body blockage at the UE is θ . Moreover, the probability that the transmission from the k th RIS to the UE is not blocked by self-body blockage is:

$$p_{\text{su}}(r_k) = \begin{cases} 1, & r_k \leq d_{\text{s}}, \\ 1 - \frac{\theta}{2\pi}, & \text{otherwise.} \end{cases} \quad (2)$$

2.3 Building Blockage Model

The blockages caused by buildings and permanent structures are modeled using random shape theory. All the building blockages are assumed to be rectangles. The centers of the blockages are distributed according to a PPP with intensity λ_{b} . The lengths and widths of the building blockages are assumed to follow two independent distributions with the expected length L and the expected width W , respectively. Meanwhile, the orientation of the building blockages follows uniform distribution in $(0, 2\pi]$. Furthermore, the probability that the transmission from the k th RIS to the UE is not blocked by building blockages is [17]:

$$p_{\text{bu}}(r_k) = e^{-\Psi r_k - \bar{\omega}}, \quad (3)$$

where $\psi = 2\lambda_b(W + L)/\pi$ and $\varpi = \lambda_b LW$. Since all the RISs are pre-deployed, no building blockage is located between the BS and the RISs. Therefore, the transmissions between the BS and the RISs always be LoS.

2.4 Received Signal Power

Both the direct transmission from the BS to the UE and the RIS-assisted transmission are considered. The wavelength of the signal is denoted by μ and the path loss exponent is α . Let P_t and G_t denote the transmit power and antenna gain of the BS. In this paper, small-scale fading is omitted because 1) it is not significant in LoS mmWave transmission [21, 27, 30, 32, 33]; 2) the effect of channel hardening exists when the number of elements of antennas/RISs is sufficiently large [34, 35]. In addition, due to high penetration loss of mmWave frequency [19], non-line-of-sight (NLoS) transmission is not considered in this paper. Furthermore, the received signal power of the direct LoS transmission from the BS to the UE is as follows:

$$P_{\text{rb}} = \frac{P_t N_t^2 G_t \mu^2}{16\pi^2 (R_b^2 + (h_b - h_u)^2)^{\frac{\alpha}{2}}}. \quad (4)$$

RIS-assisted transmission is adopted when the direct transmission is blocked. For RIS-assisted transmission, the power radiation pattern of RISs is assumed to be independent of the incident/reflected angle of the signal and the peak radiation is considered in all the directions. All the unit cells of the RIS have the same amplitude ρ of the reflection coefficient and implement perfect phase control, so that the reflected signals from the unit cells are aligned in phase at the receiver to enhance the received signal power. Therefore, the received signal power of the RIS-assisted transmission can be formulated as follows [20]:

$$P_{\text{rr}} = \frac{P_t N_t^2 G_t M_d^2 N_d^2 l_u^2 \mu^2 \rho^2}{64\pi^3 (\tilde{l}_k \tilde{r}_k)^\alpha}, \quad (5)$$

where $\tilde{l}_k = (l_k^2 + (h_b - h_r)^2)^{\frac{1}{2}}$ is the transmission distance between the BS and the k th RIS, $l_k = (R_b^2 + r_k^2 - 2R_b r_k \cos \beta_k)^{\frac{1}{2}}$, $\tilde{r}_k = (r_k^2 + (h_r - h_u)^2)^{\frac{1}{2}}$ is the transmission distance between the k th RIS and the UE, G denotes the channel gain of each RIS. Furthermore, the SNR of

the received signal is computed by:

$$\text{SNR} = \frac{P_r}{w_0}, \quad (6)$$

where P_r denotes the received signal power (depends on whether it is direct transmission from the BS to the UE or RIS-assisted transmission, $P_r = P_{\text{tb}}$ or P_{tr}) and w_0 is the noise power.

3 Coverage Probability

In this section, we derive the analytical upper and lower bounds of the coverage probability. A UE is in coverage when two conditions are met: 1) the SNR of the received signal is higher than the SNR threshold T ; 2) either the direct transmission from the BS to the UE or the RIS-assisted transmission is unblocked. Note that these two conditions are independent from each other, i.e., the received SNR in condition 1) is calculated without considering any penetration loss. Meanwhile, condition 2) does not imply condition 1) because even though the transmission is unblocked, it is possible that the SNR of the received signal is below the SNR threshold. We analyze these two conditions in the following two subsections, respectively. Moreover, we present the analytical expressions of the lower bound and upper bound of the coverage probability in the end of this section.

3.1 The RIS-assisted Transmission with Acceptable SNR

The SNR of the RIS-assisted transmission is determined by the transmission distance between the BS and the RIS and between the UE and the RIS. Therefore, given the distance between the BS and the UE, a RIS can only be located in a certain area to satisfy the SNR threshold, and this area is named the RIS area in this paper. The RIS area depends on various factors, e.g., the size of RISs, transmission distance and SNR threshold. Based on the inequation $P_{\text{tr}}/w_0 \geq T$, the mathematical expression of the RIS area is provided in the following proposition¹:

¹In previous works about stochastic geometry-based RIS-assisted network model, the works in [18, 19, 22] have only considered the scenario that the distance between the UE and RIS is much shorter than the distance

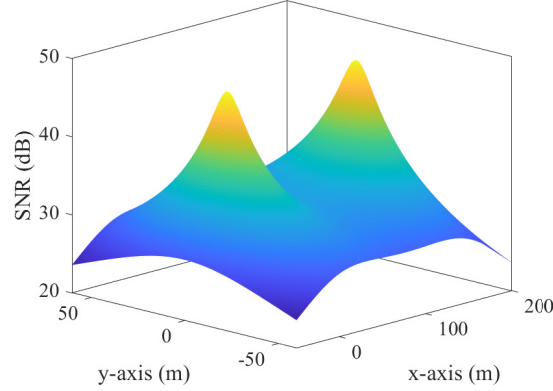


Fig. 5.5 The SNR of the received signal when the RIS is located at (x, y) . The locations of the UE and the BS are $(0, 0)$ and $(150, 0)$, respectively.

Proposition 1. For the RIS-assisted transmission, given the SNR threshold T , the RIS area can be formulated as:

$$\{(r \cos \beta, r \sin \beta) | r \geq 0, \beta \in (0, 2\pi], r^4 + br^3 \cos \beta + cr^2 + dr \cos \beta + u \geq 0\}, \quad (7)$$

where r is the horizontal distance between the RIS and the UE, β is the horizontal angle between the BS and the RIS at the UE, $b = -2R_b$, $c = R_b^2 + (h_b - h_r)^2 + (h_r - h_u)^2$, $d = -2(h_r - h_u)^2 R_b$ and $u = R_b^2(h_r - h_u)^2 + (h_r - h_u)^2(h_b - h_r)^2 - \left(\frac{P_t N_r^2 G_t M_d^2 N_d^2 l_u^2 \mu^2 \rho^2}{64\pi^3 w_0 T}\right)^{\frac{2}{\alpha}}$.

The SNR of the received signal when the RIS is located at (x, y) is shown in Fig. 5.5, where the locations of the UE and the BS are $(0, 0)$ and $(150, 0)$, respectively. The RIS area in Proposition 1 is the 2D graphic derived from Fig. 5.5 with a given SNR threshold. With different SNR threshold T , the RIS area is a various irregular graphic (e.g., Fig. 5.6-5.9), which is very difficult to be adopted for the network coverage analysis. Therefore, for the simplicity of analysis, circle/circles centered on the UE and BS are adopted to represent the upper/lower bounds of the RIS area. The principles of drawing the RIS area upper/lower bounds are: 1) the centers of the circles for the upper and lower bounds must be the UE or BS; 2) for lower bound, the circle/circles must be contained in the RIS area and cannot be

between the UE and BS, so that the distances from the BS to RIS and to UE can be assumed to be approximately the same, which is less accurate. Some other works [25–27] have calculated coverage/outage probability based on numerical integrals by integrating the distances. Different from previous works, we propose a novel approach to derive the upper and lower bounds of the coverage probability based on the RIS area.

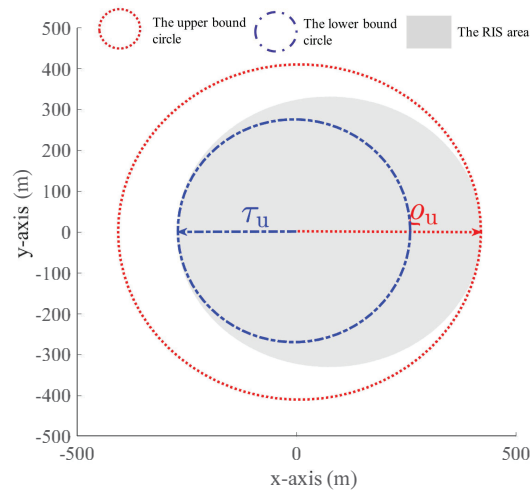


Fig. 5.6 The RIS area when the SNR threshold $T = 7\text{dB}$.

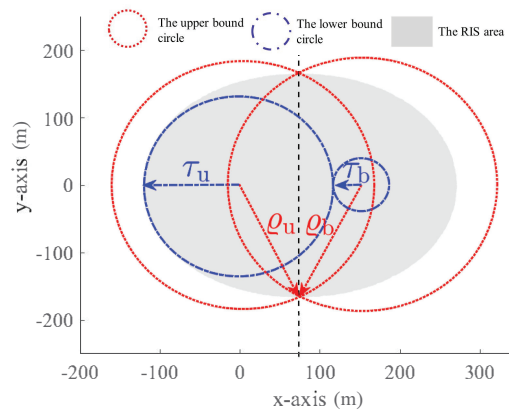


Fig. 5.7 The RIS area when the SNR threshold $T = 18\text{dB}$.

overlapped with each other if there are two circles; 3) for upper bound, the circle/circles need to be large enough to cover all the RIS area. Based on these principles, the shapes of the RIS area are classified into four typical scenarios. As the SNR threshold T increases, the four typical scenarios are shown as the grey area in Fig. 5.6-5.9:

In Fig. 5.6, a circle, which centered on the UE and has radius τ_u just large enough to be contained within the RIS area, is employed for the lower bound of the RIS area. Meanwhile, a circle, which centered on the UE and has the radius ρ_u just large enough to cover the RIS area, is adopted for the upper bound of the RIS area.

In Fig. 5.7, two circles within the RIS area are adopted for the lower bound of the RIS

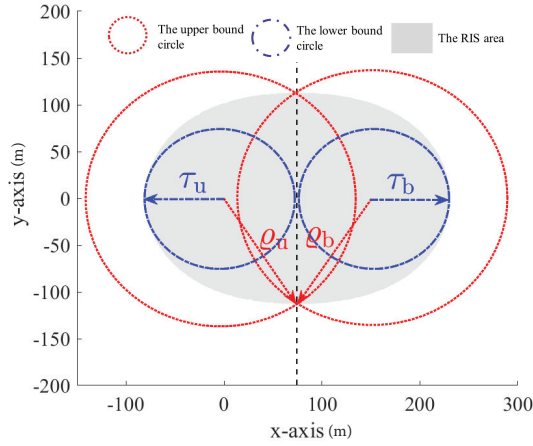


Fig. 5.8 The RIS area when the SNR threshold $T = 23\text{dB}$.

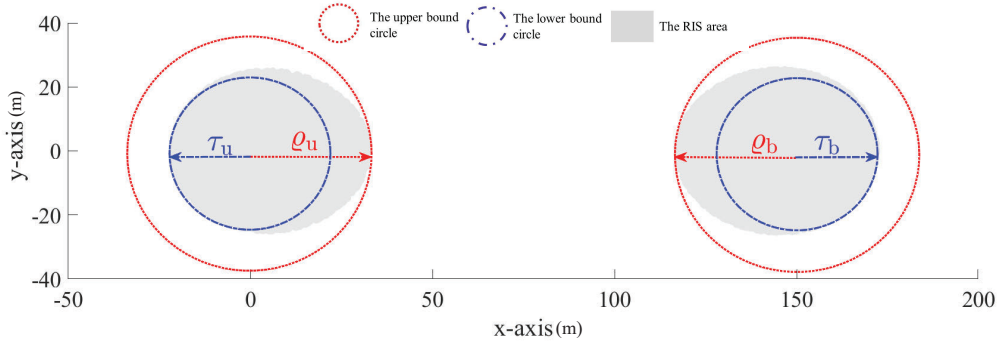


Fig. 5.9 The RIS area when the SNR threshold $T = 36\text{dB}$.

area. Specifically, one circle is centered on the UE and has radius τ_u just large enough to be contained within the RIS area; the other circle is centered on the BS and has radius τ_b satisfying $\tau_b = R_b - \tau_u$. Meanwhile, two circles, one is centered on the UE and the other is centered on the BS, with the radii ρ_u and ρ_b just large enough to cover the whole RIS area, are adopted for the upper bound of the RIS area. The radii of the circles satisfy $\rho_u = \rho_b$.

In Fig. 5.8 and Fig. 5.9, two circles, one is centered on the UE and the other is centered on the BS, with radii τ_u and τ_b just large enough to be contained within the RIS area, are employed for the lower bound of the RIS area. Meanwhile, two circles, one is centered on the UE and the other is centered on the BS, with the radii ρ_u and ρ_b just large enough to cover the whole RIS area, are adopted for the upper bound of the RIS area. Note that $\rho_u = \rho_b$ in Fig. 5.8.

In Fig. 5.9, there is the other scenario of the RIS area, which is: when the SNR threshold is high enough, the locations of the UE and the BS are not covered by the RIS area. In this case, depending on whether the RIS area is on the UE side or BS side, a circular ring centered on the UE (BS) with the small radius ρ_{u1} (ρ_{b1}) and the large radius ρ_{u2} (ρ_{b2}) is employed for the upper bound of the RIS area. Meanwhile, the lower bound of the RIS area does not exist, which means the lower bound of coverage probability is 0.

Moreover, Lemma 1 presents the radii of the circles or circular rings for the upper and lower bounds of the RIS area.

Lemma 1. *The radii of the circles for the RIS area lower and upper bound, i.e., τ_u , τ_b , ρ_u and ρ_b , are decided by the following parameters:*

$$\left\{ \begin{array}{l} \Delta = B^2 - 4AC, \\ A = D^2 - 3F, \\ B = DF - 9E^2, \\ C = F^2 - 3DE^2, \\ D = 3b^2 - 8c, \\ E = -b^3 + 4bc - 8d, \\ F = 3b^4 + 16c^2 - 16b^2c + 16bd - 64u. \end{array} \right.$$

(I) When $\Delta < 0$ and $D > 0$ and $F > 0$,

$$\left\{ \begin{array}{ll} \rho_u = \tilde{x}_2, \tau_u = |\tilde{x}_1|, & \tilde{x}_1 < 0, \\ \rho_{u1} = \tilde{x}_1, \rho_{u2} = \tilde{x}_2, \tau_u = 0, & \tilde{x}_1 \geq 0. \end{array} \right.$$

$$\left\{ \begin{array}{ll} \rho_{b1} = R_b - \tilde{x}_4, \rho_{b2} = R_b - \tilde{x}_3, \tau_b = 0, & \tilde{x}_4 \leq R_b, \\ \rho_b = R_b - \tilde{x}_3, \tau_b = \tilde{x}_4 - R_b, & \tilde{x}_4 > R_b, \end{array} \right.$$

Table 5.1 $\rho_u, \rho_b, \tau_b, \tau_u$ when $\Delta = 0, AB > 0$ and $C \neq 0$

Case	Condition	$\rho_u \vee (\rho_{u1}, \rho_{u2})$	$\rho_b \vee (\rho_{b1}, \rho_{b2})$	τ_b	τ_u
1	$x_1 < 0$	$\rho_u = x_2$	$\rho_b = 0$	0	$ x_1 $
2	$x_1 \geq 0, x_2 < R_b/2$	$\rho_{u1} = x_1, \rho_{u2} = x_2$	$\rho_b = 0$	0	0
3	$x_1 \geq R_b/2, x_2 < R_b$	$\rho_u = 0$	$\rho_{b1} = R_b - x_2, \rho_{b2} = R_b - x_1$	0	0
4	$x_2 \geq R_b$	$\rho_u = 0$	$\rho_b = R_b - x_1$	$x_2 - R_b$	0

Table 5.2 $\rho_u, \rho_b, \tau_b, \tau_u$ when $\Delta > 0, x_1 < 0$ and $x_2 > R_b$

Case	Condition	ρ_u	ρ_b	τ_b	τ_u
1	$ x_1 \geq R_b$	x_2	0	0	$ x_1 $
2	$ x_1 < R_b$	$\begin{cases} x_1 + x_2 \geq 2R_b \\ x_1 + x_2 < 2R_b \end{cases}$	$\sqrt{\frac{-\sigma + \sqrt{\sigma^2 - 4\chi}}{2}} + \frac{R_b^2}{4}$	$\begin{cases} x_2 - R_b \\ R_b - x_1 \end{cases}$	

where $\{\tilde{x}_1, \tilde{x}_2, \tilde{x}_3, \tilde{x}_4\} = \{x_1, x_2, x_3, x_4\}$ and $\tilde{x}_1 < \tilde{x}_2 < \tilde{x}_3 < \tilde{x}_4$.

$$\begin{cases} x_1, x_2 = \frac{-b + \text{sgn}(E)y_1^{1/2} \pm (y_2^{1/2} + y_3^{1/2})}{4}, \\ x_3, x_4 = \frac{-b - \text{sgn}(E)y_1^{1/2} \pm (y_2^{1/2} - y_3^{1/2})}{4}. \end{cases}$$

$$\begin{cases} y_1 = \frac{D - 2A^{1/2} \cos \frac{\Theta}{3}}{3}, \\ y_2 = \frac{D + A^{1/2} (\cos \frac{\Theta}{3} + \sqrt{3} \sin \frac{\Theta}{3})}{3}, \\ y_3 = \frac{D + A^{1/2} (\cos \frac{\Theta}{3} - \sqrt{3} \sin \frac{\Theta}{3})}{3}. \end{cases}$$

where $\Theta = \arccos \frac{3B - 2AD}{2A^{3/2}}$.

(II) When $\Delta = 0$ and $AB > 0$ and $C \neq 0$, ρ_u, ρ_b, τ_b and τ_u are shown in Table 5.1, where

$$x_1, x_2 = \frac{-b + 2AE/B \pm \sqrt{2B/A}}{4} \quad (x_1 < x_2).$$

(III) When $\Delta > 0$: when $x_1 < 0$ and $x_2 > R_b$, ρ_u, ρ_b, τ_b and τ_u are shown in Table 5.2;

Table 5.3 $\rho_u, \rho_b, \tau_b, \tau_u$ when $\Delta > 0$ (except the case that $x_1 < 0$ and $x_2 > R_b$)

Case	Condition	$\rho_u \vee (\rho_{u1}, \rho_{u2})$	$\rho_b \vee (\rho_{b1}, \rho_{b2})$	τ_b	τ_u
1	$x_1 < 0, x_2 < R_b$	$\rho_u = x_2$	$\rho_b = 0$	0	$ x_1 $
2	$x_1 \geq 0, x_2 < R_b/2$	$\rho_{u1} = x_1, \rho_{u2} = x_2$	$\rho_b = 0$	0	0
3	$x_1 \geq R_b/2, x_2 < R_b$	$\rho_u = 0$	$\rho_{b1} = R_b - x_2, \rho_{b2} = R_b - x_1$	0	0
4	$x_1 \geq 0, x_2 \geq R_b$	$\rho_u = 0$	$\rho_b = R_b - x_1$	$x_2 - R_b$	0

otherwise, ρ_u, ρ_b, τ_b and τ_u are shown in Table 5.3. The expression of each parameter is:

$$\left\{ \begin{array}{l} x_1, x_2 = \frac{1}{4} \left(-b + \text{sgn}(E) \sqrt{(D + \sqrt[3]{z_1} + \sqrt[3]{z_2})/3} \pm \sqrt{(2D - (\sqrt[3]{z_1} + \sqrt[3]{z_2}) + 2\sqrt{z})/3} \right), (x_1 < x_2), \\ \sigma = \frac{R_b^2}{2} + (h_b - h_r)^2 + (h_r - h_u)^2, \\ \chi = \left(\frac{R_b^2}{4} + (h_b - h_r)^2 \right) \left(\frac{R_b^2}{4} + (h_r - h_u)^2 \right) - \left(\frac{P_t N_t^2 G_t M_d^2 N_d^2 l_u^2 \mu^2 \rho^2}{64\pi^3 w_0 T} \right)^{\frac{2}{\alpha}}, \\ z_1, z_2 = AD + 3 \left(\frac{-B \pm \sqrt{B^2 - 4AC}}{2} \right), \\ z = D^2 - D(\sqrt[3]{z_1} + \sqrt[3]{z_2}) + (\sqrt[3]{z_1} + \sqrt[3]{z_2})^2 - 3A. \end{array} \right.$$

(IV) Otherwise, $\tau_u = 0, \tau_b = 0, \rho_u = 0$ and $\rho_b = 0$.

Proof: See Appendix I

3.2 The Probability for LoS Transmission

For RIS-assisted transmission, since the transmission between the BS and the RIS always be LoS, whether the RIS-assisted transmission is blocked or unblocked depends on whether or not any blockages are located between the RIS and the UE. Indirect LoS RIS-assisted transmission exists if no blockage is located between the RIS and the UE. The probability for LoS transmission with the horizontal distance r is provided in Lemma 2.

Lemma 2. *Given the horizontal transmission distance r , the probability that the transmission is LoS is expressed by:*

$$p_u(r) = \begin{cases} e^{\nu r - \varpi}, & r \leq d_s, \\ (1 - \frac{\theta}{2\pi})e^{\nu r - \varpi}, & \text{otherwise.} \end{cases} \quad (8)$$

where $\nu = -d_h \lambda_h \frac{h_h - h_u}{h_r - h_u} - \psi$ when the transmission is from the RIS to the UE, and $\nu = -d_h \lambda_h \frac{h_h - h_u}{h_b - h_u} - \psi$ when the transmission is from the BS to the UE.

Proof.

$$p_u(r) = p_{nu}(r)p_{su}(r)p_{bu}(r) = \begin{cases} e^{(-d_h \lambda_h \frac{h_h - h_u}{h_r - h_u} - \psi)r - \varpi}, & r \leq d_s, \\ (1 - \frac{\theta}{2\pi})e^{(-d_h \lambda_h \frac{h_h - h_u}{h_r - h_u} - \psi)r - \varpi}, & \text{otherwise.} \end{cases} \quad (9)$$

□

Based on Lemma 2, when the RISs are randomly distributed within a circle or a circular ring, the probability that the indirect LoS RIS-assisted transmission exists is presented in Lemma 3.

Lemma 3. *When RISs are randomly located within the circle centered on the UE with radius R_t , the probability that the indirect LoS RIS-assisted transmission exists can be expressed as:*

$$\Phi_{uc}(R_t) = \begin{cases} 1 - e^{\gamma_1 \varepsilon_1 - \gamma_1}, & R_t < d_s, \\ e^{-\gamma_1} (e^{\gamma_1 (\varepsilon_2 + \zeta_1)} - e^{\gamma_1 (\eta_1 + \kappa_1)}), & R_t \geq d_s, \end{cases} \quad (10)$$

where

$$\left\{ \begin{array}{l} \gamma_1 = \pi R_t^2 \lambda_r, \\ \varepsilon_1 = 1 - \frac{2e^{-\varpi} (1 + e^{\nu R_t} (\nu R_t - 1))}{\nu^2 R_t^2}, \\ \varepsilon_2 = \frac{d_s^2}{R_t^2}, \\ \zeta_1 = \frac{R_t^2 - d_s^2}{R_t^2}, \\ \eta_1 = \frac{d_s^2}{R_t^2} - \frac{2e^{-\varpi} (1 + e^{\nu d_s} (\nu d_s - 1))}{\nu^2 R_t^2}, \\ \kappa_1 = f_1(R_t, d_s) = \frac{R_t^2 - d_s^2}{R_t^2} - \frac{2(1 - \frac{\theta}{2\pi}) e^{-\varpi} (e^{\nu d_s} (1 - \nu d_s) + e^{\nu R_t} (\nu R_t - 1))}{\nu^2 R_t^2}; \end{array} \right.$$

When the RISs are randomly located within the circle centered on the BS with radius R_t , the probability that the indirect LoS RIS-assisted transmission exists can be expressed as:²

$$\Phi_{bc}(R_t) = 1 - e^{\gamma_1 \varepsilon_3 - \gamma_1}, \quad (11)$$

where

$$\left\{ \begin{array}{l} \varepsilon_3 = f_2(R_t, 0), \\ f_2(x, y) = \frac{x^2 - y^2}{x^2} - (1 - \frac{\theta}{2\pi}) \frac{2}{\pi x^2} \int_0^\pi \int_0^x r e^{\nu \sqrt{R_b^2 + r^2 - 2R_b r \cos \beta} - \varpi} dr d\beta; \end{array} \right.$$

When RISs are randomly located within the circular ring centered on the UE with small radius R_{t1} and large radius R_{t2} , the probability that indirect LoS RIS-assisted transmission

²For simplicity of analysis, when the RISs are randomly located within a circle (or a circular ring) centered on the BS, the probability that the transmission from the RIS to the UE is unblocked by self-body blockage is always $1 - \frac{\theta}{2\pi}$. This is reasonable since the distance between the RIS and the UE is longer than d_s in most cases.

exists is:

$$\Phi_{\text{ur}}(R_{t1}, R_{t2}) = \begin{cases} e^{\gamma_2 \varepsilon_4 - \gamma_2} (e^{\gamma_2 \zeta_2} - e^{\gamma_2 \eta_2}), & R_{t1} < R_{t2} < d_s, \\ e^{\gamma_2 \varepsilon_4 - \gamma_2} (e^{\gamma_2 (\xi_1 + \zeta_3)} - e^{\gamma_2 (\eta_3 + \kappa_2)}), & R_{t1} < d_s \leq R_{t2}, \\ e^{\gamma_2 \varepsilon_4 - \gamma_2} (e^{\gamma_2 \zeta_2} - e^{\gamma_2 \eta_4}), & d_s \leq R_{t1} < R_{t2}, \end{cases} \quad (12)$$

where

$$\left\{ \begin{array}{l} \gamma_2 = \pi R_{t2}^2 \lambda_r, \\ \varepsilon_4 = \frac{R_{t1}^2}{R_{t2}^2}, \\ \zeta_2 = \frac{R_{t2}^2 - R_{t1}^2}{R_{t2}^2}, \\ \eta_2 = g(R_{t2}, R_{t1}) = \frac{R_{t2}^2 - R_{t1}^2}{R_{t2}^2} - \frac{2e^{-\alpha} (e^{\nu R_{t1}} (1 - \nu R_{t1}) + e^{\nu R_{t2}} (\nu R_{t2} - 1))}{\nu^2 R_{t2}^2}, \\ \xi_1 = \frac{d_s^2 - R_{t1}^2}{R_{t2}^2}, \\ \zeta_3 = \frac{R_{t2}^2 - d_s^2}{R_{t2}^2}, \\ \eta_3 = g(d_s, R_{t1}), \\ \kappa_2 = f_1(R_{t2}, d_s), \\ \eta_4 = f_1(R_{t2}, R_{t1}); \end{array} \right.$$

When the RISs are randomly located within the circular ring centered on the BS with the small radius R_{t1} and the large radius R_{t2} , the probability that the indirect LoS RIS-assisted transmission exists is:

$$\Phi_{\text{br}}(R_{t1}, R_{t2}) = e^{\gamma_2 \varepsilon_4 - \gamma_2} (e^{\gamma_2 \zeta_2} - e^{\gamma_2 \eta_5}), \quad (13)$$

where $\eta_5 = f_2(R_{t2}, R_{t1})$.

Proof. See Appendix II

□

Furthermore, the lower bound and upper bound of the coverage probability of the RIS-assisted network without considering the direct transmission are presented in the following Theorem.

Theorem 1. *The lower bound of the coverage probability of the RIS-assisted transmission is expressed as:*

$$\Psi_l = \Phi_{uc}(\tau_u) + \Phi_{bc}(\tau_b). \quad (14)$$

The upper bound of the coverage probability of the RIS-assisted transmission is expressed as:

$$\Psi_u = \Phi_{uc}(\rho_u) + \Phi_{bc}(\rho_b). \quad (15)$$

Note that if circular rings are adopted instead of circles for the upper bound of the RIS area, $\Phi_{uc}(\rho_u)$ and $\Phi_{bc}(\rho_b)$ are changed to $\Phi_{ur}(\rho_{u1}, \rho_{u2})$ and $\Phi_{br}(\rho_{b1}, \rho_{b2})$, respectively.

Proof. The expressions of the radii τ_u , τ_b , ρ_u , ρ_b , ρ_{u1} , ρ_{u2} , ρ_{b1} and ρ_{b2} have been given in Lemma 1. The functions $\Phi_{uc}(\cdot)$, $\Phi_{bc}(\cdot)$, $\Phi_{ur}(\cdot)$ and $\Phi_{br}(\cdot)$ have been given in Lemma 3. The detailed derivations are presented in Appendix I and Appendix II. \square

Corollary 1.1 If the direct transmission between the BS and the UE is considered and $P_{rb}/w_0 \geq T$, then the lower bound and upper bound of the coverage probability of the RIS-assisted network are computed by:

$$\tilde{\Psi}_l = p_u(R_b) + \Psi_l - p_u(R_b)\Psi_l. \quad (16)$$

$$\tilde{\Psi}_u = p_u(R_b) + \Psi_u - p_u(R_b)\Psi_u. \quad (17)$$

Proof. The coverage probability is one minus the probability of outage. Outage happens if neither the direct transmission nor the RIS-assisted transmission succeeds. Hence, the lower bound of the coverage probability can be derived from:

$$\tilde{\Psi}_l = 1 - (1 - p_u(R_b))(1 - \Psi_l). \quad (18)$$

The upper bound of the coverage probability can be derived by changing Ψ_1 to Ψ_u in equation (18). \square

The lower and upper bounds of the coverage probability are functions of network parameters, building blockage density and nearby-user blockage density. Based on these analytical results, the coverage probability of RIS-assisted networks under various scenarios can be evaluated.

3.3 Special Case: RISs Are Much Closer To UE Than BS

In this subsection, we focus on a common scenario where the horizontal distance between the connected RIS and UE is much shorter than the horizontal distance between the BS and UE [18, 19, 22], i.e., $r_k \ll R_b$. In this scenario, the horizontal distance between the BS and connected RIS can be approximated as the same as the horizontal distance between the BS and UE, i.e., $l_k \approx R_b$. With a given SNR threshold T , the radius R_u of the RIS area can be derived from $P_{rr}/w_0 \geq T$, which is express by:

$$R_u = \sqrt{\frac{1}{R_b^2 + (h_b - h_r)^2} \left(\frac{Z}{Tw_0}\right)^{\frac{2}{\alpha}} - (h_r - h_u)^2}, \quad (19)$$

where $Z = \frac{P_t N_t^2 G_t M_d^2 N_d^2 I_u^2 \mu^2 \rho^2}{64\pi^3}$. Note that outage happens if $\frac{1}{R_b^2 + (h_b - h_r)^2} \left(\frac{Z}{Tw_0}\right)^{\frac{2}{\alpha}} < (h_r - h_u)^2$. Moreover, considering nearby-user blockages and building blockages, the coverage probability can be derived based on equation (10) in Lemma 3, which is presented in the following lemma:

Lemma 4. *When the horizontal distance between the connected RIS and UE is much shorter than the distance between the BS and UE, i.e., $R_u \ll R_b$ ³, the closed-form coverage probability of the RIS-assisted network can be expressed by:*

$$\Psi_a = 1 - \exp\left(\pi R_u^2 \lambda_r \left(1 - \frac{2e^{-\varpi} (1 + e^{\nu R_u} (\nu R_u - 1))}{\nu^2 R_u^2}\right) - \pi R_u^2 \lambda_r\right), \quad (20)$$

³The value of R_u is decided by different parameters, e.g., RIS size, SNR threshold T , and horizontal distance R_b between BS and UE. $R_u \ll R_b$ can be satisfied in various scenarios, e.g., relatively small RIS size, relatively high SNR threshold T , or relatively long horizontal distance R_b between BS and UE.

where R_u is decided by the SNR threshold T , $\nu = -d_h \lambda_h \frac{h_h - h_u}{h_r - h_u} - 2\lambda_b(W + L)/\pi$ and $\varpi = \lambda_b LW$ are decided by the size, height and density of the blockages, including nearby-user blockages and building blockages.

3.4 Cost Effectiveness

Even the total number of unit cells is the same, the cost of RIS implementation might be different with different number of RISs. Specifically, the costs of RIS implementation, land acquisition, channel estimation and signal processing might be increasing with the number of RISs. However, it is unclear whether the total cost linearly growth with the number of RISs or not, especially when the number of unit cells decreases as the number of RISs increases. Therefore, in this paper, we propose a general model for the total cost of RIS implementation as a function of n (as mentioned in system model, n is the number of RISs divided from the total number of unit cells). The equation is presented as follows:

$$C_{\text{ost}} = c_{\text{ost}} n^\zeta, \quad (21)$$

where c_{ost} and ζ are the cost indexes decided by the industry, particularly, ζ is the exponent to indicate how the number of RISs affects the total cost, e.g., $\zeta = 1$ means that the total cost grows linearly with the number of RISs, while $\zeta = 0$ means that the total cost is fixed despite of the number of RISs.

4 Numerical Results

In this section, the coverage probability of RIS-assisted wireless networks is analyzed and the analytical results are validated via Monte Carlo simulations. As mentioned in the system model, the parameter n decides both the RIS density and the RIS size. Under various scenarios, i.e., different building density, human density, transmission distance and SNR threshold, the optimal value of n which leads to the highest coverage probability is different. The optimal values of n under various scenarios are discussed in the following analysis. The

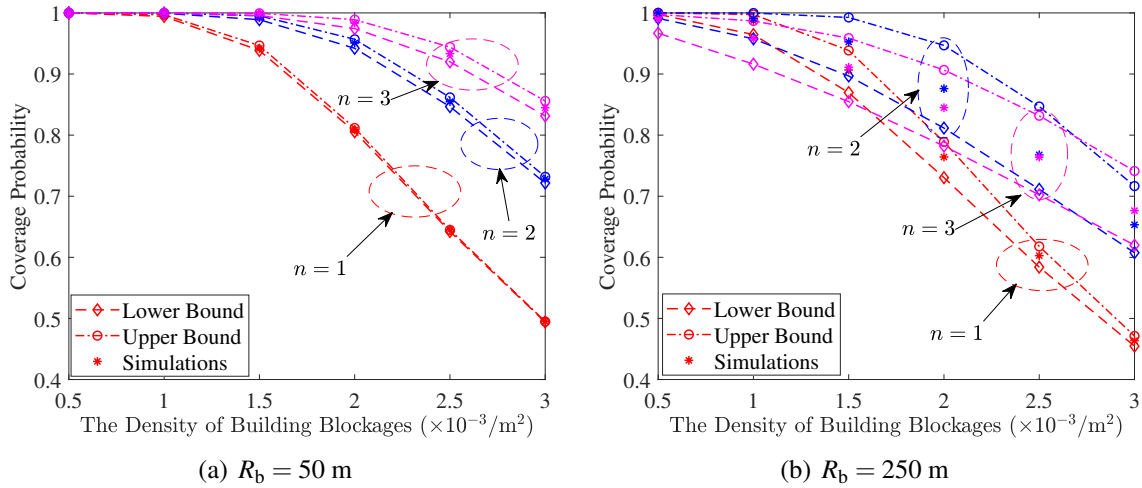


Fig. 5.10 The coverage probability versus the density of building blockages for different distance between the BS and the UE.

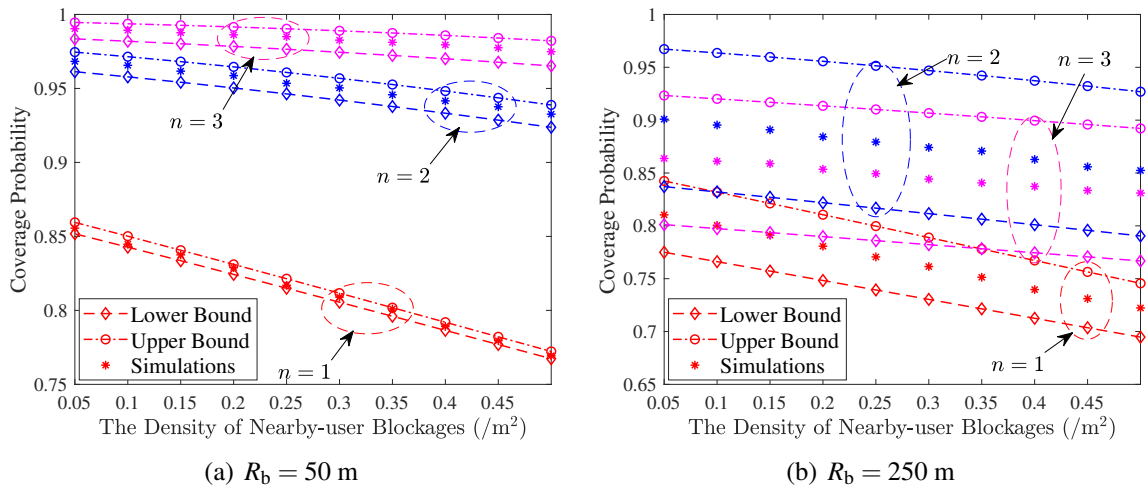


Fig. 5.11 The coverage probability versus the density of nearby-user blockages for different distance between the BS and the UE.

Table 5.4 Simulation Parameters

parameter	value	parameter	value
M	50	N	50
N_t	128	h_r	15 m
h_b	30 m	h_u	1.3 m
h_h	1.7 m	d_h	0.4 m
λ_h	0.3 /m ²	d_u	0.1 m
θ	$\pi/3$	λ_b	2×10^{-3} /m ²
λ_r'	5×10^{-4} /m ²	L	15 m
W	10 m	α	2
μ	0.01 m	P_t	1 W
G_t	1	ρ	0.9
l_u	0.005 m	w_0	-90 dBm
T	20 dB	R_b	250 m

system parameters are shown in Table 5.4 if not mentioned otherwise. Similar settings of simulation parameters can be found in [19, 20, 17, 37, 38].

In Fig. 5.10, the coverage probabilities to the building blockage density are shown. In each subfigure, different distance between the BS and the UE is applied, and the comparison between different values of n is demonstrated. Firstly, the analytical results are validated by showing that both lower bound and upper bound have the same trend as the simulation results. Secondly, it is indicated that the density of building blockages has less impact on the coverage probability with larger n . The reason is that higher value of n leads to higher RIS density, moreover, higher probability for the transmission to be unblocked. Thirdly, as the distance between the BS and the UE rises, the coverage probability with larger n decreases faster than the coverage probability with smaller n . The reason is that larger n means smaller size of RISs, which leads to lower received signal power gain and is more sensitive to the increase of transmission distance. For these reasons, when $R_b = 50$ m, the RIS-assisted networks with $n = 3$ have the highest coverage probability. However, when $R_b = 250$ m and $\lambda_b \leq 2.7 \times 10^{-3}$ /m², the networks with $n = 2$ have the highest coverage; and when $R_b = 250$ m and $\lambda_b > 2.7 \times 10^{-3}$ /m², the RIS-assisted networks with $n = 3$ have the highest coverage probability. As a result, large n is suitable for high building blockage density and/or short transmission distance, e.g., urban area, whereas small n is more applicable for low

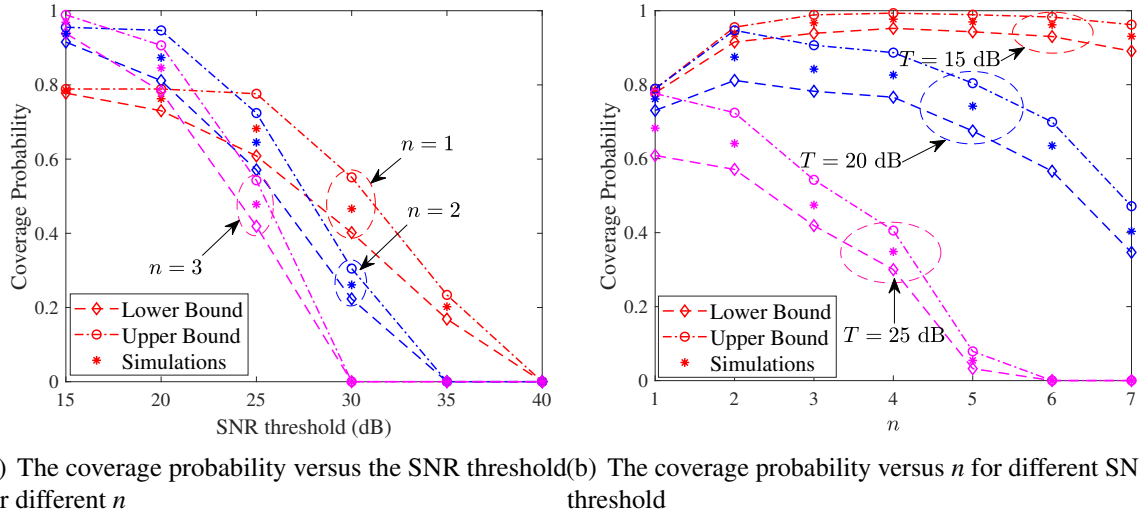
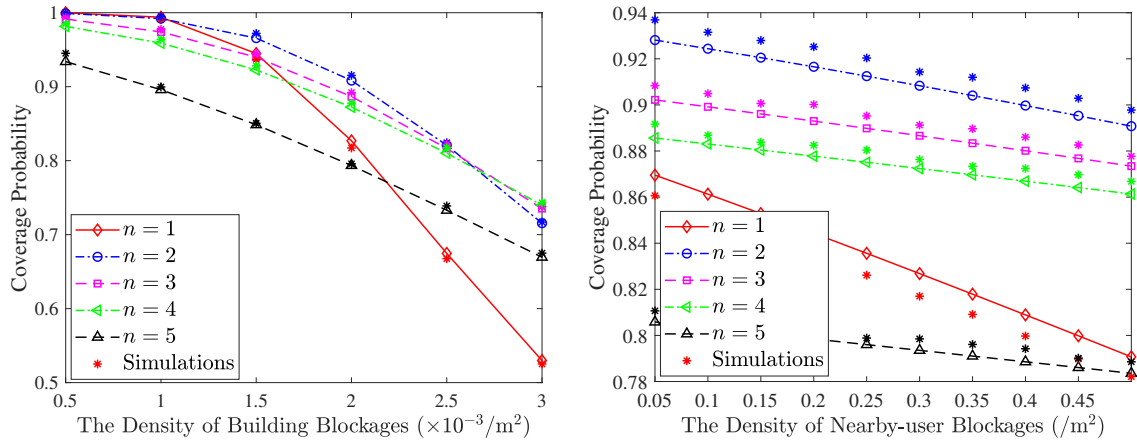


Fig. 5.12 The coverage probability versus the SNR threshold and n .

building blockage density and/or long transmission distance, e.g., rural area. In addition, in the same cell of a BS, small-scale RISs are preferable to be deployed around the cell center, while large-scale RISs are preferable to be deployed in the cell edge.

Fig. 5.11 shows the effect of the nearby-user blockages on the coverage probability. Fig. 5.11 (a) shows that when the horizontal transmission distance $R_b = 50$ m, $n = 3$ has the highest coverage. However, in Fig. 5.11 (b), when the horizontal transmission distance increases to 250 m, $n = 2$ has the highest coverage, and as the nearby-user blockage density rises to $0.5 / \text{m}^2$, $n = 2$ and $n = 3$ have almost the same coverage. Fig. 5.11 indicates that the networks with larger n are less sensitive to the increase of the nearby-user blockage density. In addition, increasing n can be more beneficial for the case with high nearby-user density. Consequently, large n is more applicable for the places which deploy small-cell networks and have high human density, e.g., malls and airports.

In Fig. 5.12, the impact of SNR threshold on the coverage probability is illustrated. When the SNR threshold is relatively low, e.g., below 20 dB, small-size RISs can provide enough received signal power gain to meet the SNR threshold. Hence, the coverage probability is mainly affected by blockages. In other words, the blockage probability is dominant in the impact on the coverage probability. Therefore, large n is preferable when SNR threshold is



(a) The coverage probability versus the density of building blockages for different n

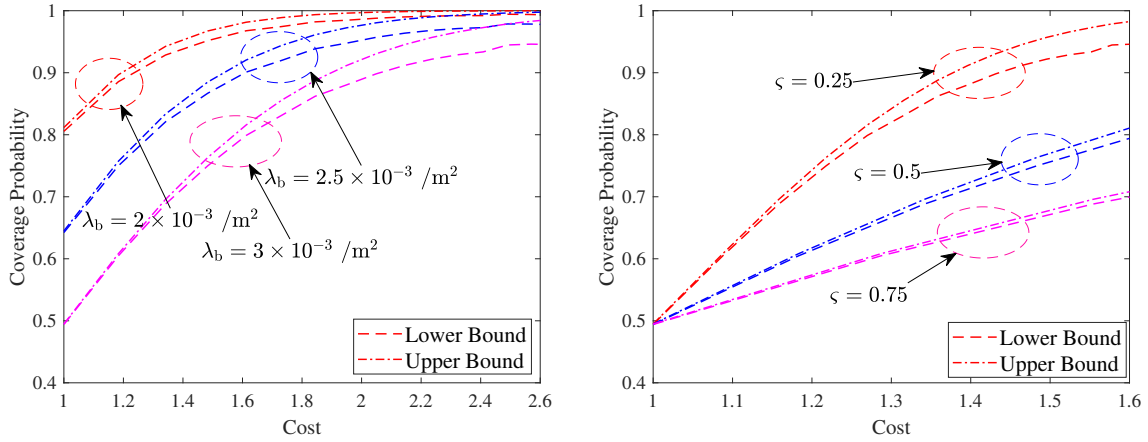
(b) The coverage probability versus the density of nearby-user blockages for different n

Fig. 5.13 The coverage probability when RISs are much closer to the UE than the BS.

low, e.g., in Fig. 5.12 (b), $n = 4$ has the highest coverage probability when the SNR threshold $T = 15$ dB. However, as the SNR threshold rises, only large-size RISs can provide enough received signal power gain to meet the SNR threshold. In other words, the received signal power gain becomes dominant in the coverage probability. Accordingly, small n is more suitable for the networks with high SNR threshold, e.g., $n = 1$ leads to the highest coverage when $T = 25$ dB.

In Fig. 5.13, the coverage probabilities of RIS-assisted network when RISs are much closer to the UE than the BS are shown. The analytical results match with simulations well, and small gaps exist because of the approximation in which the horizontal distance between the BS and connected RIS is equal to the horizontal distance between the BS and UE. In both Fig. 5.13 (a) and (b), $n = 2$ leads to the highest coverage probability except when building blockage density rises to around $2.7 \times 10^{-3} / \text{m}^2$. In addition, as blockage density increases, coverage with low value of n drops faster than coverage with high value of n . Fig. 5.13 further demonstrates that densely deployed small-scale RISs outperform sparsely deployed large-scale RISs in scenarios with dense blockages in terms of coverage enhancement.

In Fig. 5.14, the function of coverage probability to cost is illustrated. Fig. 5.14 (a) shows that the coverage probability and the cost increase as the number of RISs grows.



(a) The coverage probability versus the cost for different building density λ_b . $\zeta = 0.5$.
 (b) The coverage probability versus the cost for different cost exponent ζ . $\lambda_b = 3 \times 10^{-3} / \text{m}^2$.

Fig. 5.14 Cost effectiveness: the function of coverage probability to cost for different cost exponent ζ . $R_b = 50$ m.

Particularly, with the same amount of cost increase, higher building density causes larger growth of coverage probability. Fig. 5.14 (b) indicates the impact of the cost exponent on the coverage probability. The results show that high value of cost exponent leads to low cost effectiveness of densely deployed small-scale RISs, e.g., even in the environment with densely deployed blockages, when $\zeta = 0.75$, 60% cost growth causes only 40% coverage enhancement. Therefore, lower cost exponent leads to higher cost effectiveness when densely deployed small-scale RISs are deployed, while higher cost exponent causes higher cost effectiveness when sparsely deployed large-scale RISs are deployed.

Summary of Insights

According to the analysis of numerical results, the main insights are summarized as follows:

- For a given total number of passive elements, the RIS density and RIS size decide the tradeoff between blockage probability and path loss.
- Blockage density has more impact on coverage probability when sparsely deployed large-scale RISs are deployed, while transmission distance has more impact on coverage probability when densely deployed small-scale RISs are deployed.

- In the same cell of a BS, small-scale RISs are preferable to be deployed around the cell center to decrease blockage probability, while large-scale RISs are preferable to be deployed in the cell edge to decrease blockage probability and compensate path loss.
- Densely deployed small-scale RISs are better option when SNR threshold is relatively low, while sparsely deployed large-scale RISs win when SNR threshold is relatively high.
- Cost effectiveness of densely deployed small-scale RISs depends on how the number of RISs affects the network cost. If the cost grows linearly with the number of RISs, densely deployed small-scale RISs are not cost-effective even in the environment with densely deployed blockages.

5 Conclusion

In this paper, analytical results for RIS deployment strategy analysis considering both building blockages and human blockages have been provided. The proposed tractable upper and lower bounds of coverage probability closely match the trend of simulations, demonstrating their usefulness in replacing time-consuming simulation in RIS deployments. Moreover, the impact of building density, nearby-user density, transmission distance and SNR threshold on RIS-assisted mmWave network coverage was analyzed, respectively. The results showed that as the number of RISs grows, if the increase of network cost is below the linear increase at certain level, more small RISs are better option for high building blockage density and/or short transmission distance, e.g., urban area, whereas fewer large RISs are more suitable for low building blockage density and/or long transmission distance, e.g., rural area. In addition, if the network cost grows linearly with the number of RISs, densely deployed small-scale RISs are not a cost-effective option even in the environment with densely deployed blockages. Our works can be used as a guidance for practical RIS deployment in built environments where blockages are common.

Appendix I

Geometrically, whether it is the scenario in Fig. 5.9 or the scenarios in Fig. 5.6-5.8 depends on the number of intersections between the RIS area boundary and $y = 0$. For example, the number of intersections between the RIS area boundary and $y = 0$ is 2 in Fig. 5.6-5.8, and that is 4 in Fig. 5.9. Furthermore, if the number of intersections between the RIS area boundary and $y = 0$ is 2, then which scenario the RIS area belongs to depends on the distance between the 2 intersections. Mathematically, the number of intersections between the RIS area boundary and $y = 0$ equals to the number of real solutions of the equation (22), which is shown as follows:

$$r^4 + br^3 + cr^2 + dr + u = 0. \quad (22)$$

Equation (22) is derived from the equation (7) by letting $\cos \beta = 1$. We denote the number of real solutions of the equation (22) as ω . Moreover, let $\{x_1, \dots, x_\omega\}$ denote the real solutions of the equation (22). The absolute values of the real solutions $\{|x_1|, \dots, |x_\omega|\}$ represent the distances between the UE and the intersections. Since the UE is located at $(0, 0)$, x_1, \dots, x_ω are the X-axis coordinate values, and $x_1 < 0$ means that one of the intersection is in the X-axis negative direction of the UE. ω and $\{x_1, \dots, x_\omega\}$ can be found based on the discriminants Δ, A, B, C, D, E, F of the single variable quartic equation (22). Furthermore, the scenarios (I)-(III) in Lemma 1 are explained as follows:

(I) When $\Delta < 0$ and $D > 0$ and $F > 0$, $\omega = 4$ and the real solutions are $\{\tilde{x}_1, \tilde{x}_2, \tilde{x}_3, \tilde{x}_4\}$ ($\tilde{x}_1 < \tilde{x}_2 < \tilde{x}_3 < \tilde{x}_4$). The RIS area belongs to the scenario in Fig. 5.9.

(1) For the RIS area on the UE side:

when $\tilde{x}_1 < 0$, for the RIS area lower bound, a circle centered on the UE with radius $\tau_u = |\tilde{x}_1|$ is formed within the RIS area; for the RIS area upper bound, a circle centered on the UE with radius $\rho_u = \tilde{x}_2$ is formed to cover the RIS area;

when $\tilde{x}_1 \geq 0$, the location of the UE is not covered by the RIS area, hence, there is no circle centered on the UE for the RIS area lower bound, i.e., $\tau_u = 0$. And a circular ring centered on the UE with the small radius $\rho_{u1} = \tilde{x}_1$ and the large radius $\rho_{u2} = \tilde{x}_2$ is formed for the RIS area upper bound.

(2) For the RIS area on the BS side:

when $\tilde{x}_4 > 0$, for the RIS area lower bound, a circle centered on the BS with radius $\tau_b = \tilde{x}_4 - R_b$ is formed within the RIS area; for the RIS area upper bound, a circle centered on the BS with radius $\rho_b = R_b - \tilde{x}_3$ is formed to cover the RIS area;

when $\tilde{x}_4 \leq R_b$, the location of the BS is not covered by the RIS area, hence, there is no incircle centered on the BS for the RIS area lower bound, i.e., $\tau_b = 0$. And a circular ring centered on the BS with the small radius $\rho_{p1} = R_b - \tilde{x}_4$ and the large radius $\rho_{p2} = R_b - \tilde{x}_3$ is formed for the RIS area upper bound.

(II) When $\Delta = 0$ and $AB > 0$ and $C \neq 0$, $\omega = 4$ and there are 2 unequal real solutions $\{x_1, x_2\}$ ($x_1 < x_2$) and 2 equal real solutions, which means the SNR threshold T is high enough that the RIS area only cover one side (either the BS side or the UE side).

When $x_2 < R_b/2$, the RIS area is on the UE side, then:

(1) Case 1 in Table 5.1: when $x_1 < 0$, for the RIS area lower bound, a circle centered on the UE with radius $\tau_u = |x_1|$ is formed within the RIS area; for the RIS area upper bound, a circle centered on the UE with radius $\rho_u = x_2$ is formed to cover the RIS area;

(2) Case 2 in Table 5.1: when $x_1 \geq 0$, the location of the UE is not covered by the RIS area, hence, there is no incircle centered on the UE for the RIS area lower bound, i.e., $\tau_u = 0$. Meanwhile, a circular ring centered on the UE with the small radius $\rho_{u1} = x_1$ and the large radius $\rho_{u2} = x_2$ is formed for the RIS area upper bound;

When $x_1 \geq R_b/2$, the RIS area is on the BS side, then:

(3) Case 3 in Table 5.1: when $x_2 \leq R_b$, the location of the BS is not covered by the RIS area, hence, there is no incircle centered on the BS for the RIS area lower bound, i.e., $\tau_b = 0$. Meanwhile, a circular ring centered on the BS with the small radius $\rho_{b1} = R_b - x_2$ and the large radius $\rho_{b2} = R_b - x_1$ is formed for the RIS area upper bound;

(4) Case 4 in Table 5.1: when $x_2 > R_b$, for the RIS area lower bound, a circle centered on the BS with radius $\tau_b = x_2 - R_b$ is formed within the RIS area; for the RIS area upper bound, a circle centered on the BS with radius $\rho_b = R_b - x_1$ is formed to cover the RIS area;

(III) When $\Delta > 0$, $\omega = 2$ and the real solutions are $\{x_1, x_2\}$ ($x_1 < x_2$).

When $x_1 < 0$ and $x_2 > R_b$, a circle centered on UE with radius $\tau_u = |x_1|$ is formed within the

RIS area for the RIS area lower bound. Then:

Case 1 in Table 5.2: when $|x_1| \geq R_b$, the RIS area belongs to the scenario in Fig. 5.6. For the RIS area upper bound, a circle centered on the UE with radius $\rho_u = x_2$ is formed to cover the RIS area. In addition, no circle centered on the BS is formed since the location of the BS has already been covered by the circle centered on UE with radius τ_u ;

Case 2 in Table 5.2: when $|x_1| < R_b$, the RIS area belongs to the scenarios in Fig. 5.7 and Fig. 5.8. The radii of the circle for the RIS area upper bound are equal to the distance from the UE/BS to $(\frac{R_b}{2}, y_p)$. Note that $(\frac{R_b}{2}, y_p)$ and $(\frac{R_b}{2}, -y_p)$ are the intersections of the RIS area boundary and $x = R_b/2$, where y_p can be found by solving the following equation:

$$\frac{P_t N_t^2 G_t M^2 N^2 l_u^2 \mu^2 \rho^2}{64\pi^3 \left(\left(\frac{R_b}{2} \right)^2 + y_p^2 + (h_b - h_r)^2 \right)^{\frac{\alpha}{2}} \left(\left(\frac{R_b}{2} \right)^2 + y_p^2 + (h_r - h_u)^2 \right)^{\frac{\alpha}{2}} w_0} = T. \quad (23)$$

The left side of equation (23) represents the SNR of the received signal when the RIS is located at one of the intersections, and the right side of equation (23) is the SNR threshold. The expression of y_p is shown in the following equation:

$$y_p = \sqrt{\frac{-\sigma + \sqrt{\sigma^2 - 4\chi}}{2}}, \quad (24)$$

Since the circles for the RIS area upper bound must cover all the RIS area, the radii ρ_u and ρ_b must equal to the distance between the intersections and the UE (or the BS, it is symmetric), as shown in Fig. 5.7 and Fig. 5.8. Hence, the radii $\rho_u = \rho_b = \sqrt{\frac{-\sigma + \sqrt{\sigma^2 - 4\chi}}{2} + \frac{R_b^2}{4}}$. Then, for RIS area lower bound, to ensure that the circle centered on the BS is within the RIS area and not overlapped with the circle centered the UE, the radius τ_b of the circle is: when $|x_1| + x_2 \geq 2R_b$, $\tau_b = x_2 - R_b$; when $|x_1| + x_2 < 2R_b$, $\tau_b = R_b - |x_1|$;

The scenarios in Table 5.3 are the same as the scenarios in Table 5.1.

Appendix II

Since the distribution of RISs follows PPP, the probability that i RISs are located within the circle with radius R_t is [17]:

$$P_{\text{pr1}}(i) = \frac{(\pi R_t^2 \lambda_r)^i e^{-\pi R_t^2 \lambda_r}}{i!} = \frac{\gamma_1^i e^{-\gamma_1}}{i!}. \quad (25)$$

When the circle is centered on the UE, and $R_t < d_s$, and i RISs located within the circle, based on equation (8), the probability that at least an RIS is unblocked from the UE is:

$$P_{\text{pr2}}(i) = 1 - \prod_{k=1}^i (1 - e^{\nu r_k - \varpi}), \quad (26)$$

where r_k is the horizontal distance between the UE and the k th RIS. Moreover, with i RISs randomly located within the circle, the probability that at least an RIS is unblocked from the UE is:

$$\begin{aligned} \hat{P}_{\text{pr2}}(i) &= \underbrace{\int_0^{R_t} \dots \int_0^{R_t}}_i \left(1 - \prod_{k=1}^i (1 - e^{\nu r_k - \varpi}) \right) \prod_{k=1}^i \frac{2r_k}{R_t^2} dr_1 \dots dr_i \\ &= 1 - \left(1 - \frac{2e^{-\varpi} (1 + e^{\nu R_t} (\nu R_t - 1))}{\nu^2 R_t^2} \right)^i = 1 - \varepsilon_1^i. \end{aligned} \quad (27)$$

By combining equation (25) and (27), the probability that i RISs are located within the circle and at least 1 RIS is unblocked from the UE is:

$$P_{\text{co}}(i) = P_{\text{pr1}}(i) \hat{P}_{\text{pr2}}(i) = \frac{\gamma_1^i e^{-\gamma_1}}{i!} (1 - \varepsilon_1^i). \quad (28)$$

Furthermore, when the circle is centered on the UE and $R_t < d_s$, the probability that the LoS RIS-assisted transmission exists is:

$$\Phi_{\text{uc1}} = \sum_{i=1}^{\infty} P_{\text{co}}(i) = \sum_{i=1}^{\infty} \frac{\gamma_1^i e^{-\gamma_1}}{i!} (1 - \varepsilon_1^i) = 1 - e^{\gamma_1 \varepsilon_1 - \gamma_1}. \quad (29)$$

When the circle is centered on the UE, and $R_t \geq d_s$, and j RISs located within the circle with radius d_s and i RISs located within the circle with radius R_t , based on equation (8), the

probability that at least 1 RIS is unblocked from the UE is:

$$P_{\text{pr3}}(j, i) = 1 - \prod_{k=1}^j (1 - e^{vr_k - \varpi}) \prod_{k=j+1}^i \left(1 - \left(1 - \frac{\theta}{2\pi}\right) e^{vr_k - \varpi}\right). \quad (30)$$

Furthermore, with i RISs randomly located within the circle with radius R_t , the probability that at least 1 RIS is unblocked from the UE is computed by:

$$\begin{aligned} \hat{P}_{\text{pr3}}(i) &= \sum_{j=0}^i \frac{i!}{j!(i-j)!} \underbrace{\int_0^{d_s} \dots \int_0^{d_s}}_j \underbrace{\int_{d_s}^{R_t} \dots \int_{d_s}^{R_t}}_{i-j} \left(1 - \prod_{k=1}^j (1 - e^{vr_k - \varpi})\right) \\ &\quad \times \prod_{k=j+1}^i \left(1 - \left(1 - \frac{\theta}{2\pi}\right) e^{vr_k - \varpi}\right) \prod_{k=1}^i \frac{2r_k}{R_t^2} dr_1 \dots dr_i \\ &= \sum_{j=0}^i \frac{i!}{j!(i-j)!} \left(\left(\frac{d_s^2}{R_t^2}\right)^j \left(\frac{R_t^2 - d_s^2}{R_t^2}\right)^{i-j} - \left(\frac{d_s^2}{R_t^2} - \frac{2e^{-\varpi}(1 + e^{vd_s}(vd_s - 1))}{v^2 R_t^2}\right)^j \right) \\ &\quad \times \left(\frac{R_t^2 - d_s^2}{R_t^2} - \frac{2(1 - \frac{\theta}{2\pi})e^{-\varpi}(e^{vd_s}(1 - vd_s) + e^{vR_t}(vR_t - 1))}{v^2 R_t^2} \right)^{i-j} \\ &= \sum_{j=0}^i \frac{i!}{j!(i-j)!} (\varepsilon_2^j \zeta_1^{i-j} - \eta_1^j \kappa_1^{i-j}) = (\varepsilon_2 + \zeta_1)^i - (\eta_1 + \kappa_1)^i. \end{aligned} \quad (31)$$

Moreover, by combining equation (25) and (31), the probability that i RISs are located within the circle and at least 1 RIS is unblocked from the UE is:

$$P_{\text{co2}}(i) = P_{\text{pr1}}(i) \hat{P}_{\text{pr3}}(i) = \frac{\gamma_1^i e^{-\gamma_1}}{i!} \left((\varepsilon_2 + \zeta_1)^i - (\eta_1 + \kappa_1)^i \right). \quad (32)$$

Furthermore, when the circle is centered on the UE and $R_t \geq d_s$, the probability that the indirect LoS RIS-assisted transmission exists is:

$$\Phi_{\text{uc2}} = \sum_{i=1}^{\infty} \frac{\gamma_1^i e^{-\gamma_1}}{i!} \left((\varepsilon_2 + \zeta_1)^i - (\eta_1 + \kappa_1)^i \right) = e^{-\gamma_1} (e^{\gamma_1(\varepsilon_2 + \zeta_1)} - e^{\gamma_1(\eta_1 + \kappa_1)}). \quad (33)$$

Finally, by combining equation (29) and (33), equation (10) in Lemma 3 is derived. Equation (11)-(13) in Lemma 3 can be derived based on the same method. Hence, the proofs are omitted.

References

- [1] J. G. Andrews, S. Buzzi, W. Choi *et al.*, “What will 5G be?,” *IEEE J. Sel. Areas Commun.*, vol. 32, no. 6, pp. 1065-1082, Jun. 2014.
- [2] Z. Li, H. Hu, J. Zhang *et al.*, “Enhancing indoor mmWave wireless coverage: Small-cell densification or reconfigurable intelligent surfaces deployment?,” *IEEE Wirel. Commun. Lett.*, vol. 10, no. 11, pp. 2547-2551, Nov. 2021.
- [3] Q. Wu and R. Zhang, “Towards smart and reconfigurable environment: Intelligent reflecting surface aided wireless network,” *IEEE Commun. Mag.*, vol. 58, no. 1, pp. 106-112, Jan. 2020.
- [4] C. Huang, S. Hu, G. Alexandropoulos *et al.*, “Holographic MIMO Surfaces for 6G Wireless Networks: Opportunities, Challenges, and Trends,” *IEEE Wirel. Commun.*, vol. 27, no. 5, pp. 118-125, Oct. 2020.
- [5] E. Basar, M. Di Renzo, J. De Rosny *et al.*, “Wireless communications through reconfigurable intelligent surfaces,” *IEEE Access*, vol. 7, pp. 116753-116773, Aug. 2019.
- [6] Y. Zhu, M. Li, Y. Liu, Q. Liu, Z. Chang, and Y. Hu, “DRL-based Joint Beamforming and BS-RIS-UE Association Design for RIS-Assisted mmWave Networks,” [Online] <https://arxiv.org/abs/2202.09524>
- [7] C. Huang, Z. Yang, G. C. Alexandropoulos *et al.*, “Multi-Hop RIS-Empowered Terahertz Communications: A DRL-Based Hybrid Beamforming Design,” *IEEE J. Sel. Areas Commun.*, vol. 39, no. 6, pp. 1663-1677, Jun. 2021.

-
- [8] W. Xu, J. An, C. Huang *et al.*, “Deep Reinforcement Learning Based on Location-Aware Imitation Environment for RIS-Aided mmWave MIMO Systems,” *IEEE Wirel. Commun. Lett.*, vol. 11, no. 7, pp. 1493-1497, Jul. 2022.
- [9] L. Wei, C. Huang, G. C. Alexandropoulos *et al.*, “Channel Estimation for RIS-Empowered Multi-User MISO Wireless Communications,” *IEEE Trans. Commun.*, vol. 69, no. 6, pp. 4144-4157, Jun. 2021.
- [10] T. Van Chien, L. T. Tu, S. Chatzinotas *et al.*, “Coverage probability and ergodic capacity of intelligent reflecting surface-enhanced communication systems,” *IEEE Commun. Lett.*, vol. 25, no. 1, pp. 69-73, Jan. 2021.
- [11] L. Yang, Y. Yang, D. B. d. Costa *et al.*, “Outage probability and capacity scaling law of multiple RIS-aided networks,” *IEEE Wirel. Commun. Lett.*, vol. 10, no. 2, pp. 256-260, Feb. 2021.
- [12] Y. Zhang, J. Zhang, M. D. Renzo *et al.*, “Performance analysis of RIS-aided systems with practical phase shift and amplitude response,” *IEEE Trans. Veh. Technol.*, vol. 70, no. 5, pp. 4501-4511, May 2021.
- [13] A. Papazafeiropoulos, C. Pan, A. Elbir *et al.*, “Coverage probability of distributed IRS systems under spatially correlated channels,” *IEEE Wirel. Commun. Lett.*, vol. 10, no. 8, pp. 1722-1726, Aug. 2021.
- [14] T. Van Chien, A. K. Papazafeiropoulos, L. T. Tu *et al.*, “Outage probability analysis of IRS-assisted systems under spatially correlated channels,” *IEEE Wirel. Commun. Lett.*, vol. 10, no. 8, pp. 1815-1819, Aug. 2021.
- [15] Q. Tao, J. Wang and C. Zhong, “Performance analysis of intelligent reflecting surface aided communication systems,” *IEEE Commun. Lett.*, vol. 24, no. 11, pp. 2464-2468, Nov. 2020.

-
- [16] A. M. Salhab and M. H. Samuh, "Accurate performance analysis of reconfigurable intelligent surfaces over Rician fading channels," *IEEE Wirel. Commun. Lett.*, vol. 10, no. 5, pp. 1051-1055, May 2021.
- [17] J. G. Andrews, F. Baccelli, and R. K. Ganti, "A tractable approach to coverage and rate in cellular networks," *IEEE Trans. Commun.*, vol. 59, no. 11, pp. 3122–3134, Nov. 2011.
- [18] J. Lyu and R. Zhang, "Spatial throughput characterization for intelligent reflecting surface aided multiuser system," *IEEE Wirel. Commun. Lett.*, vol. 9, no. 6, pp. 834-838, Jun. 2020.
- [19] J. Ye, A. Kammoun and M. -S. Alouini, "Spatially-distributed RISs vs relay-assisted systems: A fair comparison," *IEEE Open J. Commun. Soc.*, vol. 2, pp. 799-817, Feb. 2021.
- [20] M. Nemati, J. Park and J. Choi, "RIS-assisted coverage enhancement in millimeter-wave cellular networks," *IEEE Access*, vol. 8, pp. 188171-188185, Oct. 2020.
- [21] Y. Zhu, G. Zheng and K. -K. Wong, "Stochastic geometry analysis of large intelligent surface-assisted millimeter wave networks," *IEEE J. Sel. Areas Commun.*, vol. 38, no. 8, pp. 1749-1762, Aug. 2020.
- [22] J. Lyu and R. Zhang, "Hybrid active/passive wireless network aided by intelligent reflecting surface: System modeling and performance analysis," *IEEE Trans. Wireless Commun.*, vol. 20, no. 11, pp. 7196-7212, Nov. 2021.
- [23] T. Shafique, H. Tabassum and E. Hossain, "Stochastic geometry analysis of IRS-assisted downlink cellular networks," *IEEE Trans. Commun.*, vol. 70, no. 2, pp. 1442-1456, Feb. 2022.
- [24] M. Di Renzo and J. Song, "Reflection probability in wireless networks with metasurface-coated environmental objects: An approach based on random spatial processes," *EURASIP J. Wireless Commun. Netw.*, vol. 2019, no. 1, p. 99, Dec. 2019.

- [25] C. Psomas, H. A. Suraweera and I. Krikidis, "On the Association with Intelligent Reflecting Surfaces in Spatially Random Networks," *Proc. IEEE Int. Conf. Commun. (ICC)*, Montreal, QC, Canada, 2021, pp. 1-6.
- [26] Y. Chen, B. Zhang, M. Ding, D. López-Pérez and H. Zheng, "Performance Analysis of Wireless Networks with Intelligent Reflecting Surfaces," *IEEE Wirel. Commun. Netw. Conf. (WCNC)*, Nanjing, China, 2021, pp. 1-6.
- [27] M. A. Kishk and M. -S. Alouini, "Exploiting randomly located blockages for large-scale deployment of intelligent surfaces," *IEEE J. Sel. Areas Commun.*, vol. 39, no. 4, pp. 1043-1056, Apr. 2021.
- [28] W. Tang, M. Chen, X. Chen *et al.*, "Wireless communications with reconfigurable intelligent surface: Path loss modeling and experimental measurement," *IEEE Trans. Wireless Commun.*, vol. 20, no. 1, pp. 421-439, Jan. 2021.
- [29] A. Thornburg, T. Bai, and R. W. Heath, Jr., "Performance analysis of outdoor mmWave ad hoc networks," *IEEE Trans. Signal Process.*, vol. 64, no. 15, pp. 4065–4079, Aug. 2016.
- [30] Y. Zhu, L. Wang, K.-K. Wong, and R. W. Heath, Jr., "Secure communications in millimeter wave ad hoc networks," *IEEE Trans. Wireless Commun.*, vol. 16, no. 5, pp. 3205–3217, May 2017.
- [31] T. Bai, R. Vaze and R. W. Heath, "Analysis of blockage effects on urban cellular networks," *IEEE Trans. Wireless Commun.*, vol. 13, no. 9, pp. 5070-5083, Sep. 2014.
- [32] P. Liu and A. Springer, "Space shift keying for LOS communication at mmWave frequencies," *IEEE Wireless Commun. Lett.*, vol. 4, no. 2, pp. 121-124, Apr. 2015.
- [33] Y. Zhang, J. Zhang, X. Chu and J. Zhang, "Lower-bound capacity-based wireless friendliness evaluation for walls as reflectors," *IEEE Trans. Broadcast.*, vol. 67, no. 4, pp. 917-924, Dec. 2021.

-
- [34] E. Björnson, J. Hoydis, and L. Sanguinetti, “Massive MIMO networks: Spectral, energy, and hardware efficiency,” *Found. Trends Signal Process.*, vol. 11, nos. 3–4, pp. 154–655, 2017.
- [35] E. Björnson and L. Sanguinetti, “Rayleigh Fading Modeling and Channel Hardening for Reconfigurable Intelligent Surfaces,” *IEEE Wirel. Commun.*, vol. 10, no. 4, pp. 830-834, Apr. 2021.
- [36] T. S. Rappaport, S. Sun, R. Mayzus *et al.*, “Millimeter wave mobile communications for 5G cellular: It will work!,” *IEEE Access*, vol. 1, pp. 335-349, May 2013.
- [37] M. Gapeyenko, A. Samuylov, M. Gerasimenko *et al.*, “Analysis of human-body blockage in urban millimeter-wave cellular communications,” *Proc. IEEE Int. Conf. Commun. (ICC)*, May 2016, pp. 1-7.
- [38] X. Yang, W. Lu; N. Wang *et al.*, “Design and implementation of a tdd-based 128-antenna massive MIMO prototype system,” *China Commun.*, vol. 14, no. 12, pp. 162-187, Dec. 2017.

Chapter 6

Paper III - Coverage Analysis of Multiple Transmissive RIS-aided Outdoor-to-Indoor mmWave Networks

Zeyang Li, Haonan Hu, Jiliang Zhang and Jie Zhang.

This paper has been published in IEEE Transactions on Broadcasting.

Coverage Analysis of Multiple Transmissive RIS-aided Outdoor-to-Indoor mmWave Networks

Zeyang Li¹, Haonan Hu^{1,2}, Jiliang Zhang^{1,3}, Jie Zhang^{1,3}

¹ Department of Electronic and Electrical Engineering, the University of Sheffield, Sheffield, S10 2TN, UK

² Chongqing Key Laboratory of Mobile Communications Technology Engineering Research Center of Mobile Communications, the School of Communication and Information Engineering, Chongqing University of Posts and Telecommunications, Chongqing 400065

³ Ranplan Wireless Network Design Ltd., Cambridge, CB23 3UY, UK

Abstract

Transmissive reconfigurable intelligent surfaces (RISs) are a promising solution for coverage enhancement of the future outdoor-to-indoor (O2I) millimeter wave (mmWave) network. In this work, the coverage probability of the multiple transmissive RIS-aided O2I mmWave network is investigated. Firstly, the system model of the three-dimensional O2I mmWave network considering random blockages is proposed. Moreover, the spatial correlation of blockages is analyzed to derive the accurate blockage probability. Furthermore, based on the blockage probability, the closed-form approximation of the signal-to-noise ratio (SNR) coverage probability is derived and verified. Finally, the impact of blockage density, the number and locations of RISs on the coverage probability is analyzed. According to the numerical results, the highest coverage enhancement caused by four small-scale RISs with appropriate locations reaches 69.5% higher compared with a large-scale RIS located at the center of the building envelope.

1 Introduction

As the vast majority of data transmission take places indoors [1, 2], great challenges are brought to indoor wireless networks. Since most base stations (BSs) are deployed outdoor,

outdoor-to-indoor (O2I) networks are a promising solution to satisfy the immense indoor data demand. However, the adoption of millimeter-wave (mmWave) frequency causes a new problem for O2I networks, which is the high penetration loss of building walls [3]. The O2I propagation has been investigated in [4–6] and the results showed that the network performance is limited by the high penetration loss. To tackle this problem, reconfigurable intelligent surface (RIS)-aided O2I networks have been proposed to guide mmWave signals to specific position of indoor user equipment (UE).

A RIS is a two-dimensional (2D) surface composed of many sub-wavelength and conductive passive elements (unit cells). All the unit cells are intelligently controlled by a smart controller so that the RIS can implement phase shift and modify amplitude on the incident signal. RISs can be categorized into three types depends on their function, i.e., reflective RISs, transmissive RISs and simultaneously transmitting and reflecting (STAR) RISs. Many existing works about RIS-aided networks focus on reflective RISs. For example, in [7] and [8], indoor and outdoor mmWave physical channel models for RIS were proposed. The results showed that RIS-aided networks provide significant enhancement in achievable data rate and error performance. The performance and cost comparison between indoor RIS-aided networks and ultra-dense small-cell networks were proposed in [9]. The results indicated that the proper number of BSs is crucial for RIS-aided networks to achieve certain coverage probability with the lowest network cost. For the application in O2I networks, reflective RISs require that the BS and UE are located on the same side of the surface, which is hard to be achieved.

Transmissive RISs and STAR RISs have been investigated in recent works. A prototype developed by NTT DOCOMO verifies the practicability of STAR RISs [10]. The work in [11] presented a hardware model of STAR RISs, and proposed the near-field and far-field channel models. The work in [12] investigated a downlink RIS-aided multi-user network. All three types of RISs, i.e., reflective, transmissive and STAR RISs, were considered. The system sum-rate of each type was derived. By optimizing the transmission and reflection coefficients at the RIS and resource allocation at the BS, the work in [13] maximized the sum coverage range of the STAR RIS-aided two-user networks. Moreover, the work in [14]

minimized the power consumption of STAR RIS-aided two-user networks by optimizing active and passive beamforming at the BS and RIS. Furthermore, in [15], the downlink STAR RIS-aided multi-user network was considered. The work optimized the beamforming at both the BS and RIS to maximize the system sum-rate. The downlink RIS-aided O2I network was investigated in [16]. A wall deployed with many chipless radio frequency identification sensors was adopted as the RIS in the network. The locations of blockages were modeled using Poisson point process (PPP). Two closed-form approximations of the signal-to-noise (SNR) coverage probability were derived.

To our best knowledge, only the work in [16] studied the RIS-aided O2I network. The work ignored the spatial correlation of blockages, thereby overestimated the network coverage. The reason is that the space is limited and the sensors are very close to each other in the indoor environment. If the network is deployed according to the analysis which ignores the correlation, the actual network performance cannot meet the expectation. In addition, it is neither practical nor cost-effective to deploy transmissive RISs on the whole wall. Therefore, to assist the transmission effectively, the positions of the RISs on the wall require further investigation. To fill the gaps discussed above, in this paper, we propose the first investigation on multi-RIS-aided O2I network considering blockage correlation. To model the complex indoor environment and provide a general insight, the indoor blockages are modeled based on PPP. Our contributions are summarized as follows:

- A system model of the three-dimensional (3D) multi-RIS-aided O2I network is proposed. The spatial correlation of blockages is analytically analyzed and the line-of-sight (LoS) probability is derived;
- A closed-form approximation of the SNR coverage probability is provided and verified by simulations. Then, a tractable method for incorporating multi-RIS deployment into the average coverage probability is presented.
- The impact of RIS quantity, RIS size, RIS locations and the ratio of the room (the length / width of the room) on the network coverage is discussed with a given total number of unit cells. For the network with high blockage density and low SNR threshold,

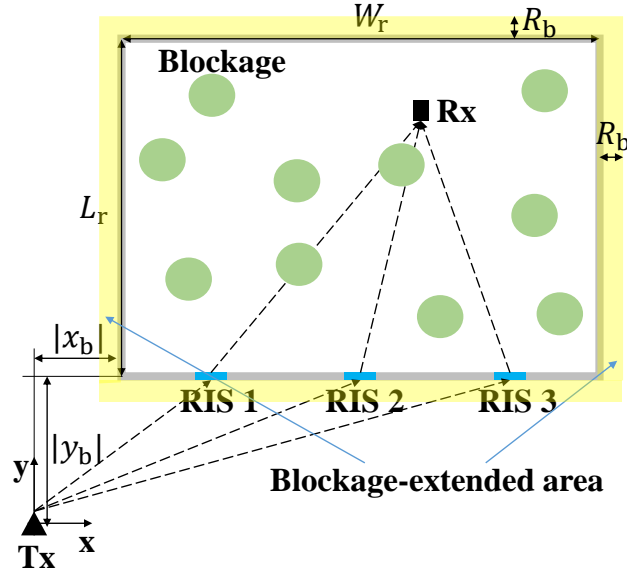


Fig. 6.1 Network model.

significant coverage enhancement can be achieved by optimizing the locations of more small-scale RISs, while for the network with low blockage density and high SNR threshold, fewer large-scale RISs with optimized locations are preferable for coverage enhancement.

The paper is organized as follows. In Section II, we present the system model of multi-RIS-aided O2I network. In Section III, we derive the blockage probability and approximation of coverage probability, and we present a method to evaluate multi-RIS deployment. In Section IV, we verify the analytical results and analyze the number of RISs and positions of RISs on network coverage. In Section V, we draw conclusions.

2 System Model

A downlink multi-RIS-aided O2I network with a BS and N RISs is considered. Table 6.1 presents a summary of main notations used. The BS has M_b antennas and the UE has single antenna. Each RIS has M_r unit cells and the size of each unit cell is $d_u \times d_u$ [20]. As shown in Fig. 6.1, the BS is located outside the building. A rectangular room with size $W_r \times L_r$ is considered. N RISs are deployed on the building envelope, so that the BS can transmit signals

Table 6.1 Main Notations

Symbol	Description
N	number of RISs
(x_u, y_u)	location of the UE
(x_b, y_b)	location of left side of RIS-deployment building envelope
P_{ri}	average received power of the transmission with i th RIS
β_i	elevation angle from the center of i th RIS to transmitter
Υ_{ri}	instantaneous received power of transmission with i th RIS
$R_{i,j}$	overlapped blockage region shared by i th, $(i+1)$ th, \dots , j th RISs only
$A_{i,j}$	overlapped blockage region shared by i th, $(i+1)$ th, \dots , j th RISs
$S(\cdot)$	area of blockage region \cdot
$p(n)$	probability that n th RIS is non-blocked from UE
$q(i, j)$	probability that i th RIS is non-blocked under condition that j th RIS is non-blocked from UE
$\tau_{i,j}(\varepsilon_{i,j})$	probability that region $R_{i,j}$ contains blockages ($\varepsilon_{i,j} = 1$) / no blockage ($\varepsilon_{i,j} = 0$)
$E_{i,j}$	event that i th, $(i+1)$ th, \dots , j th RISs are blocked from UE
ϕ	set indicating which regions have blockages and which regions have no blockage
$\Phi_{i,j}$	set containing all the sets ϕ which make event $E_{i,j}$ happen
$\rho(i, j)$	probability that the i th, $(i+1)$ th, \dots , j th RISs are blocked under condition that $(i-1)$ th and $(j+1)$ th RISs are non-blocked from the UE
$P_{LoS}(\cdot)$	probability that RISs in set \cdot are non-blocked while other RISs are blocked from the UE
z	set containing all the non-blocked RISs
Z	set containing all the combinations z of non-blocked RISs
Ψ_i	set containing all the combinations z of the i th non-blocked RIS and all the other non-blocked RISs
ξ_i	probability that the i th RIS is selected for transmission
C_h, C_m	without/with cooperation of multiple RISs, coverage probability with a given receiver location
W_{r2}	length of the RIS-deployment wall
x_d	distance between the center of RIS-deployment wall and the left side of building envelope
A_h, A_m	without/with cooperation of multiple RISs, average coverage probability of the room

to the UE in the room through RIS-aided communication [16]. Without loss of generality, in the horizontal plane, we assume that the BS is located at $(0, 0)$ and the left side of the RIS-deployment building envelope is located at (x_b, y_b) . The locations of the UE and the i th RIS are (x_u, y_u) and (x_{ri}, y_b) , respectively. The height difference between the BS and the i th RIS is h_{bi} . And the height difference between the i th RIS and the UE is h_{ri} .

Non-line-of-sight (NLoS) transmission is not considered in this paper due to high penetration loss of mmWave frequency [3, 19]. Hence, the direct transmission between the BS and UE, which is blocked by the building envelope, is not considered. Meanwhile, we assume that the transmission from the BS to each RIS is LoS because the BS and RISs are pre-deployed to guarantee the transmission is non-blocked. Meanwhile, because of complex indoor environment, e.g., furniture, humans and decorations, the transmission from RISs to UE might be blocked. The blockages are modeled as cylinders and the average radius of the blockages R_b is considered. Note that $R_b \ll W_r$ and $R_b \ll L_r$. In addition, for the sake of simplicity, we assume that the distribution of the centers of blockages follows Poisson point process (PPP) in the room and the blockage-extended area, as shown in Fig. 6.1. The density of blockages is denoted by λ_b . The transmission is blocked when blockages are located between the RIS and UE.

Two serving-RIS-selection schemes are considered: 1) The RIS providing highest average received signal power is selected to assist the transmission; 2) All the non-blocked RISs are selected to assist the transmission. The average received power of the transmission aided by i th RIS is [20]:

$$P_{ri} = \frac{P_t G M_b^2 M_r^2 d_u^2 \lambda^2 \omega \cos^3 \beta_i}{64 \pi^3 d_i^\alpha l_i^\alpha}, \quad (1)$$

where P_t is the transmit power of each antenna, G is the gain of the unit cell, λ is the wavelength of the signal, ω is the penetration loss of the RIS, $d_i = \sqrt{(x_{ri} - x_u)^2 + y_b^2 + h_{bi}^2}$ is the distance between the BS and the i th RIS, $l_i = \sqrt{(x_{ri} - x_u)^2 + y_u^2 + h_{ri}^2}$ is the distance between the i th RIS and the UE, β_i is the elevation angle from the center of the i th RIS to the transmitter ($\cos \beta_i = \frac{y_b}{d_i}$), $\cos^3 \beta_i$ represents the normalized power radiation pattern of the RIS, and it reaches the highest when the RIS faces the BS, i.e. $\cos \beta_i = 1$ when $y_b = d_i$. Moreover, by assuming Nakagami- m fading channel in each link, the instantaneous received

signal power of the transmission aided by i th RIS is [16]:

$$\Upsilon_{ri} = \frac{P_t G M_b^2 d_u^2 \lambda^2 \omega \cos^3 \beta_i \left(\sum_{j=1}^{M_r} \delta_{i,j} v_{i,j} \right)^2}{64 \pi^3 d_i^\alpha l_i^\alpha}, \quad (2)$$

where $\delta_{i,j}$ and $v_{i,j}$ are the Nakagami- m fading channel gain from the BS to the j th unit cell of the i th RIS and from the j th unit cell of the i th RIS to the UE, respectively. The distribution of the Nakagami- m fading channel gain is:

$$f(x) = \frac{2m^m x^{2m-1}}{\Omega^m \Gamma(m)} \exp\left(-\frac{mx^2}{\Omega}\right), x > 0, \quad (3)$$

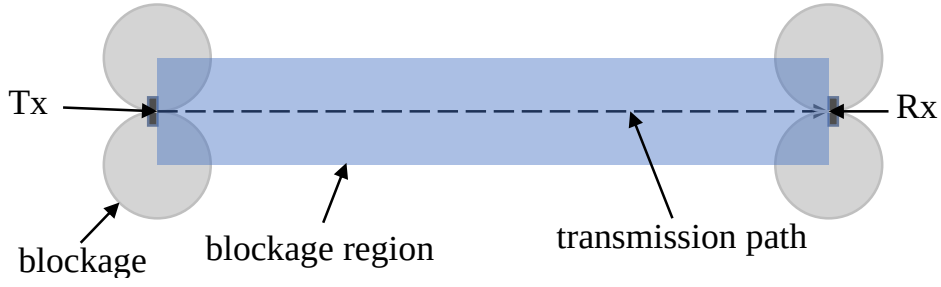
where m is the fading severity parameter, Ω is the mean fading power, $\Gamma(\cdot)$ is the gamma function.

3 O2I Network Coverage Analysis

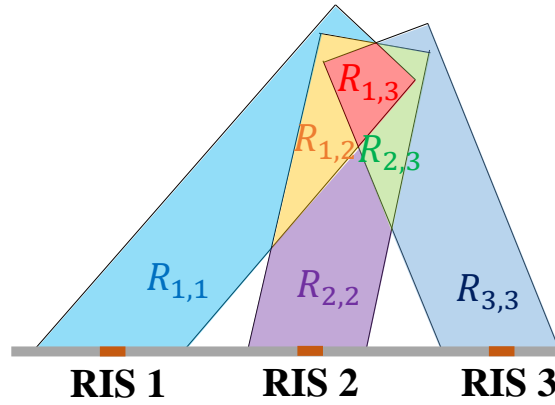
In this section, we analyze the network coverage of the multi-RIS-aided O2I network. Firstly, we only consider the average radius of the blockages and derive the blockage probability with a given UE location. Then, we consider that the radii of the blockages follow a distribution with probability density function (PDF) $f_{R_v}(r_v)$, and derive the blockage probability approximation. Furthermore, we derive the coverage probability approximation of the multi-RIS-aided O2I network. Finally, we propose a tractable method to incorporate locations of multiple RISs into average coverage probability.

3.1 Blockage Probability considering Blockages with the Same Size

A blockage region of a transmission is adopted to decide if the transmission is blocked or not. As shown in Fig. 6.2 (a), a blockage region of a transmission is determined by the locations of transceivers and size of blockages (Specifically, as shown in Fig. 6.2 (a), the blockage region is determined by the four blockages which block the transmission by their edge.). If and only if the center of any blockages is located in the blockage region, the transmission



(a) Illustration of blockage region of a transmission. If the center of a blockage is located in the blockage region, the transmission is blocked. For a given size of blockages, a blockage region is decided by the locations of the transmitter (RIS) and receiver.



(b) The blockage regions when 3 RISs are deployed on the building envelope. For a given location of the receiver, each RIS has its own fixed blockage region. Part of each RIS's blockage region is overlapped with other RISs' blockage region.

Fig. 6.2 Top views to show blockage region/regions.

is blocked [17]. In addition, we assume that the transmission is blocked only when the blockages are located between the RIS and UE. Hence, the blockage region is rectangular [18]. To consider the correlation for different RISs being blocked, the blockage region $R_{c,d}$ is defined as follows:

Remark 1: Each RIS has its blockage regions, as shown in Fig. 6.2 (b). If the center of any blockages is located in the blockage regions, the corresponding RIS is blocked from the UE. Some blockage regions are shared by different RISs. Specifically, $R_{c,d}$ is defined as the blockage region only shared by the RIS $c, c+1, \dots, d$. Note that $1 \leq c \leq d \leq N$. $R_{c,d}$ is non-overlapped blockage region when $c = d$, while $R_{c,d}$ is overlapped blockage region when $c \neq d$. If the center of any blockage locates in $R_{c,d}$, the RISs $c, c+1, \dots, d$ are blocked. For example, in Fig. 6.2 (b), if the center of a blockage is located in blockage region $R_{2,2}$, then

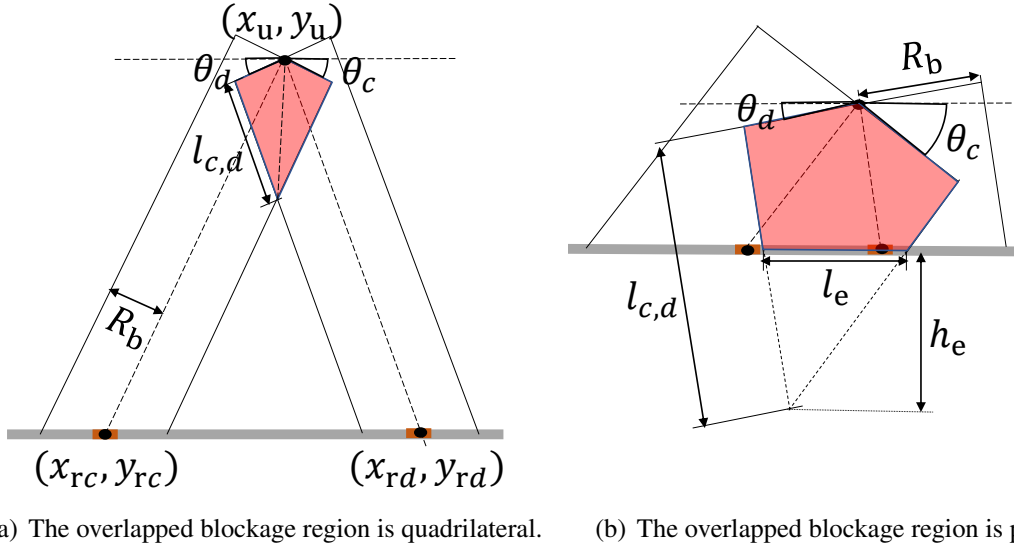


Fig. 6.3 The overlapped blockage region (red) of two RISs.

the transmission from the 2nd RIS to the UE is blocked. And if the center of a blockage is located in blockage region $R_{1,3}$, then RIS 1, RIS 2 and RIS 3 are all blocked.

Moreover, to derive the blockage probability, the area of each blockage region needs to be calculated. $A_{c,d}$ is defined as the overlapped blockage region shared by the RIS $c, c+1, \dots, d$.¹ The value $S(\cdot)$ is defined as the area of the blockage region \cdot , e.g., $S(A_{c,d})$ is the area of the blockage region $A_{c,d}$, $S(R_{c,d})$ is the area of the blockage region $R_{c,d}$. Note that $S(R_{c,d}) \leq S(A_{c,d})$. Lemma 1 provides the equations to calculate the area of $A_{c,d}$.

Lemma 1. For the case of $c = d$, the area $S(A_{c,d})$ of the overlapped blockage region $A_{c,d}$ is presented as follows:

$$S(A_{c,d}) = 2R_b \sqrt{(x_u - x_{rc})^2 + (y_u - y_b)^2}. \quad (4)$$

¹The difference between $R_{c,d}$ and $A_{c,d}$ is: $R_{c,d}$ is only shared by the RIS $c, c+1, \dots, d$ while other RISs besides the RIS $c, c+1, \dots, d$ might share part of $A_{c,d}$. Normally, $R_{c,d}$ is contained by $A_{e,f}$ ($c \leq e$ and $d \geq f$), e.g., in Fig. 6.2, $A_{1,2}$ is the combination of $R_{1,2}$ and $R_{1,3}$.

For the case of $c \neq d$, when $x_{wc} < x_{wd}$,

$$S(A_{c,d}) = \begin{cases} R_b^2 \tan\left(\frac{\pi - \theta(c) - \theta(d)}{2}\right), & x_c < x_u < x_d, \\ R_b^2 \tan\left(\frac{\pi - |\theta(c) - \theta(d)|}{2}\right), & \text{otherwise}; \end{cases} \quad (5)$$

when $x_{wc} \geq x_{wd}$, $S(A_{c,d})$ is provided as follows:

$$S(A_{c,d}) = \begin{cases} R_b^2 \tan\left(\frac{\pi - \theta(c) - \theta(d)}{2}\right) - \frac{h_e l_e}{2}, & x_c < x_u < x_d, \\ R_b^2 \tan\left(\frac{\pi - |\theta(c) - \theta(d)|}{2}\right) - \frac{h_e l_e}{2}, & \text{otherwise}; \end{cases} \quad (6)$$

where $x_{wc} = x_{rc} + \frac{R_b \sqrt{(x_u - x_{rc})^2 + (y_u - y_b)^2}}{y_u - y_b}$, $x_{wd} = x_{rd} - \frac{R_b \sqrt{(x_u - x_{rd})^2 + (y_u - y_b)^2}}{y_u - y_b}$, $\theta(\cdot) = \arctan\left|\frac{x_u - x_r}{y_u - y_b}\right|$, $l_e = x_{wc} - x_{wd}$ and the expression of h_e is presented as follows:²

$$h_e = \begin{cases} \frac{l_e(y_u - y_b)}{|x_u - x_{rc}|}, & x_{rd} = x_u, \\ \frac{l_e(y_u - y_b)}{|x_u - x_{rd}|}, & x_{rc} = x_u, \\ y_b - y_u - \frac{R\sqrt{(x_u - x_{rc})^2 + (y_u - y_b)^2} + R\sqrt{(x_u - x_{rd})^2 + (y_u - y_b)^2}}{x_{rc} - x_{rd}}, & \text{otherwise}. \end{cases} \quad (7)$$

Proof. With the given locations of any two RISs and UE, the overlapped blockage region shared by the two RISs is either quadrilateral or pentagon, which is shown in Fig. 6.3 (a) and Fig. 6.3 (b). The area of the overlapped blockage region is derived based on the geometric properties. \square

Before $S(R_{c,d})$ is derived, we present Proposition 1:

Proposition 1. *When the radius of each blockage is the same, the overlapped blockage region $A_{c,d}$ will be covered by the overlapped blockage region $A_{e,f}$ if $x_{re} \geq x_{rc}$ and $x_{rf} \leq x_{rd}$.*

Based on Proposition 1, given the total number of RISs, the area of $R_{c,d}$ can be calculated based on recursion, which is presented in the following lemma.

²This method can be less accurate when the distance between the UE and the RIS-deployment wall is shorter than R_b , i.e., $y_u - y_b < R_b$. However, since $R_b \ll W_r$ and $R_b \ll L_r$, those area is much smaller than the whole room area. For simplicity, we only consider the lower bound of the blockage probability of those area by assuming the coverage probability $C(x_u, y_{u1}) = C(x_u, y_b + R_b)$ for any $y_{u1} < y_b + R_b$.

Lemma 2. *If N RISs are deployed on the wall, then the area of each blockage region $R_{c,d}$ can be expressed in a recursive manner, which is:*

$$\begin{aligned} S(R_{e,f}) &= S(A_{e,f}) - \sum_{c=e, f < d \leq N} S(R_{c,d}) \\ &- \sum_{1 \leq c < e, d=f} S(R_{c,d}) - \sum_{1 \leq c < e, f < d \leq N} S(R_{c,d}). \end{aligned} \quad (8)$$

Proof. Lemma 2 is derived based on the geometric properties presented in *Proposition 1* and in a recursive manner, which is:

$$\begin{aligned} S(R_{1,N}) &= S(A_{1,N}); \\ S(R_{1,N-1}) &= S(A_{1,N-1}) - S(R_{1,N}); \\ S(R_{2,N}) &= S(A_{2,N}) - S(R_{1,N}); \\ S(R_{1,N-2}) &= S(A_{1,N-2}) - S(R_{1,N}) - S(R_{1,N-1}); \\ S(R_{2,N-1}) &= S(A_{2,N-1}) - S(R_{1,N}) - S(R_{1,N-1}) \\ &\quad - S(R_{2,N}); \\ S(R_{3,N}) &= S(A_{3,N}) - S(R_{1,N}) - S(R_{2,N}); \\ &\vdots \end{aligned}$$

□

Since the centers of blockages are distributed following PPP, and the number of points in a certain blockage area $A_{n,n}$ with size $S(A_{n,n})$ follows Poisson distribution with mean value $\lambda_b S(A_{n,n})$. Accordingly, the probability $p(n)$ that the n th RIS is non-blocked from the UE can be calculated as follows:

$$p(n) = \exp\left(-\lambda_b S(A_{n,n})\right). \quad (9)$$

Moreover, we denote the probability that the n_j th RIS is non-blocked from the UE under the condition that the n_{j-1} th RIS is non-blocked from the UE as $q(n_j, n_{j-1})$, which is:

$$q(n_j, n_{j-1}) = \prod_{c>n_{j-1}, c\leq n_j \leq d} \tau_{c,d}(0), \quad (10)$$

where the function $\tau_{c,d}(\varepsilon_{c,d})$ ($\varepsilon_{c,d} \in \{0, 1\}$), which is adopted to calculate the probability that region $R_{c,d}$ contains blockages/no blockage, is defined as follows:

$$\tau_{c,d}(\varepsilon_{c,d}) = \begin{cases} 1 - \exp\left(-\lambda_b S(R_{c,d})\right), & \varepsilon_{c,d} = 1, \\ \exp\left(-\lambda_b S(R_{c,d})\right), & \varepsilon_{c,d} = 0, \end{cases} \quad (11)$$

where $\varepsilon_{c,d} = 1$ means that blockages are located in region $R_{c,d}$, and $\varepsilon_{c,d} = 0$ means that no blockage is located in region $R_{c,d}$.

We define event $E_{c,d}$ as that the c th, $(c+1)$ th, \dots , d th RISs are blocked from the UE. The event $E_{c,d}$ can be achieved in many scenarios, e.g., scenario 1: region $R_{c,d}$ contains blockages while other regions do not contain blockages, i.e., $\varepsilon_{c,d} = 1$ and $\varepsilon_{e,f} = 0$ ($(c \leq e \leq f \leq d) \wedge (\neg(e=c) \wedge (f=d))$); or scenario 2: region $R_{c,d-1}$ and $R_{d,d}$ contain blockages while other regions do not contain blockages, i.e., $\varepsilon_{c,d-1} = 1$, $\varepsilon_{d,d} = 1$ and $\varepsilon_{e,f} = 0$ ($(c \leq e \leq f \leq d) \wedge (\neg(e=c) \wedge (f=d-1)) \wedge (\neg(e=d) \wedge (f=d))$). We use ϕ to represent the set indicating which regions have blockages and which regions have no blockage, i.e., $\phi = \{\varepsilon_{c,c}, \dots, \varepsilon_{e,f}, \dots, \varepsilon_{d,d}\}$ ($c \leq e \leq f \leq d$). Moreover, the set containing all the sets which make event $E_{c,d}$ happen can be expressed as:

$$\begin{aligned} \Phi_{c,d} = \\ \{\phi = \{\varepsilon_{c,c}, \dots, \varepsilon_{e,f}, \dots, \varepsilon_{d,d}\} | \phi \Rightarrow E_{c,d}, c \leq e \leq f \leq d\}. \end{aligned} \quad (12)$$

For example, $\Phi_{1,2}$ for event $E_{1,2}$ is shown in Table 6.2. Furthermore, we denote the probability that the (n_i) th, (n_i+1) th, \dots , (n_j) th RISs are blocked from the UE under the condition that

Table 6.2 $\Phi_{1,2}$ for event $E_{1,2}$

Set	Index	Index Value					
$\Phi_{1,2}$	$\varepsilon_{1,1}$	0	1	0	1	1	
	$\varepsilon_{1,2}$	1	1	1	1	0	
	$\varepsilon_{2,2}$	0	0	1	1	1	

$(n_i - 1)$ th and $(n_j + 1)$ th RISs are non-blocked ($n_i \geq 1$ and $n_j \leq N$) as $\rho(n_i, n_j)$ ³. Based on probability theory, the expression of $\rho(n_i, n_j)$ is provided as follows:

$$\rho(n_i, n_j) = \sum_{\phi \in \Phi_{n_i, n_j}} \prod_{\varepsilon_{e,f} \in \phi} \tau_{e,f}(\varepsilon_{e,f}). \quad (13)$$

$\rho(n_i, n_j) = 0$ if $n_i > n_j$.

Then by combining equation (9), (10) and (13), the probability that the RISs n_1, n_2, \dots, n_k are non-blocked while other RISs are blocked from the UE is expressed by the following equation:

$$P_{\text{LoS}}(n_1, n_2, \dots, n_k) = \rho(1, n_1 - 1) p(n_1) \rho(n_k + 1, N) \prod_{j=2}^k q(n_j, n_{j-1}) \rho(n_{j-1} + 1, n_j - 1). \quad (14)$$

Note that $1 \leq n_1 < n_2 < \dots < n_k \leq N$ and $1 \leq k \leq N$.

We use the set z to represent all the non-blocked RISs, i.e., $z = \{n_1, \dots, n_i, \dots, n_k\}$ ($1 \leq n_i \leq N, 1 \leq i \leq k \leq N$). Then Z is defined as the set containing all the combinations z of non-blocked RISs, which can be expressed as the following equation:

$$Z = \{z = \{n_1, \dots, n_i, \dots, n_k\} | n_i \in z, 1 \leq n_i \leq N, 1 \leq i \leq k \leq N\}. \quad (15)$$

³If $n_i = 1$, $\rho(1, n_j)$ is the probability that the 1st, 2nd, \dots , n_j th RISs are blocked from the UE under the condition that $(n_j + 1)$ th RIS is non-blocked; if $n_j = N$, $\rho(n_i, N)$ is the probability that the n_i th, $(n_i + 1)$ th, \dots , N th RISs are blocked from the UE under the condition that $(n_i - 1)$ th RIS is non-blocked.

Meanwhile, we define Ψ_a as the set containing all the combinations z of the a th non-blocked RIS and all the other non-blocked RISs, which can be expressed as the following equation:

$$\Psi_a = \{z = \{a, n_1, \dots, n_i, \dots, n_k\} | a \in z, n_i \in z, 1 \leq n_i \leq N, 1 \leq i \leq k \leq N, n_i \neq a\}. \quad (16)$$

Furthermore, if the RIS providing highest average received power is selected to assist the transmission, then the probability that the a th RIS is selected for transmission is:

$$\xi(a) = \sum_{z \in \Psi_a} P_{\text{LoS}}(z) \prod_{n_i \in z, n_i \neq a} G(a, n_i). \quad (17)$$

where the function $G(n_i, n_j)$, which is defined as the following equation:

$$G(n_i, n_j) = \begin{cases} 1, & \left((P_r(n_i) \geq P_r(n_j)) \wedge (n_i > n_j) \right) \vee \left((P_r(n_i) > P_r(n_j)) \wedge (n_i < n_j) \right), \\ 0, & P_r(n_i) < P_r(n_j). \end{cases} \quad (18)$$

Equation (18) is adopted to decide if the average received power from the n_i th RIS is higher than that from the n_j th RIS.

3.2 Blockage Probability Approximation considering Blockages with Different Size

In this subsection, the radius of each blockage is represented by the random variable R_v with PDF $f_{R_v}(r_v)$. Note that $0 \leq R_v \leq R_{\max}$, $R_{\max} \ll W_r$ and $R_{\max} \ll L_r$. In this case, it is challenging to derive the exact blockage probability. However, the approximation of the blockage probability can be obtained. Firstly, instead of considering that R_v is continuous on the interval $[0, R_{\max}]$, we consider that the discrete function $\hat{R}_v \in \mathbb{R} = \{\frac{d_R}{2}, \frac{3d_R}{2}, \dots, R_{\max} - \frac{d_R}{2}\}$, where $d_R \ll R_{\max}$. Then, the density of the blockages with the radius \hat{R}_v is

$$\lambda_v(\hat{R}_v) = \lambda_b \int_{\hat{R}_v - \frac{d_R}{2}}^{\hat{R}_v + \frac{d_R}{2}} f_{R_v}(r_v) dr_v. \quad (19)$$

Moreover, for each value \hat{R}_v , we can use equation (14) to calculate the probability that the RISs n_1, n_2, \dots, n_k are non-blocked while other RISs are blocked from the UE with blockage radius \hat{R}_v and blockage density $\lambda_v(\hat{R}_v)$, i.e., $P_{\text{LoS}}(n_1, n_2, \dots, n_k, \hat{R}_v, \lambda_v(\hat{R}_v))$. Furthermore, for all the values $\hat{R}_v \in \mathbb{R}$, the probability that the RISs n_1, n_2, \dots, n_k are non-blocked while other RISs are blocked from the UE can be approximated by:

$$\begin{aligned} & \hat{P}_{\text{LoS}}(n_1, n_2, \dots, n_k) \\ & \approx \prod_{\hat{R}_v \in \mathbb{R}} P_{\text{LoS}}(n_1, n_2, \dots, n_k, \hat{R}_v, \lambda_v(\hat{R}_v)). \end{aligned} \quad (20)$$

3.3 Coverage Probability

The coverage probability is defined as the probability that the SNR of the received signal is higher than the SNR threshold T . For large values of M_r , the channel amplitude of the signal $v_i = \sqrt{Y_{ri}}$ follows Gaussian distribution with mean $\sqrt{P_{ri}}\mu$ and variance $P_{ri}\sigma^2$, i.e., $v_i \sim \mathcal{N}(\sqrt{P_{ri}}\mu, P_{ri}\sigma^2)$ [21]. μ and σ^2 are given as follows:

$$\mu = \prod_{i=1}^2 \frac{\Gamma(m_i + \frac{1}{2})}{\Gamma(m_i)} \left(\frac{\Omega_i}{m_i} \right)^{\frac{1}{2}}, \quad (21)$$

$$\sigma^2 = \prod_{i=1}^2 \frac{\Gamma(m_i + 1)}{\Gamma(m_i)} \left(\frac{\Omega_i}{m_i} \right) - \left(\prod_{i=1}^2 \frac{\Gamma(m_i + \frac{1}{2})}{\Gamma(m_i)} \left(\frac{\Omega_i}{m_i} \right)^{\frac{1}{2}} \right)^2. \quad (22)$$

Moreover, given the location of the UE, the coverage probability of the multi-RIS-aided O2I network is provided in the following theorem.

Theorem 1. *When the RIS providing highest average received power is selected to transmit the signal, the coverage probability of the RIS-aided O2I network is:*

$$\begin{aligned} C_h &= \sum_{a=1}^N \sum_{z \in \Psi_a} P_{\text{LoS}}(z) \prod_{n_i \in z, n_i \neq a} G(a, n_i) \\ & \times \left(\frac{1}{2} - \frac{1}{2} \operatorname{erf} \left(\frac{\sqrt{T} \sigma_w^2 - \sqrt{P_{ra}} \mu}{\sqrt{P_{ra}} \sigma \sqrt{2}} \right) \right), \end{aligned} \quad (23)$$

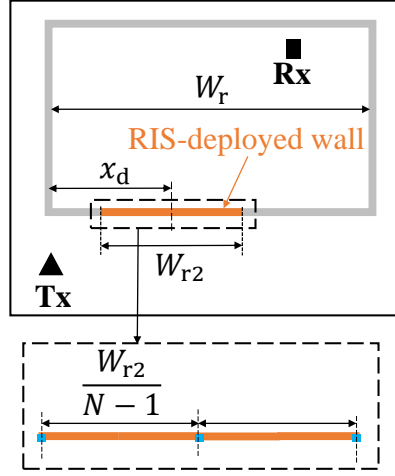


Fig. 6.4 Multi-RIS deployment strategy.

where σ_w^2 is the noise power, T is the SNR threshold. For the cooperation of multiple RISs, the coverage probability of the RIS-aided O2I network is:

$$C_m = \sum_{z \in Z} P_{\text{LoS}}(z) \left(\frac{1}{2} - \frac{1}{2} \operatorname{erf} \left(\frac{\sqrt{T \sigma_w^2} - \sum_{n \in z} \sqrt{P_{rn}} \mu}{\sum_{n \in z} \sqrt{P_{rn}} \sigma \sqrt{2}} \right) \right). \quad (24)$$

Proof. The probability that the a th RIS is selected for transmission and the UE is in coverage is:

$$P_a = \xi(a) \cdot P(\Upsilon_{ra} > T \sigma_w^2), \quad (25)$$

where $\xi(a)$ is presented in (17) and $\sqrt{\Upsilon_{ri}}$ follows Gaussian distribution. Moreover, the coverage probability, which is the summation of the probability that each RIS is selected for transmission and the UE is in coverage, can be calculated by:

$$C_h = \sum_{a=1}^N P_a. \quad (26)$$

When multiple RISs are serving the UE simultaneously, the coverage probability is:

$$C_m = \sum_{z \in Z} P_{\text{LoS}}(z) \cdot P \left(\left(\sum_{n \in z} \sqrt{\Upsilon_{rn}} \right)^2 > T \sigma_w^2 \right). \quad (27)$$

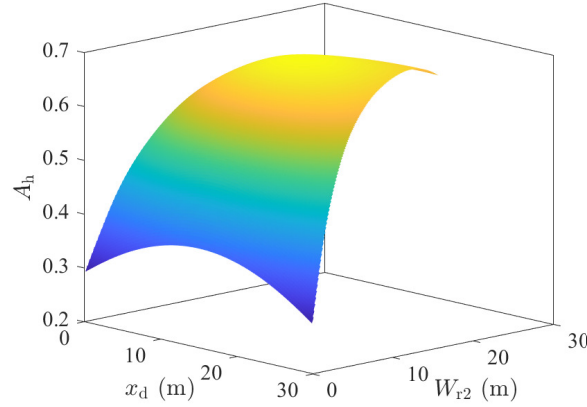


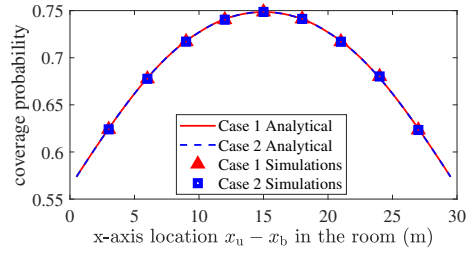
Fig. 6.5 The effect of W_{r2} and x_d on the average coverage probability when 4 RISs are deployed.

Table 6.3 Simulation Parameters

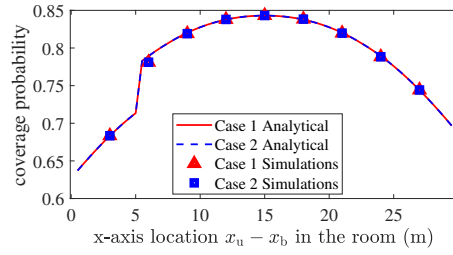
Parameter	Value	Parameter	Value
λ	0.01 m	ω	-5 dB
L_r	30 m	T	15 dB
W_r	30 m	d_u	0.005 m
x_b	20 m	R_b	1 m
y_b	30 m	P_t	1 W
h_{ri}	0 m	λ_b	0.03 m^{-2}
h_b	20 m	σ_w^2	-120 dB
α	2	G	8
M_b	32	M_c	900
m_1	3	m_2	3

We assume that the channels of each RIS are independent from the channels of other RISs. Therefore, the amplitude of the signal $\sum_{n \in \mathcal{Z}} \sqrt{\Upsilon_{rn}}$ also follows Gaussian distribution with mean $\sum_{n \in \mathcal{Z}} \sqrt{P_{ri}} \mu$ and variance $\sum_{n \in \mathcal{Z}} P_{ri} \sigma^2$. \square

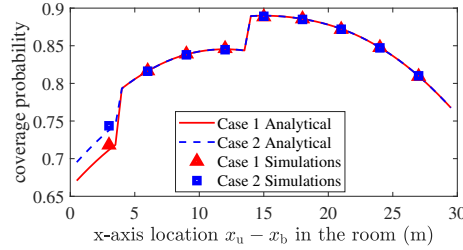
For blockages with random radii, the coverage probability approximation can be calculated by substituting P_{LoS} into \hat{P}_{LoS} in equation (23) and (24). \hat{P}_{LoS} is provided in equation (20).



(a) 2 RISs are deployed.



(b) 3 RISs are deployed.



(c) 4 RISs are deployed.

Fig. 6.6 With different number of RISs, the coverage probability when the UE is 10 m away from the building envelope. In case 1, the RIS providing the highest average received power is selected to transmit the signal; in case 2, all the RISs that are not blocked are selected to transmit the signal.

3.4 Method for Describing Locations of Multiple RISs

For the deployment of multiple RISs, it is highly complicated to find the optimal positions for all the RISs. In this paper, we focus on the RIS deployment strategy where 1) the distance between any two adjacent RISs is the same; 2) all the RISs are located in a line on the RIS-deployment building envelope, as shown in Fig. 6.4. To describe the locations of multiple RISs, firstly, we define the RIS-deployment wall as a part of the building envelope which the RISs can be deployed on. Then, the location of the RIS-deployment wall is described by two factors, i.e., the length of the RIS-deployment wall W_{r2} and the distance between the

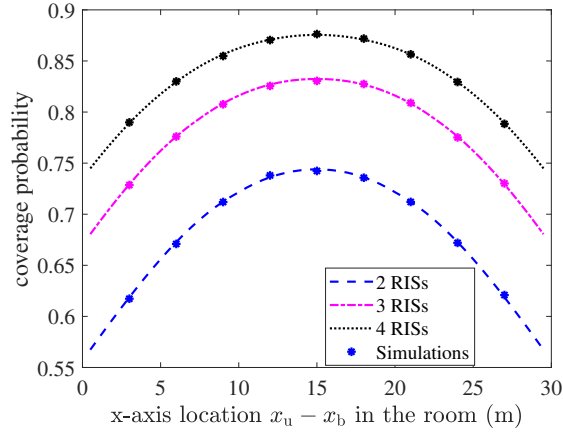


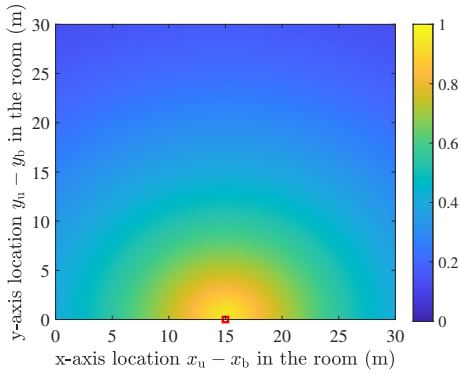
Fig. 6.7 Considering the blockages with different size, the coverage probability when the UE is 10 m away from the building envelope.

center of the RIS-deployment wall and the left side of the building envelope x_d . Note that $0 \leq W_{r2} \leq W_r$ and $\frac{W_{r2}}{2} \leq x_d \leq W_r - \frac{W_{r2}}{2}$. In addition, the distance between any two adjacent RISs is $\frac{W_{r2}}{N-1}$. By adjusting the values of W_{r2} and x_d , all the locations of evenly distributed multiple RISs can be represented.

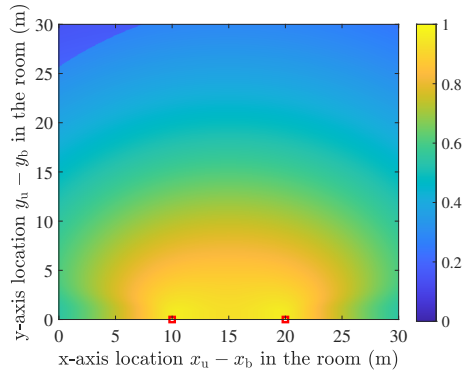
The coverage probabilities in equation (23) and equation (24) are the functions of the location of the UE, the length and the center location of the RIS-deployment wall, i.e., $C_h(x_u, y_u, W_{r2}, x_d)$ and $C_m(x_u, y_u, W_{r2}, x_d)$. Moreover, the average coverage probability of the room is defined as:

$$A_h(W_{r2}, x_d) = \frac{l_u^2}{W_r L_r} \sum_{x_u \in X_u, y_u \in Y_u} C_h(x_u, y_u, W_{r2}, x_d), \quad (28)$$

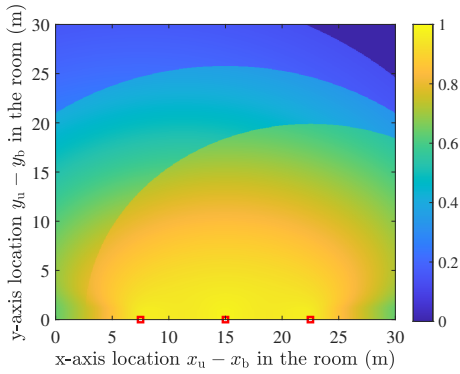
$$A_m(W_{r2}, x_d) = \frac{l_u^2}{W_r L_r} \sum_{x_u \in X_u, y_u \in Y_u} C_m(x_u, y_u, W_{r2}, x_d), \quad (29)$$



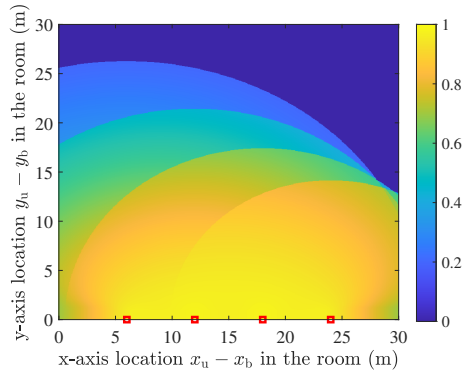
(a) The network coverage in the room with 1 RIS.



(b) The network coverage in the room with 2 RISs.



(c) The network coverage in the room with 3 RISs.



(d) The network coverage in the room with 4 RISs.

Fig. 6.8 The network coverage in the room with different number of RISs deployed in the building envelope.

where $X_u = \{\frac{l_u}{2}, \frac{3l_u}{2}, \frac{5l_u}{2}, \dots, W_r - \frac{l_u}{2}\}$, $Y_u = \{\frac{l_u}{2}, \frac{3l_u}{2}, \frac{5l_u}{2}, \dots, L_r - \frac{l_u}{2}\}$. By optimizing W_{r2} and x_d , the average coverage probability can be maximized, which is:

$$\begin{aligned}
 \mathbf{P1} : & \max_{W_{r2}, x_d} A_h \\
 \text{s.t.} & \quad \text{C0} : 0 \leq W_{r2} \leq W_r, \\
 & \quad \text{C1} : \frac{W_{r2}}{2} \leq x_d \leq W_r - \frac{W_{r2}}{2},
 \end{aligned} \tag{30}$$

Fig. 6.5 shows the average coverage probability with different W_{r2} and x_d when 4 RISs are deployed. The numerical parameters in Table III are used.

Table 6.4 With different room size $W_r \times L_r$ and different number of RISs, the optimized length W_{r2} and the optimized location x_d of the RIS-deployment wall, and the optimal average coverage probability A_h of the room.

$W_r \times L_r$	2 RISs				3 RISs				4 RISs			
	W_{r2} (m)	x_d (m)	A_h (%)	I (%)	W_{r2} (m)	x_d (m)	A_h (%)	I (%)	W_{r2} (m)	x_d (m)	A_h (%)	I (%)
20 m \times 45 m	7.71	9.96	46.3%	46.5%	8.25	9.99	50.1%	58.5%	9.16	10.15	45.8%	44.9%
25 m \times 36 m	8.93	12.46	52.7%	46.4%	9.28	12.35	59.6%	65.6%	9.64	12.71	55.5%	54.2%
30 m \times 30 m	10.23	14.96	56.9%	46.2%	10.66	14.75	65.2%	67.5%	10.13	15.28	63.8%	63.9%
36 m \times 25 m	12.16	17.96	59.9%	46.5%	13.64	17.40	68.8%	68.2%	11.59	18.16	69.0%	68.7%
45 m \times 20 m	15.63	22.45	61.7%	48.0%	18.13	21.63	70.3%	68.6%	14.82	23.55	70.7%	69.5%

Table 6.5 With different blockage density λ_b and different number of RISs, the optimized length W_{r2} and the optimized location x_d of the RIS-deployment wall, and the optimal average coverage probability A_h of the room with size 30 m \times 30 m.

λ_b	2 RISs				3 RISs				4 RISs			
	W_{r2} (m)	x_d (m)	A_h (%)	I (%)	W_{r2} (m)	x_d (m)	A_h (%)	I (%)	W_{r2} (m)	x_d (m)	A_h (%)	I (%)
0.01 m ⁻²	11.42	14.96	88.3%	23.9%	10.3	14.68	91.7%	28.6%	7.97	16.05	87.1%	22.2%
0.015 m ⁻²	11.27	14.96	80.0%	31.7%	10.38	14.68	85.5%	40.8%	8.64	15.75	81.1%	33.5%
0.02 m ⁻²	10.85	14.96	71.7%	37.7%	10.52	14.68	78.7%	51.1%	9.25	15.58	75.1%	44.2%
0.025 m ⁻²	10.54	14.96	63.9%	42.4%	10.53	14.73	71.8%	60.0%	9.76	15.42	69.3%	54.4%
0.03 m ⁻²	10.23	14.96	56.9%	46.2%	10.66	14.75	65.2%	67.5%	10.13	15.28	63.8%	63.9%

4 Numerical Results

In this section, the analytical coverage probabilities of RIS-aided networks are validated and evaluated. We focus on the scenarios in which all the RISs in the same room have the same size, i.e., all the RISs in the same figure/sub-figure have the same size. Meanwhile, a practical scenario is investigated, which is: given the total number of unit cells M_c and the number of RISs N , the number of unit cells per RIS is $M_r = \lfloor M_c/N \rfloor$. The system numerical parameters are provided in Table 6.3 unless otherwise specified [9, 16, 18, 20].

Fig. 6.6 shows the coverage probability when the UE is 10 m away from the building envelope. $x_d = W_r/2$ and $W_{r2} = \frac{N-1}{N+1}W_r$. In case 1, the RIS providing highest average received power is selected to transmit the signal, and in case 2, all the RISs which are not blocked are selected to transmit the signal. The figure illustrates that the analytical results match Monte Carlo simulations. In addition, the coverage probability of case 1 and that of case 2 are the same in Fig. 6.6 (a) and (b), the only difference is shown in Fig. 6.6 (c), i.e., when 4 RISs are deployed and the location $x_u - x_b$ in the room is between 0 and 5 m. The reason is: the cooperation of multiple RISs only leads to limited coverage enhancement

because it only benefits certain scenarios. Those scenarios need to satisfy two conditions: 1) a proportion of outage happens because of the high path loss; 2) the power gain caused by adopting multiple-RIS cooperation is high enough to reduce that proportion of outage. In Fig. 6.7, case 1 is adopted and the blockages with different size are considered. The radii of the blockages R_v are uniformly distributed in the range of $[0, 2]$. It shows that the analytical results match with simulations.

To indicate how the RIS deployment affects the network coverage in the room, Fig. 6.8 shows the coverage probability in the considered room with different number of RISs. The RIS with the highest average received power is selected for transmission. The position of the UE in the room are described by x axis and y axis. In addition, the square red marks on the x axis represent RISs. In Fig. 6.8 (a), only one large-size RIS is deployed on the center of the wall, i.e., $(15, 0)$. In this scenario, blockages are the main reason for the low-coverage area. In Fig. 6.8 (b), two smaller RISs, whose size is half of the RIS in Fig. 6.8 (a), are deployed on the wall. Compared with Fig. 6.8 (a), the coverage in Fig. 6.8 (b) is improved. However, since smaller RIS leads to lower power gain, the coverage in the area around $(0, 30)$ is extreme low. Furthermore, as more RISs with smaller size are deployed on the different positions of the wall, the high path loss becomes the main reason for the low-coverage area, as shown in Fig. 6.8 (c) and Fig. 6.8 (d). Therefore, to achieve high network coverage, both the size of each RIS and the number of RISs should be designed carefully to provide enough power gain and space diversity.

The optimized length W_{r2} and location x_d of the RIS-deployment wall, and the optimal average coverage probabilities are demonstrated in Table 6.4 with different room size $W_r \times L_r$ and different number of RISs, and in Table 6.5 with different blockage density λ_b and different number of RISs. Meanwhile, compared with that a RIS comprised of M_c unit cells is located at the center of the building envelope, the coverage enhancement I is also indicated in the tables. It shows that the highest coverage enhancement is 69.5 %. In addition, the optimized length of RIS-deployment wall, i.e., W_{r2} , does not equal to the length of the building envelope, and the optimized location of RIS-deployment wall, i.e., x_d , is almost the center of the building envelope. Additionally, with the same number of RISs and

same area of the room, the room with longer building envelope has higher optimal average coverage probability. The reason is: on average, longer building envelope leads to shorter transmission distance between the RISs and the UE, moreover, lower path loss and lower blockage probability. Table 6.5 shows that when the number of RISs is 2, the optimal W_{r2} of the RIS-deployment wall decreases as blockage density increases; and when the number of RISs is 3 or 4, on the contrary, W_{r2} increases as blockage density increases. The reason is: as blockage density increases, blockage probability becomes more dominant in causing network outage than path loss, thereby it is more necessary to reduce blockage probability. When the number of RISs is 2, non-overlapped blockage regions have more influence on blockage probability than overlapped blockage region. Meanwhile, decreasing W_{r2} from 11.42 m to 10.23 m reduces the area of non-overlapped blockage regions in average with the cost of increasing the area of overlapped blockage region; on the other hand, overlapped blockage regions matter more when the number of RISs is 3 or 4, hence, W_{r2} increases to reduce the area of overlapped blockage regions.

5 Conclusion

In this paper, the transmissive multiple RIS-aided O2I network has been investigated. The indoor blockage effect considering the correlation among multiple RISs being co-blocked has been analyzed. Based on the system model, the network coverage probability has been evaluated. With the same room area, the room with longer building envelope leads to higher network coverage. In addition, the optimal average coverage probability with optimized locations of multiple RISs can reach at most 69.5% higher than that with a large-size RIS located at the center of the building envelope. Our works can provide guidance for the future multiple transmissive RIS-aided O2I network deployment.

References

- [1] 5G PPP Technology Board. (Sep. 2021). Delivery of 5G Services Indoors – the wireless wire challenge and solutions [Online]. Available: <https://5g-ppp.eu/wp-content/uploads/2021/09/Delivery-of-5G-services-indoors-v1.0-final-2.pdf>
- [2] K. Doppler *et al.*, “Future indoor network with a sixth sense: Requirements, challenges and enabling technologies,” *Pervasive and Mobile Computing*, vol. 83, p. 101571, Jul. 2022.
- [3] H. Zhang, Y. Zhang, J. Cosmas *et al.*, “MmWave indoor channel measurement campaign for 5G new radio indoor broadcasting,” *IEEE Trans. Broadcast.*, early access, Jan. 2022.
- [4] Z. Zhong, J. Zhao, and C. Li, “Outdoor-to-indoor channel measurement and coverage analysis for 5G typical spectrums,” *Int. J. Antennas Propag.*, vol. 2019, pp. 1–10, Sep. 2019.
- [5] C. Umit Bas, R. Wang, S. Sangodoyin *et al.*, “Outdoor to indoor propagation channel measurements at 28 GHz,” *IEEE Trans. Wireless Commun.*, vol. 18, no. 3, pp. 1477-1489, Mar. 2019.
- [6] D. Plets, W. Joseph, L. Verloock *et al.*, "Extensive penetration loss measurements and models for different building types for DVB-H in the UHF band," *IEEE Trans. Broadcast.*, vol. 55, no. 2, pp. 213-222, Jun. 2009.
- [7] E. Basar, I. Yildirim and F. Kilinc, “Indoor and outdoor physical channel modeling and efficient positioning for reconfigurable intelligent surfaces in mmWave bands,” *IEEE Trans. Commun.*, vol. 69, no. 12, pp. 8600-8611, Dec. 2021.

- [8] I. Yildirim, A. Uyrus and E. Basar, "Modeling and analysis of reconfigurable intelligent surfaces for indoor and outdoor applications in future wireless networks," *IEEE Trans. Commun.*, vol. 69, no. 2, pp. 1290-1301, Feb. 2021.
- [9] Z. Li, H. Hu, J. Zhang *et al.*, "Enhancing Indoor mmWave Wireless Coverage: Small-Cell Densification or Reconfigurable Intelligent Surfaces Deployment?," *IEEE Wireless Commun. Lett.*, vol. 10, no. 11, pp. 2547-2551, Nov. 2021.
- [10] NTT DOCOMO, (Jan. 2020) *DOCOMO Conducts World-s First Successful Trial of Transparent Dynamic Metasurface*. [Online]. Available: https://www.docomo.ne.jp/english/info/media_center/pr/2020/0117_00.html
- [11] J. Xu, Y. Liu, X. Mu *et al.*, "STAR-RISs: simultaneous transmitting and reflecting reconfigurable intelligent surfaces," *IEEE Commun. Lett.*, vol. 25, no. 9, pp. 3134-3138, Sept. 2021.
- [12] S. Zeng, H. Zhang, B. Di *et al.*, "Reconfigurable intelligent surfaces in 6G: Reflective, transmissive, or both?," *IEEE Commun. Lett.*, vol. 25, no. 6, pp. 2063-2067, Jun. 2021.
- [13] C. Wu, Y. Liu, X. Mu *et al.*, "Coverage characterization of STAR-RIS networks: NOMA and OMA," *IEEE Commun. Lett.*, vol. 25, no. 9, pp. 3036-3040, Sept. 2021.
- [14] X. Mu, Y. Liu, L. Guo *et al.*, "Simultaneously transmitting and reflecting (STAR) RIS aided wireless communications," *IEEE Trans. Wireless Commun.*, vol. 21, no. 5, pp. 3083-3098, May 2022.
- [15] S. Zhang, H. Zhang, B. Di *et al.*, "Intelligent omni-surfaces: Ubiquitous wireless transmission by reflective-refractive metasurfaces," *IEEE Trans. Wireless Commun.*, vol. 21, no. 1, pp. 219-233, Jan. 2022.
- [16] M. Nemati, B. Maham, S. R. Pokhrel *et al.*, "Modeling RIS empowered outdoor-to-indoor communication in mmWave cellular networks," *IEEE Trans. Commun.*, vol. 69, no. 11, pp. 7837-7850, Nov. 2021.

-
- [17] T. Bai, R. Vaze and R. W. Heath, "Analysis of Blockage Effects on Urban Cellular Networks," *IEEE Trans. Wireless Commun.*, vol. 13, no. 9, pp. 5070-5083, Sep. 2014.
- [18] M. Gapeyenko, A. Samuylov, M. Gerasimenko *et al.*, "Spatially-Consistent Human Body Blockage Modeling: A State Generation Procedure," *IEEE Trans. Mob. Comput.*, vol. 19, no. 9, pp. 2221-2233, 1 Sep. 2020.
- [19] T. S. Rappaport, S. Sun, R. Mayzus *et al.*, "Millimeter wave mobile communications for 5G cellular: It will work!," *IEEE Access*, vol. 1, pp. 335-349, May 2013.
- [20] W. Tang, M. Chen, X. Chen *et al.*, "Wireless communications with reconfigurable intelligent surface: Path loss modeling and experimental measurement," *IEEE Trans. Wireless Commun.*, vol. 20, no. 1, pp. 421-439, Jan. 2021.
- [21] H. Ibrahim, H. Tabassum and U. T. Nguyen, "Exact coverage analysis of intelligent reflecting surfaces with Nakagami-M channels," *IEEE Trans. Veh. Technol.*, vol. 70, no. 1, pp. 1072-1076, Jan. 2021.

Revisions of Paper III

As mentioned in the Introduction of the thesis, the coverage probability without considering blockage spatial correlation might lead to overestimation. In this research work, we provide results to verify this statement. In Fig. 6.9, the coverage probabilities with/without considering blockage spatial correlation are shown as functions of blockage density. Two different UE positions in the room are considered. In addition, 4 RISs are deployed on the building envelope. Other simulation parameters are shown in Table 6.3. The results show that the coverage probabilities without considering blockage spatial correlation are higher than that considering blockage spatial correlation. Therefore, the coverage probability without considering blockage spatial correlation leads to an overestimation of the actual network coverage.

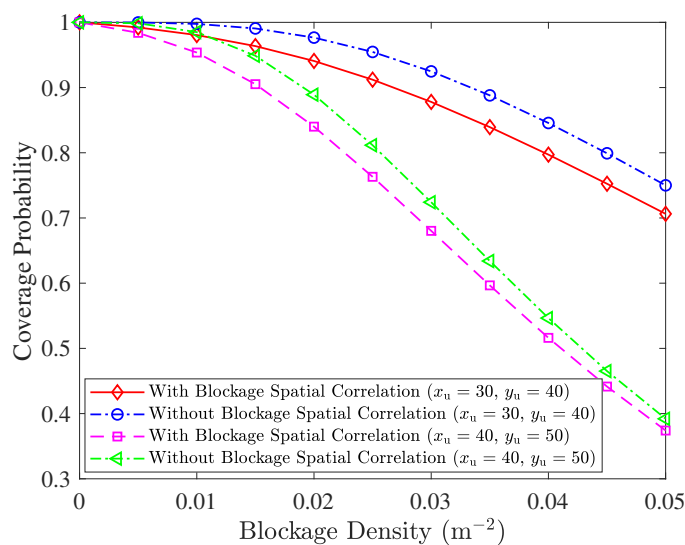


Fig. 6.9 The coverage probability considering / without considering blockage spatial correlation.